UNIVERSITAT DE BARCELONA

Field-effects on single molecular circuitry

Electronic transport from synthetic to biological models

Albert Cortijos i Aragonès

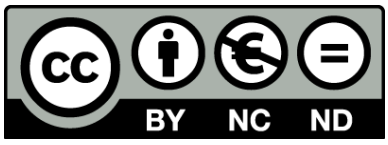

Part I

MAGNETIC FIELDS AND ELECTRON TRANSPORT

Chapter 2

Fundamental study: Metal complexes

The specific ability to control of the electrons' and molecules' spin (see *Section "Spintronics: When electronics and spins meet"* on Page 36) and tune the *spin-injection* and *manipulation* at the *nanoscale*, nowadays has become the cornerstone for the Spintronics field,[117,118] therefore to find tools which allow the manipulation of spin-polarized currents, represents one of the most important milestones to reach for the field researchers. The understanding and control of the transported electrons' spin degree of freedom beyond the electron charge in metals, semiconductors, ferromagnets, metallic or semiconducting heterostructures will open a new dimension of high-performance *spin-based* electronics and optoelectronics with outstanding improvements and new functionalities: downscaled sizes, larger bandwidths, ultrafast switches,[203] *non-volatility* and increased data processing speed, decreased electric power consumption or increased integration densities.[162,163,272]

Manipulate a spin-polarized current and regulate the MR effect through a single-molecule at RT is the aim of this Chapter and exist some precedents based on spin-valves which can help to achieve it. As has been explained in *Section "Magnetic fields and molecules: Molecular Spintronics"* (Page 43) single-molecule spin-valves have been used as the simplest test-benches for fundamental Spintronics research. Between the two kind of employed molecules, magnetic and non-magnetic, the former have been discarded because the MR effect and spin-discrimination energy mechanisms roles are due the electrodes,[181] thus we will focus on the works using magnetic molecules.[188,189,192,193,219,273–276] In such studies have been explored the spin-dependent current response of individual transition metal complexes molecules[37] with *open-shell* electronic configuration as essential requirement.[273,274,276] The parameter that possibilities the enhancement of the sensibility to the injected spins' polarization is the SOC effect,[203,219] widely explained on *Section "Spintronic surface effects: SOC and Rashba splitting"* (Page 47). As a consequence of such enhancement, is generated a strong MR effect and its associated highly efficient spin-discrimination, as shown different single-molecule devices based on the well-known

Tb(III) SMMs.[188,189,192,193,275,277]

Notwithstanding the relevance of all the previous works and their significant repercussion on the Spintronics field, the presented project involves two relevant differences respect such precedents regarding the *(i)* control and the *(ii)* applicability of the MR effect.

1. For all the above single-molecule spin-valve devices, the presented MR effect is related with the excess of transmission for one spin-polarization over the other proportionally to the total transmission. Depending on the contribution of such asymmetric spin-selection, calculated as spin filter efficiency (SFE),[191,278–280] some magnetic molecules used in spin-valves have been proposed as efficient spin-filters singe-molecule devices.[188,189,191,281–284] Such molecules present differentiated spin-states interacting with the electrodes by lifting the spin degeneracy. As a consequence of such Zeeman-splitting of the spin-levels,[285,286] the energy differences between them is enough representative to cause on the transported electrons different energy penalties according its polarization, as Figure 2.1 shows for a spin-valve mechanism based in a Tb(III) SMM.[188,189]

   Based on such spin-discrimination molecular capabilities, in this Chapter the control of the spin-dependent current response of the presented device is aimed to be tuned with the magnetic polarization direction of only one junction's subsystem, role taken by a ferromagnetic electrode which behaves as the polarizing source. Since tuning of the MR effect for the presented device is controlled via one subsystem, a part from representing a breakthrough respect the precedent studies because they used two different subsystems, involves that the presented single-molecule device cannot be considered strictly a spin-valve since it requires at least two different magnetic polarized subsystems. Therefore, from now and on we refer to it as a spin-filter.

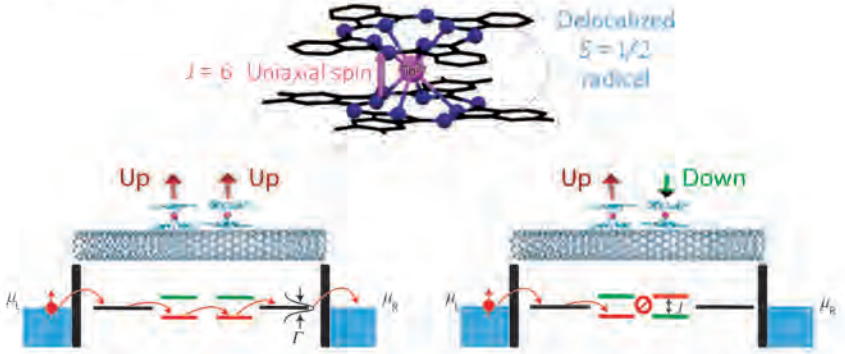

Figure 2.1: Spin-valve using Tb(III) SMM (top). Depending on the parallel (bottom-left) or antiparallel (bottom-right) configuration the spin-transport is allowed or prevented, respectively. Adapted from Urdampilleta et al.[188]

2. The applicability of the presented device will represent a breakthrough respect the precedents, since all the cited Spintronics fundamental studies were

performed far from practical operating conditions, such as Ultrahigh Vacuum (UHV) and most of them at LT regimes. For this reason the objective of this Chapter is achieve the first approach to design a spin-filtering device at the single-molecule scale and operating at RT.

2.1 Molecules as Spin-filters

As is explained above, the objective of this Section is a test-bench development for a single-molecule device based in a open-shell molecule behaving as a spin filter.[151,153,287–290]) Traditionally Spin filters have been studied in multi-layered systems and characterized via conductance variations measurements under a variable EMF.[119,152–155] The variations on the captured current are a direct consequence to the spin-filters' preferences for the transported electron polarization, such behavior allows the tunning of the current across the system via the control of the EMF, so is MR effect at single-molecule scale. The discrimination exerted between electron polarizations is the result of efficient spin-selective channels[151,154,291–293] presented by the spin-filter due to the presence of occupied and empty orbitals for each electron polarization close to the ε_F of the metal leads.[151,288,289,294]

To develop the spin-filtering single-molecule device presented on this Chapter, different *key-parameters* are be gathered to design it and attest the proposed model above. The *first key-parameter* is the ***open-shell*** electronic structure of the device's central molecule.[188,189,288,289,295–299] The used molecules should present a specific *high-spin* electronic configuration which allows the presence of the explained above α or β channels,[300] where the transported electrons suffer distinct energy penalties according the their polarization causing a current blockage or allowing the electron transmission, as it was explained before. Such discrimination represents the cornerstone of the presented Spintronic devices of this thesis, because they provide an "asymmetry" to the system. *From now and on, asymmetry concept will refer to the system's dual behavior which results in opposite responses due its properties and as a reaction of an external stimulus.*

A well-known molecular family that gathers the *first key-parameter* specifications are the Spin-Crossover complexes (SCO) with remarkable electron transport properties based on ground-state spin switching, where the *high-spin* open-shell electronic structure present higher conductance than the closed-shell *low-spin* state.[121,288,289,301] This switching behavior between the possible two electronic states is due to the change in the electronic configuration more than the structural changes (larger metal-ligand bond distances in the *high-spin* state) which play a minor role.[288,289] Regarding the electronic configuration, it is controlled by means of an external stimulus,[121,302–308] i.e. temperature, light, X-rays, pressure, electric field or solvent interactions. These features, as well as the small size (and the inherent low resistivity) and ease of manipulation of such molecules, have been exploited in many electronic and Spintronic devices, such as memories,[309] switchable nano-devices,[309,310] thin-film transistors[310] or single-molecule storage-platforms[311]

or test-bench for fundamental effects such Kondo splitting.[312]

The *second key-parameter* is ***magnetic polarization*** of an electrode used as a polarized electronic source, because depending such magnetization will inject α or β electrons to the spin-filter. The electrode ***magnetic polarization*** provides the second *asymmetry* to the single-molecule device, under this scenario the spin-filter receives polarized current from the magnetized electrode and depending the interplay between the α or β current polarization with the molecule's spin-selective channels the conductance is tunned. The use of a ***open-shell molecule*** and a single one ferromagnetic magnetized electrode behaving as electronic source or drain, represents the breakthrough compared to all previous molecular spintronics experiments, where the MR response depend on the magnetic orientation of two polarized electrodes and the molecule was just a linker between them used merely to close the electrical circuit under polarized current,[151,184–187]) or in the other cases where molecules' magnetic moment direction were controlled but the current was unpolarized. The presented single-molecule is conceived as a mixture between both mentioned kind of spintronic single-molecule devices, because the spin-filtering is due a molecular origin but the control of the polarized current and thus the device is due the magnetized ferromagnetic electrode.

In summary, the two asymmetric *key-parameters* ascribe a specific functionality to obtain the proposed spin-filtering device, the magnetized electrode is emitting polarized current according to its ***magnetic polarization*** and is injected to a ***open-shell molecule*** which acts as a spin-filter since its spin-selective channels impose energy penalties to the injected current depending the electron polarization defined by the magnetized electrode polarization. The best way to combine the *key-parameters* is through the STM microscope. At the following subsection is detailed how the different *ingredients* were combined employing such instrument with the aim to study the spin-dependent transport of the proposed single-molecule device.

2.1.1 The experimental research

In the presented experimental study was developed the proposed single-molecule spin-filter device at RT with the target capacity to tune the current by the Ni tip magnetic moment direction (see Figure 2.2). To proceed with such target was employed a *set-up* based on an STM microscope modified for molecular electronic proposes, to allow the single-molecule conductance measurements, as was explained in *Section "STM Break-Junction Technique"* (Page 26). Through the STM *set-up* were gather two different *ingredients* analogous the two chosen and previously described asymmetric *key-parameters*. Mainly, the first *ingredient* was the used synthesized on purpose[313–315] series of $[M(tzpy)_2(NCSe)_2]$ hexacoordinate complexes molecules (i) where M= Co(II), Mn(II) or Ni(II). All the mentioned complexes were synthetically designed for the purpose to be used specifically in the performed single-molecule current experiments, as a model molecules join different requirements such as stability, neutral charge, symmetry,[43] diamagnetic ligands and the

presence of two -SeCN terminal axial ligands acting as *anchoring groups* (see *Section "Beyond than Moore: Molecules as electronic components"* on Page 19) thanks to the expected affinity to the metal electrodes.[316,317] The employed Co(II) metal complex is a SCO and present switchable character depending on the working temperature, between the diamagnetic S=0 *low-spin* $t_2g^6e_g^0$ electron configuration and the open-shell *high-spin* $t_2g^5e_g^2$ electron configuration S=3/2, the compound presents the latter electronic configuration due the experimental conditions performed at RT because the the *Critical Transition Temperature* (T_{CTC}) value is 35K. In contrast, since S=5/2 Mn(II) and S=1 Ni(II) metal complexes are not SCO molecules, they keep temperature independently the *high-spin* configuration $t_2g^3e_g^2$ and $t_2g^6e_g^2$, respectively. In summary all of the studied metal complexes present an ***open-shell*** electronic structure at RT and therefore they have potential spin-filtering capabilities. The other required *ingredient* is the electrode used as the electronic source, a ferromagnetic Ni STM tip (*ii*) capable to inject spin orientated current according to its ***magnetic polarization***. Such tip is *ex-situ* magnetized in the up direction (↑Ni) respect the substrate electrode and equivalent to α-polarization, likewise it can be magnetized in down direction(↓Ni) and equivalent to β-polarization.[151,318–320] Figure 2.2 pretends to illustrate the proposed single-molecule device with spin-filtering capabilities by means of the representation of the STM main components and the above explained *ingredients*, showing the two different scenarios under the two Ni tip magnetic polarization.

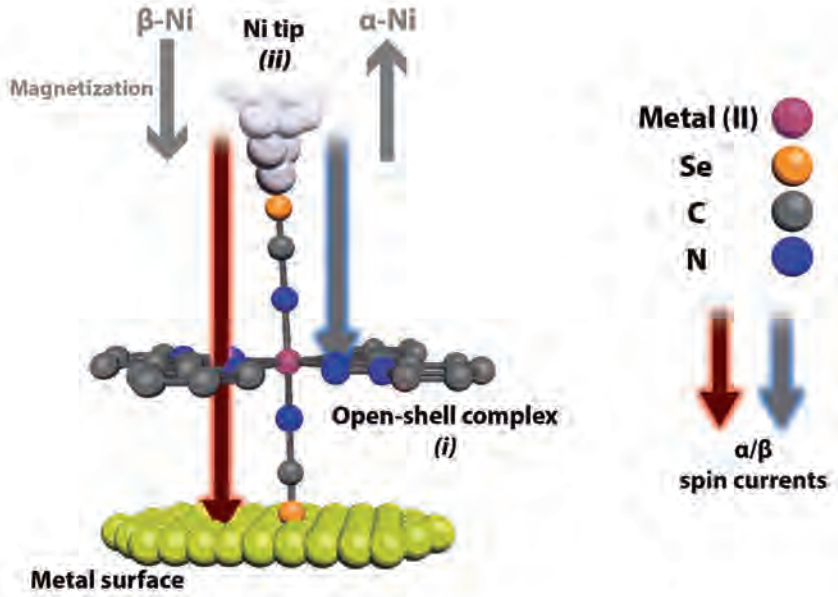

Figure 2.2: Schematic representation of the single-molecule device showing spin-filtering capabilities with the two "ingredients" labeled. M(II) corresponds to Co(II), Mn(II) and Ni(II).

The STM experiments were carried out employing polycrystalline Ni wire to obtain the STM tips electrodes and Au(111), Cu(111) or Pt(111) monocrystals were utilized as substrate electrodes, the used medium was mesitylene, an organic solvent with very low oxygen and water solubility and with a very low vapor pressure. The employed procedure was the STM-BJ into its two common approaches (see *Section "STM Break-Junction Technique"* on Page 26): the dynamic *tapping* and the static *blinking* (see *Appendix C.1*, Page 325) with different objectives. The former was used in order to capture in a statistic and very robust way, thousands of currents decays from *Tip electrode*-molecule-*Substrate electrode* junctions. The contribution of latter is an added value to the conductance measurements, through this approach can be extracted information about the junction lifetime and relate it with the affinity and bond properties between the trapped molecules and the electrodes. Also, can be used to perform the experiments when the stability of the junction and its life is affected due the low electrode-molecule affinity and the *tapping* dynamic approach has no enough time-resolution to capture the current signals. Both approaches were used under the different experimental conditions detailed above. A detailed description of the sample, substrate and tip preparation can be found from Page 328 (*Appendix C.2*).

The performed single-molecule conductance measurements were supported by computational calculations based on DFT+*NEGF* combined with non-equilibrium Green functions, *ATK code* and *NEVPT2*, in order to corroborate the spin-dependence of the current focused on the existence of α or β channels defined by electronic structure of the junctions with the metal complexes, studying the mixing of the Au surface levels with the spin-polarized molecular orbitals and the DOS and transmission curves.

2.1.2 Objectives and Summary of the experimental work

- To study the spin-dependent current response on the established singe-molecule device for the Co(II), Mn(II) and Ni(II) metal complexes, the experiments were done employing both α-↑Ni and β-↓Ni polarizations and a bias voltage between the -15 mV and -25 mV for the *Au substrate-to-Ni tip* current sense.

- In order to assess the effect of the current sense over the spin-dependent transport were inverted the electrodes source and drain roles. The single-current measurements were conducted under the *Ni tip-to-Au substrate* current sense applying a bias voltage range between the +15 mV and +25 mV employing both α-↑Ni and β-↓Ni polarizations.

- To evaluate the effects of the different metal substrates, $[Co(tzpy)_2(NCSe)_2]$ complex was measured replacing the Au substrate electrode by another ones made from Cu or Pt. Due the poor mechanical ductility of the Ni-Pt junction these control experiments were carried out using the *blinking* approach. Despite Au and Cu present enough ductility to carry out the *tapping* experiments, the *blinking* measurements were done for all the three substrate materials in order to obtain an appropriate comparison. The experimental conditions were set to -10 mV as bias voltage and for the *blinking* experiments the selected set-point was current was 1 nA for Au and Pt substrates and 0.1 nA for Cu substrate.

- To ascertain unequivocally the establishment of a molecular junction between the two electrodes during the *blinking* experiments, a mechanical pullings over a *blinking* event were exerted in different occasions during the experiments. During the mechanical pullings the Ni tip electrode was retracted few nanometers away from the surface resulting in the molecular junction collapse, the distinctive current signature of the molecular junctions is the presence of small plateaus just before the molecular rupture and the consequent sudden drop of current,[62,94,95] such plateaus are due the molecular stretching and the effects over the conductance.[43,62] As a reference of a junction-free scenario also was applied the same procedure under a tunneling current through the gap. For a more detailed description of this procedure see *Appendix C.1* (Page 325).

In the following pages is shown summarized the research as a published paper and its Supplementary Information reduced to the experimental Section as a consequence of the extension of the computational data (see on-line complete version at `http://pubs.acs.org/doi/suppl/10.1021/jacs.6b11166`*):*

"Albert C. Aragonès, Daniel Aravena, Francisco J. Valverde-Muñoz, José Antonio Real, Fausto Sanz, Ismael Díez-Pérez, and Eliseo Ruiz. Metal-Controlled Magnetoresistance at Room Temperature in Single-Molecule Devices. *Journal of the American Chemical Society*, page jacs.6b11166, mar 2017".

JACS
JOURNAL OF THE AMERICAN CHEMICAL SOCIETY
Article
pubs.acs.org/JACS

Metal-Controlled Magnetoresistance at Room Temperature in Single-Molecule Devices

Albert C. Aragonès,[†,∇,‡] Daniel Aravena,[§,∥] Francisco J. Valverde-Muñoz,[⊥] José Antonio Real,[⊥] Fausto Sanz,[†,‡] Ismael Díez-Pérez,*[,†,∇,‡] and Eliseo Ruiz*[,#,∇]

[†]Departament de Ciència de Materials i Química Física, Universitat de Barcelona, Martí i Franquès 1 and Institut de Bioenginyeria de Catalunya (IBEC), Baldiri Reixac 15-21, Barcelona 08028, Spain

[‡]Centro Investigación Biomédica en Red (CIBER-BBN), Campus Río Ebro-Edificio I+D, Poeta Mariano Esquillor s/n, 50018 Zaragoza, Spain

[§]Departamento de Química de los Materiales, Facultad de Química y Biología, Universidad de Santiago de Chile (USACH), Casilla 40, Correo 33, Santiago, Chile

[∥]Centro Para El Desarrollo de Nanociencias y Nanotecnología, CEDENNA, Santiago, Chile

[⊥]Institut de Ciència Molecular (ICMol), Universitat de València, 46980 Paterna, València, Spain

[#]Departament de Química Inorgànica i Orgànica, Universitat de Barcelona, Diagonal 645, 08028 Barcelona, Spain

[∇]Institut de Química Teòrica i Computacional, Universitat de Barcelona, Diagonal 645, 08028 Barcelona, Spain

Supporting Information

ABSTRACT: The appropriate choice of the transition metal complex and metal surface electronic structure opens the possibility to control the spin of the charge carriers through the resulting hybrid molecule/metal *spinterface* in a single-molecule electrical contact at room temperature. The single-molecule conductance of a Au/molecule/Ni junction can be switched by flipping the magnetization direction of the ferromagnetic electrode. The requirements of the molecule include not just the presence of unpaired electrons: the electronic configuration of the metal center has to provide occupied or empty orbitals that strongly interact with the junction metal electrodes and that are close in energy to their Fermi levels for one of the electronic spins only. The key ingredient for the metal surface is to provide an efficient *spin texture* induced by the spin−orbit coupling in the topological surface states that results in an efficient spin-dependent interaction with the orbitals of the molecule. The strong magnetoresistance effect found in this kind of single-molecule wire opens a new approach for the design of room-temperature nanoscale devices based on spin-polarized currents controlled at molecular level.

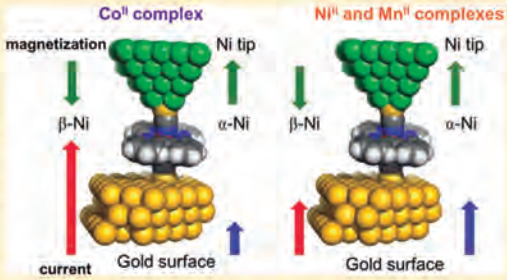

■ INTRODUCTION

Many new transport properties have been recently found by combining the spin of magnetic materials with large spin−orbit coupling (SOC) effects.[1] The control of the spin is one of the main challenges in the spintronics field, and it has been already shown a large number of remarkably performing devices based mainly in multilayered materials.[2,3] Most such devices have been built with a nonmagnetic layer sandwiched between two magnetic electrodes showing, among other properties, magnetoresistance. The use of molecular entities in spintronic devices could add new dimensionalities thanks to their longer spin relaxation times, low cost, and self-assembling capabilities.[4] However, the use of molecules in this research field is relatively new, and most of the reported experiments have been performed far from room conditions, such as in ultrahigh vacuum and at low temperatures. A wide range of examples of molecular devices displaying spin-dependent functionalities have been proven at low dimensionality, ranging from the nanoscale down to the single-molecule level. For instance, the characterization of magnetoresistive molecular nanoscale devices based on terbium(III) complexes[5,6] resulted in a number of spin-based properties such as spin valves,[7] spin transistors,[8] or spin resonators.[9] Also, slight changes in the magnetoresistance properties have been observed in single-molecule junctions built with diamagnetic molecules connected to Ni beads.[10,11] All of the above examples were typically conducted at cryogenic temperatures where the intrinsic molecular magnetic properties are preserved. To the best of our knowledge, there are only two reported molecular-based

Received: October 31, 2016
Published: February 18, 2017

DOI: 10.1021/jacs.6b11166
J. Am. Chem. Soc. XXXX, XXX, XXX−XXX

devices displaying room-temperature spin-dependent transport: (i) Self-assembled monolayers (SAMs) of chiral structures such as DNA are deposited on gold surfaces;[12,13] here, the proposed mechanism, chiral induced spin selectivity (CISS), is a combined effect of spin–orbit interaction in the chiral molecular backbone[14,15] and the induced Au–S bond magnetization at the molecule–metal interface.[16,17] Recently, such systems have been reviewed by Naaman and co-workers.[18,19] Furthermore, this effect also has been investigated in the single-molecule break-junction STM technique, consisting of individual peptide molecules of well-defined chirality bridged between a magnetized STM Ni tip and an Au.[20] Also (ii), single-molecule junctions are built by bridging individual small magnetic molecules such as spin-crossover Fe^{II} complexes $[Fe(tzpy)_2(NCX)_2]$, (X = S or Se) in a high-spin $S = 2$ configuration.[21] The observed room-temperature magnetoresistance in this case occurs when the electrons are injected from the gold (large spin–orbit effect) to a magnetic nickel electrode through the Fe^{II} complex that acts as spin filter.[22−27] The single-molecule magnetoresistance effect disappears either by employing low-spin $S = 0$ Fe^{II} complexes (also by decreasing the temperature that switches the high-spin $[Fe(tzpy)_2(NCX)_2]$ complex to the nonmagnetic low-spin state) or by using a Cu substrate (small spin–orbit) instead of Au. In the last two examples, a fundamental difference from previous experiments is the likely requirement of a heavy diamagnetic electrode as one of the electrodes of the molecular device.

In this contribution, we design, synthesize, and characterize single-molecule spin-dependent transport of a series of metal complexes $[M(tzpy)_2(NCSe)_2]$ (M = Mn, Co, and Ni) with two axial $SeCN^-$ anchoring groups (see Figure 1) that were

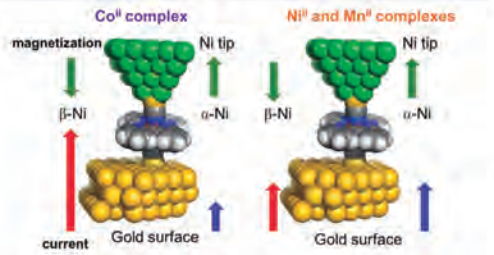

Figure 1. Schematic representation of the single-molecule devices studied under two opposite Ni tip magnetic polarizations (green arrows, labeled α and β). Among the paramagnetic $[M(tzpy)_2(NCSe)_2]$ complexes (M = Mn, Co, and Ni), only the Co^{II} complex shows high tunneling magnetoresistance (red and blue arrows indicate currents for the two opposite magnetizations of the Ni tip), while transport in the Mn^{II} and Ni^{II} complexes remains invariable versus the Ni magnetization directions.

proven to be a mechanically stable metal–molecule attachment.[21] The spin-dependent single-molecule transport study was conducted by trapping the metal complexes between a dielectric Au electrode (electron source) and a magnetically polarized Ni electrode (spin-polarized electron drain). We observed that the single-molecule wire with the $S = {}^3/_2$ Co^{II} complex shows a conductance change of at least 100-fold under opposite Ni magnetizations along the main junction axis (Figure 1), similar to those reported for the homologous Fe^{II} complex.[21] In contrast, the devices based on Ni^{II} and Mn^{II} complexes do not exhibit such magnetoresistance. Our theoretical calculations indicate that the presence of unpaired electrons in the molecule is mandatory, but that the metal electronic configuration is the key factor. The $t_{2g}^5e_g^2$ electronic configuration of the Co^{II} complex provides an efficient spin-selective channel due to the presence of one occupied and one empty β orbitals close to the Fermi level of the junction electrodes. Contrarily, for the $t_{2g}^6e_g^2$ electronic configuration of the $S = 1$ Ni^{II} complex, the proximal e_g orbital to the electrode Fermi energy lacks the appropriate symmetry to mix with the π orbitals of the $SeCN^-$ ligands that interact with the electrodes. In the $t_{2g}^3e_g^2$ electronic configuration of the $S = {}^5/_2$ Mn^{II} complex, the absence of the observed magnetoresistance is explained by the lack of Mn^{II} orbitals close to the electrodes' Fermi levels. The differences in the molecule/Au spinterface between the two axial directions of the Ni magnetic polarization[21] are indispensable to explain the observed magnetoresistance in the former (Figure 1).

RESULTS AND DISCUSSION

Room-Temperature Single-Molecule Transport of the $[M(tzpy)_2(NCSe)_2]$ Complexes (M = Mn, Co, and Ni). Single-molecule conductance experiments were performed at room temperature using a spin-polarized version of the STM break-junction approach.[21,28,29] Briefly, an individual $[M(tzpy)_2(NCSe)_2]$ complex (M = Mn, Co, and Ni) was trapped between a Au and a ferromagnetic Ni electrode under opposite magnetic polarization directions along the axial molecular junction (Figure 1). For this purpose, a freshly mechanically cut Ni tip was magnetically polarized *ex situ* by placing it in close proximity to a 1 T NdFeB magnet for a period of 2 h, and then it was placed into the STM tip holder. To avoid Ni oxidation during the magnetization stage, the Ni tip was kept under anaerobic conditions (see detailed Ni tip preparation and characterization elsewhere[21]). The magnitude and direction of the magnetic polarization of the Ni tip were characterized before and after the STM break-junction experiment using SQUID magnetometry to check that they persisted over the entire time frame of the experiments.[21] The magnetized STM Ni probe was then driven toward the surface and pulled back again in successive cycles, using a 2-point feedback loop on the tunneling current flowing between the two electrodes under a constant bias voltage. Representative current traces during the pulling stage are shown in the insets of Figure 2a–c for the three $[M(tzpy)_2(NCSe)_2]$ complexes (M = Mn, Co, and Ni), respectively. When a molecule bridges between the two electrodes, a plateau appears in the current trace during the pulling stage at a specific molecular conductance.[28,30] The absence of other exposed interacting groups in these compounds as well as the single plateau features in the decay curves suggests the axial $SeCN^-$ ligand as the only anchoring points.[21] Hundreds of these individual traces are then accumulated into the same conductance histogram where the average single-molecule conductance value is extracted from the Gaussian fitting of the peaks (Figures 2a–c). The α and β labels correspond to the magnetic moment of the Ni electrode, pointing upward and downward, respectively, along the main molecular junction axis (see Figure 1).

The analysis of the histograms in Figure 2 reveals two markedly different charge transport behaviors: (i) The single-molecule junctions built with the Mn^{II} and Ni^{II} complexes display similar characteristic conductance values for both α-up and β-down directions of the Ni magnetization (see Figure 2a,c) and, consequently, no magnetoresistance. The [Mn-

DOI: 10.1021/jacs.6b11166
J. Am. Chem. Soc. XXXX, XXX, XXX−XXX

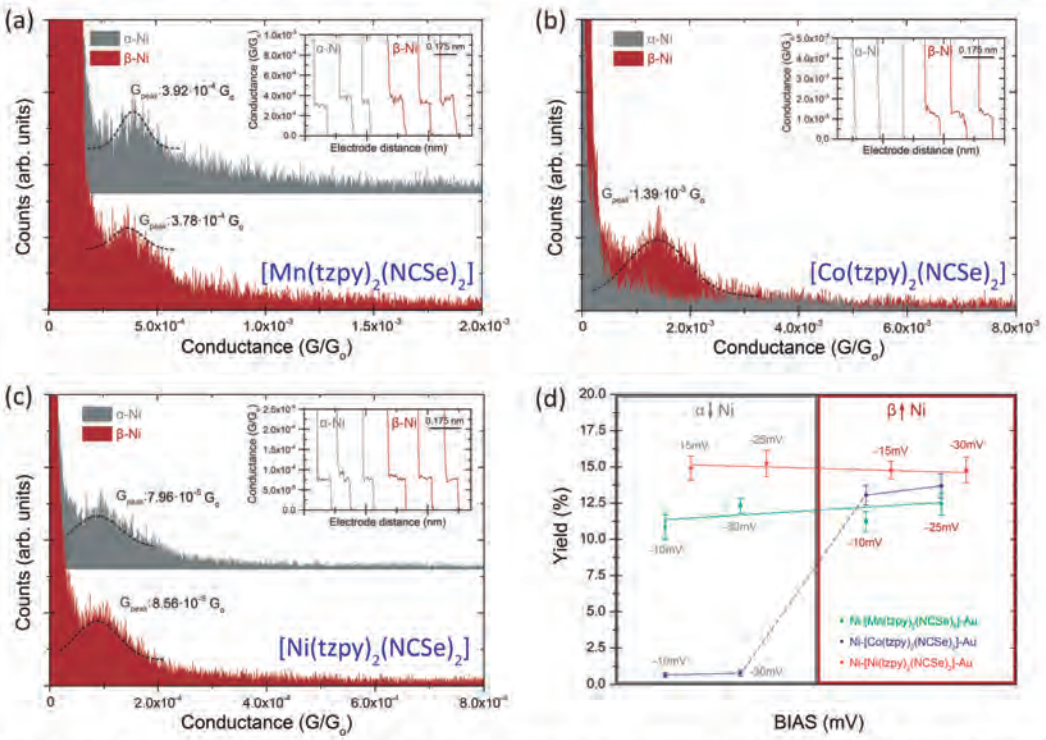

Figure 2. Single-molecule conductance histogram for the metal complexes: (a) $S = {}^5/_2$ $[Mn(tzpy)_2(NCSe)_2]$, (b) $S = 3/2$ $[Co(tzpy)_2(NCSe)_2]$, and (c) $S = 1$ $[Ni(tzpy)_2(NCSe)_2]$ bridging between Au and both α-up polarized (gray) and β-down (maroon) magnetically polarized Ni electrodes. The two histograms in parts a and c have been vertically offset for clarity. All conductance values have been extracted from Gaussian fits of the peaks. Insets show representative individual current versus pulling traces for the α-up polarized (left) and the β-down polarized (right) Ni electrodes used to build the conductance histograms. The applied bias was set to −15 mV in part c and −25 mV in parts a and b as indicated in the figure. (d) Single-molecule junction yield (%) for the three compounds under the two Ni magnetic polarizations. Different points correspond to different employed bias voltages, and the error bars denote the standard deviation from the average conductance results of different experiments.

$(tzpy)_2(NCSe)_2]$ displays a conductance around $3.8 \times 10^{-4}G_0$ (with $G_0 = 77.5\ \mu S$), ~5-fold higher that of $[Ni(tzpy)_2(NCSe)_2]$, $8.2 \times 10^{-5}G_0$. (ii) In contrast, the single-molecule junctions built with the $[Co(tzpy)_2(NCSe)_2]$ complex display a measurable conductance value for the β-down polarized Ni electrode only (Figure 2b). This measured magnetoresistance for the Co^{II} compound is comparable to that previously reported for a homologous Fe^{II} complex while the obtained conductance value, $1.39 \times 10^{-3}G_0$, is ~3-fold larger than that previously reported for the equivalent $[Fe(tzpy)_2(NCSe)_2])$ complex, $4.4 \times 10^{-4}G_0$ for the same β-down Ni polarization direction.[21] No current plateaus were then appreciable in the individual pulling traces for the $[Co(tzpy)_2(NCSe)_2]$ complex in the single-molecule experiments with α-up polarized Ni electrodes (gray traces in the Figure 2b, inset). The single-molecule conductance is in this case below the detection limit of our current amplifiers ($<10^{-6}G_0$, see gray histogram in Figure 2b).

Figure 2d summarizes the experimental yield of the single-molecule transport experiments for the three studied compounds under the two Ni magnetic polarizations. As previously described,[21] the single-molecule yield is expressed as the percentage of individual pulling traces showing plateau features. Typically, single-molecule experimental values of >10% are routinely obtained experimentally[31,32] and allow the single-molecule conductance characterization. All three systems show yields above 10% for the formation of single-molecule junctions between the two metal electrodes for a β-down Ni polarization direction. When the Ni polarization is inverted, the yield drops down to values below 1% for the $[Co(tzpy)_2(NCSe)_2]$ compound, whereas the yield remains constant for the other two.

Effect of the Metal Substrate on the Single-Molecule Magnetoresistance. In order to highlight the role of the metal substrate on the observed magnetoresistance for the single-molecule contact formed with the $[Co(tzpy)_2(NCSe)_2]$ compound, we have performed single-molecule charge transport measurements on $M/[Co(tzpy)_2(NCSe)_2]/Ni$ junctions (M = Au, Cu, Pt) under opposite magnetization directions of the Ni tips along the main molecular junction axis. Due to the poor mechanical ductility of the Ni−Pt junction, the length of the plateaus in the break-junction pulling traces resulting from the single-molecule bridge formation was almost unappreciable,[33] a fact that forced us to exploit a previously presented *blinking* approach to build and characterize the single-molecule conductance (see a detailed description elsewhere[34,35]). Briefly, in the blinking approach, the Ni STM electrode is held at a nanometer distance from the metal surface. When a molecule

DOI: 10.1021/jacs.6b11166
J. Am. Chem. Soc. XXXX, XXX, XXX−XXX

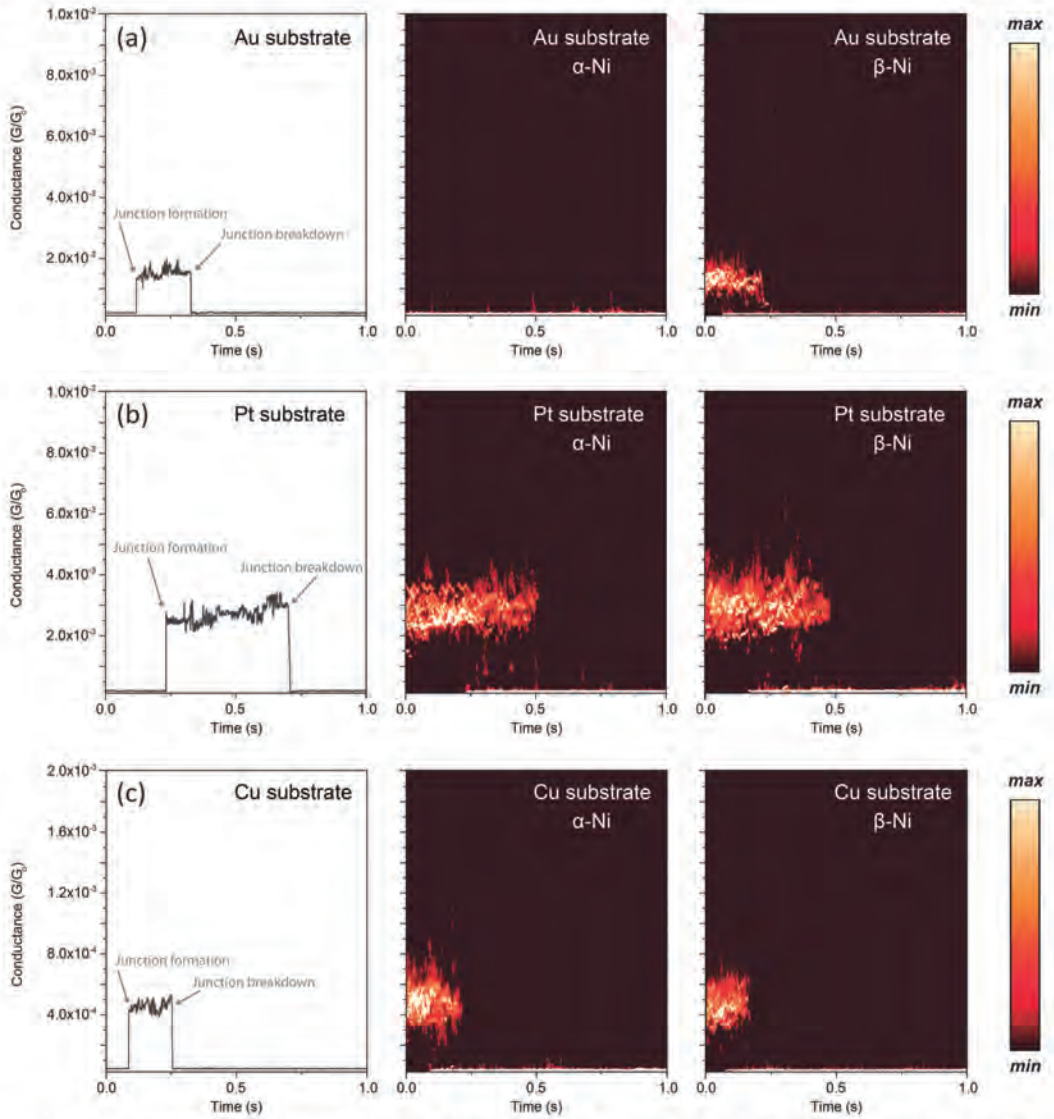

Figure 3. Single-molecule charge transport of the $[Co(tzpy)_2(NCSe)_2]$ compound on different metal surfaces. The horizontally expanded panels show, from left to right, a representative *blinking* event of the single-molecule bridge formation, and the two 2D *blinking* maps show the average of several tens of individual *blinking* traces for the two opposite directions of the Ni electrode magnetization α/β, respectively (see Figure 1), on (a) Au, (b) Pt, and (c) Cu surfaces. The 2D maps were normalized to a color scale versus the total number of counts, representing 100 counts as the maximum and 0 counts as the minimum. The applied bias was set to −10 mV.

spans the gap, a telegraphic signal is recorded in the current transient (see Figure 3, left panels) whose amplitude equals the conductance of the molecular junction. The existence of a molecular bridge is ascertained by performing pulling stages during the ON telegraphic signal to promote the molecular breakdown (see Supporting Information section 5). Up to a hundred of the individual blinking traces are accumulated in a 2D *blinking* map without any selection by setting all of them to a common time origin and background tunneling current subtraction.

Figure 3 shows a comparison of the three 2D *blinking* maps recorded for the $[Co(tzpy)_2(NCSe)_2]$ single-molecule junctions formed between the magnetically polarized Ni STM electrode and Au, Pt, and Cu surfaces, respectively. The central and right panels correspond to the 2D *blinking* maps with the Ni electrode magnetically polarized upward and downward, respectively. The results obtained using the Au substrate (Figure 3a) are essentially the same as those shown in Figure 2b employing the break-junction approach; i.e., the level of conductance and the magnetoresistance effect displaying

DOI: 10.1021/jacs.6b11166
J. Am. Chem. Soc. XXXX, XXX, XXX−XXX

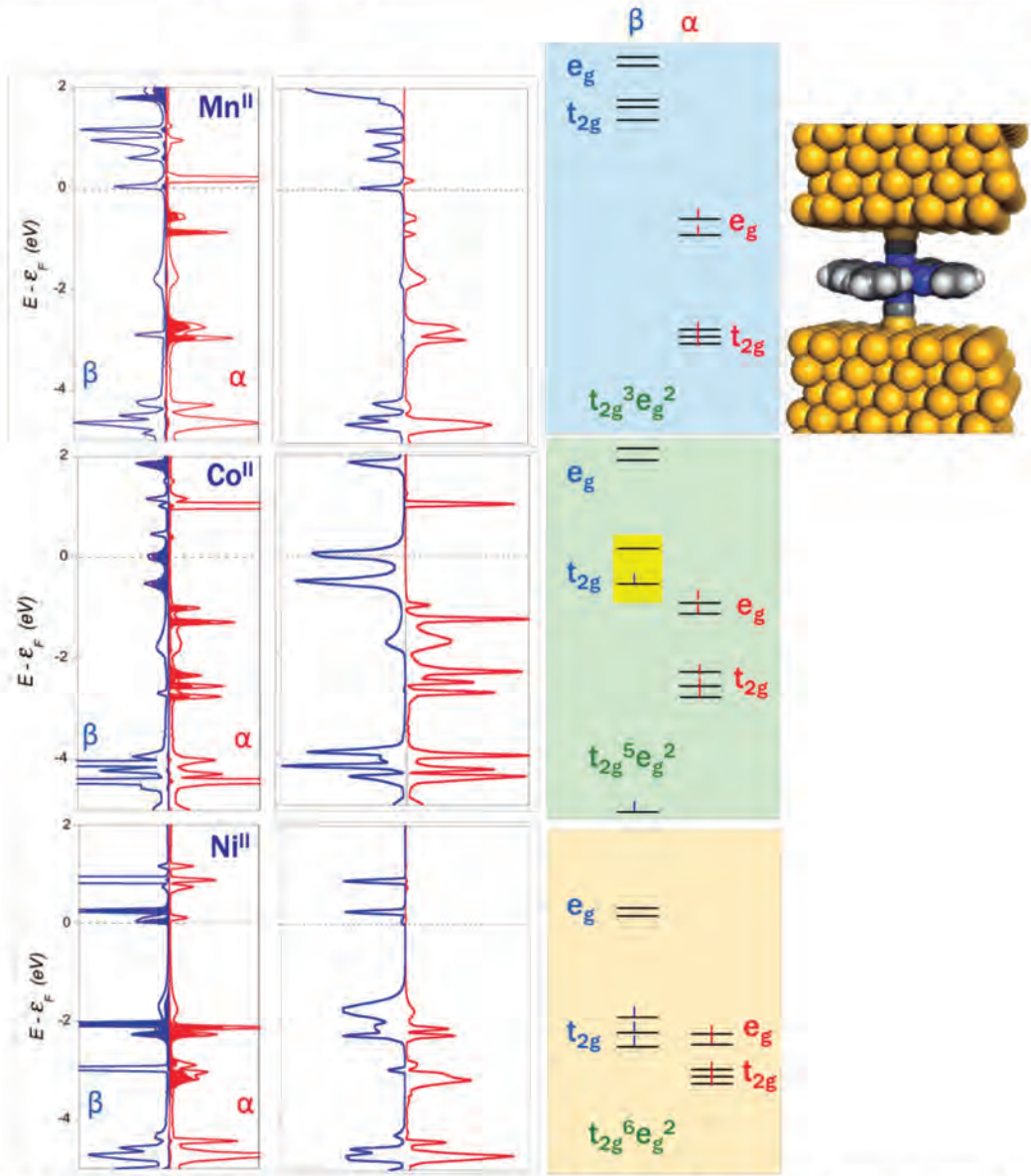

Figure 4. DFT calculated spin-resolved projected density of states (left) of the Mn^{II}, Co^{II}, and Ni^{II} complexes (filled curve corresponds to the transition metal levels and metal orbitals, and their occupations are represented in the right side) and transmission spectra (right, between 0 and 2 for each spin) for a 2.5 Å constant gold–ligand bond distance. Red and blue colors correspond to the α and β spin contributions, respectively. Transition metal d orbitals out of the energy range have just been placed without considering their orbital energy values. The highlighted t_{2g} unpaired β orbitals in the Co^{II} complex correspond to the main spin-dependent electron channels.

suppression of the single-molecule conductance at the α-up Ni magnetization direction are equally observed. In contrast, the molecular junctions built on either Pt or Cu surfaces are insensitive to the magnetic polarization direction of the top Ni electrode, showing essentially no magnetoresistance of the single-molecule wire conductance for the $[Co(tzpy)_2(NCSe)_2]$ complex (Figure 3b,c, respectively). The suppression of magnetoresistance observed in the single-molecule wire built on Cu was also confirmed by characterizing the single-molecule transport of $[Co(tzpy)_2(NCSe)_2]$ using the previous dynamic STM break-junction approach (see Supporting Information section 3). These results evidence the importance that molecule/metal interfacial effects have on the final observed

DOI: 10.1021/jacs.6b11166
J. Am. Chem. Soc. XXXX, XXX, XXX–XXX

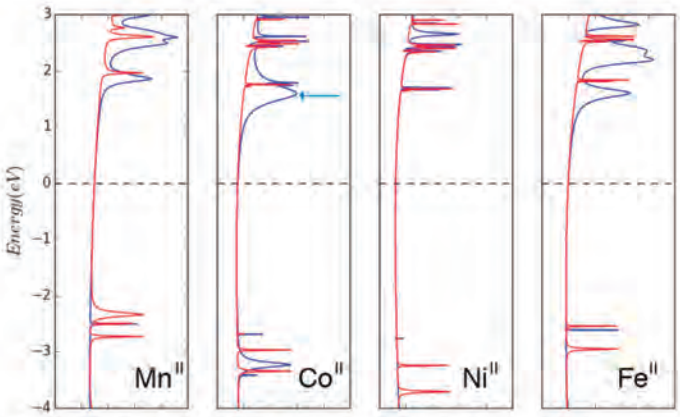

Figure 5. DFT transmission (between 0 and 2.5 for each spin) calculated with the hybrid B3LYP functional for the single $[M(tzpy)_2(NCSe)_2]$ complexes (M = Co, Mn, Ni, and Fe) sandwiched between two electrodes (red and blue are α and β contributions, respectively). The Fe^{II} system is included for comparison (see text) and was investigated with periodic models elsewhere.[21] The Fermi level was chosen to be −5 eV and set to 0 eV in the plot (marked with a dashed line). The blue arrow indicates in the Co^{II} case the crucial t_{2g} orbital for the magnetoresistance effect.

device magnetoresistance as will be discussed in the next section.

Spin-Dependent Density of States and Transmission Calculation. To rationalize the origin of the observed differences in magnetoresistance in the studied single-molecule junctions, we first performed spin-polarized DFT-NEGF calculations.[36−38] The structural model for the calculations consisted of two true semi-infinite Au surface electrodes with the molecule attached to both Au(111) surfaces by the Se atoms in a 3-fold hollow configuration. The calculations were carried out using two equivalent gold surfaces in order to simplify the system, with the consideration that the spin-filter effect arises from the mixing of the gold surface levels with the spin-polarized molecular orbitals.[21] The nickel tip is not included in the calculation since it just controls the final device conductance because the transport of minority spin carriers is more efficient in the magnetically polarized Ni electrode.[39] Furthermore, the magnetic effect of the nickel tip on the molecule is included using a spin-polarized single determinant to describe the electronic structure of the molecule.

The calculated density of states (DOS) and transmission curves for the three complexes (M = Mn, Co, and Ni) adsorbed between two Au(111) surfaces are plotted in Figure 4. The main observed differences between the three studied cases can be summarized as follows for each metal system: (i) The Mn^{II} system has a $t_{2g}^3e_g^2$ electronic configuration, where either the highest occupied α e_g orbital and the lowest unoccupied β t_{2g} orbitals are far from the Au Fermi level (around 0.5 eV below and 1.8 eV above in the DOS, Figure 4, left and right panels, respectively). Hence, despite the molecule having the largest total spin, $S = {}^5/_2$, the single-molecule device is unlikely to show magnetoresistance effects at low applied voltage biases as experimentally observed. Despite the lack of 3d orbitals close to the Fermi energy, there is a non-negligible contribution to $T(E)$ starting from the Fermi level (Figure 4, central panel) that corresponds to narrow levels with a poor interaction with the electrodes. Furthermore, the states contributing to the $T(E)$ in this range are highly delocalized unoccupied orbitals, which appear too close to the Fermi level due to the typical gap underestimation of the PBE functional. We expect these states to be further away from the Fermi level, having a much lower contribution to the electronic transmission. To check this assumption, we performed a model calculation of the Mn^{II} system coupled to two small gold clusters and obtained the transmission function for zero bias. We employed the B3LYP functional to incorporate an improved description of the HOMO−LUMO gap (see Computational Details section for further reference). We observe a notorious increase of the energy gap, where the main contributions to the electronic transport come from d orbital levels that are far from the Fermi level (~1.5−2.0 eV apart, see Figure 5). This is in line with the relatively low single-molecule conductance of this system (~3.8 × $10^{-4}G_0$, see Figure 2a). (ii) The Co^{II} case displays two t_{2g} β orbitals (highlighted in yellow in Figure 4 , right) that are closer to the Au electrode Fermi level in comparison with the α channel orbitals that display the highest occupied orbitals appearing ~1.0 eV apart. The observed broadening of these two t_{2g} β orbitals is evidence of its effective hybridization to the metal orbitals, which also results in a higher measured conductance of the single-molecule junction for this molecular system through the β orbital channel (~1.4 × $10^{-3}G_0$, see Figure 2b). The analysis of these two orbitals shows correspondence to the π antibonding d_{xz} and d_{yz} t_{2g} orbitals with strong interaction with the gold electrode through the π system of the axial ligands, while the third t_{2g} orbital (nonbonding d_{xy}) is located below −5 eV. B3LYP results for the corresponding model system support this picture, with relatively broad transmission peaks that are 1.0−1.5 eV apart from the Fermi level (see Figure 5) suggesting that the transport proceeds through the β LUMO. As a result, β spin-polarized orbital channels are responsible for the pronounced spin filtering of the current transmitted through the Co^{II} complex single-molecule junction. We have calculated the energy involved in the flipping of the molecular spin with the complex adsorbed on a hollow site of a spin-polarized Ni(111) surface. The value is 90 cm^{-1} favorable for the parallel spin alignment using the PBE functional (see Computational Details section). Considering that the magnetically polarized Ni tip induces the same spin alignment at the molecule through magnetic exchange interactions,[40] the observed single-molecule

DOI: 10.1021/jacs.6b11166
J. Am. Chem. Soc. XXXX, XXX, XXX−XXX

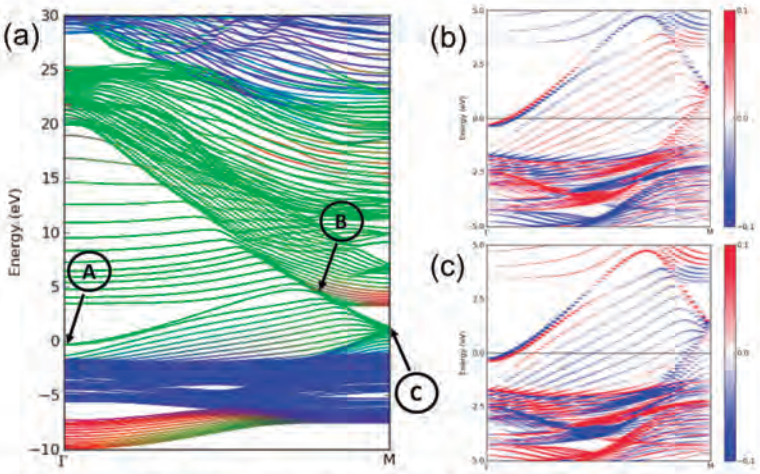

Figure 6. (a) Calculated band structure of Au(111) surface along the $\Gamma \rightarrow M$ (π/a, 0, 0) path. Bands were obtained from an 18-atom slab calculation of a 1 × 1 surface. The color of the bands represents the contributions from s, p, and d orbitals, coded in an RGB scheme. In this way, pure red, green, and blue represent bands dominated by s, p, and d contributions, respectively. Intermediate colors are weighted by each contribution. (b and c) Spin polarization (red and blue colors for the two spin orientations) along the (b) *x*- and (c) *y*-directions projected on one surface gold atom. There is no spin polarization along the *z*-axis.

magnetoresistance is explained by an asymmetric hybridization of the molecular orbitals to the magnetically polarized molecule/Au interface (*spinterface*).[41,42] This effect is similar to that presented in the previously reported Fe^{II} systems, which also display DOS and transmission curves with two of the β t_{2g} orbitals close to the Fermi level.[21,22] The role of the spinterface effect in the appearance of magnetoresistance in the single-molecule junction built with the Co^{II} system is corroborated by the experimental results shown in Figure 3, where the interfacial magnetic polarization is suppressed by using other metal surfaces (e.g., Cu, Pt magnetoresistance for the Co^{II} system vanishes in Figure 3b,c) with less tendency to be spin-polarized than Au. Hence, the gold surface is a key ingredient to produce the magnetoresistance behavior due to the existence of spin unbalanced topological surface states detected by angle-resolved photoemission spectroscopy (ARPES),[43] wherein the spin−orbit effect results in spin texture on this surface. Although gold, copper, and platinum exhibit the same qualitative structure with respect to their sp band crossing,[43] we observe that magnetoresistance effects are only observed when the Co^{II} complex is deposited on gold. In the case of Cu, this behavior is related to the low spin−orbit coupling constant due to its lower atomic weight. In the case of Pt, despite having a structure similar to that of Au, it has one valence electron less that yields a different mixing with the $SeCN^-$ ligands in comparison to that of Au. We will come back to this point in the next section. (iii) The Ni^{II} system is similar to the Mn^{II} case, as it has delocalized orbitals close to the Fermi level for both β and α electrons, with a higher β contribution (Figure 4, right panel). In this case, the β empty e_g orbitals also appear relatively close to the Fermi level. The corresponding transmission peaks are narrow, manifesting the very weak mixing of the frontier σ e_g orbitals of the Ni^{II} complex to the π nature of axial $SeCN^-$ orbitals that interact with the gold surface levels. This poor hybridization also explains the low conductance measured in this case (~$8.6 \times 10^{-5} G_0$, Figure 2c). The B3LYP calculation effectively corrects for the position of the delocalized empty orbitals, which appear now far from the Fermi level (see Figure 5). Furthermore, the transmission peaks corresponding to e_g orbitals are extremely narrow, confirming the low mixing of these orbitals and the low experimental conductivity of the Ni^{II} derivative. Figure 5 shows satisfactorily the relation between the measured conductance and the energy profile of the transmission function. The most conductive ion is Co^{II}, in agreement with the experimental data, due to their highly coupled empty β t_{2g} levels that appear relatively close to the Fermi level (indicated with a blue arrow in Figure 5). The less conducting cases are observed for the Mn^{II} and Ni^{II} complexes that only present poor mixing of the e_g-type orbitals near the Fermi level. If we include the Fe^{II} derivative in this analysis, we observe that it presents lower conductivity than Co^{II}, but higher than those of Mn^{II} and Ni^{II}. Similar to the case of Co^{II}, this system presents significantly broadened β t_{2g} orbitals that appear further away from the Fermi level in comparison to the Co^{II} derivative, explaining its lower conductivity.[21] On the other hand, the conductivity associated with t_{2g} orbitals in Fe^{II} (the last occupied t_{2g} orbital of Co^{II} close to the Fermi level is empty for Fe^{II}, and it is the main responsible of transport for such complex) should be higher than the contributions from e_g orbitals, which are dominant for Mn^{II} and Ni^{II} systems. The observed lack of magnetoresistance for the Mn^{II} and Ni^{II} single-molecule junctions is then explained by the ineffective spin-filter behavior of the molecule due to the poor differences in the transmission efficiency between the α and β channels.

An important message is deduced from the above discussion: An appropriate electronic structure of the magnetic molecule is necessary to develop magnetoresistance in a single-molecule device, similar to what is required to show large magnetic anisotropy effects, i.e., low-lying excitations and differentiated α–β electronic configurations.[44−46] The existence of low-lying excitations warrants the presence of occupied and empty orbitals in a narrow energy range that allows available channels for efficient transport if they lie close to the Fermi level of the

DOI: 10.1021/jacs.6b11166
J. Am. Chem. Soc. XXXX, XXX, XXX−XXX

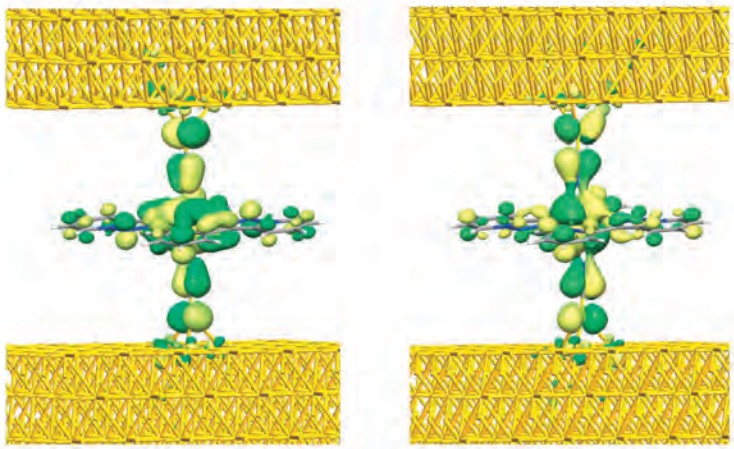

Figure 7. Main transmission eigenstates corresponding to the β transmission peaks at −0.52 and +0.04 eV for the Co^{II} complex (occupied and empty t_{2g} orbitals, see Figure 4). The transmission eigenstates are obtained by diagonalizing the transmission matrix, and the corresponding eigenvalues indicate the importance of each eigenstate in the transport. As it is a complex wave function, the color map indicating the phase of the function is represented from 0 to 2π by dark green to yellow colors. The isovalue employed for the isosurface is 0.2.

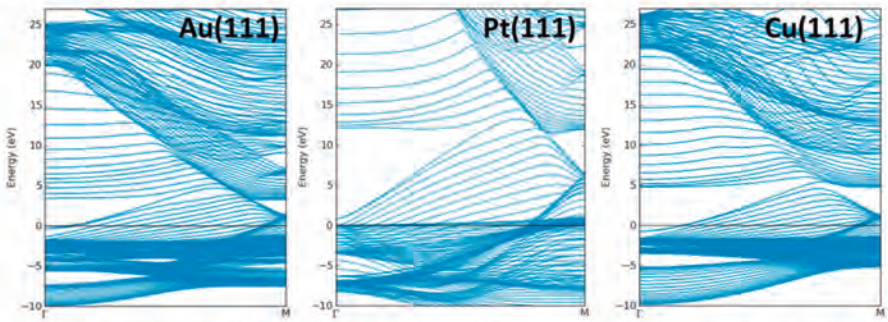

Figure 8. Band diagram along the Γ → M path for the 18 layer Au(111) (left), Pt(111)(center), and Cu(111) (right). (All surfaces are 1 × 1.) The Fermi level is indicated by a black line.

electrodes. For instance, the $[Co(tzpy)_2(NCSe)_2]$ complex has mononuclear single-molecule magnet behavior (see Supporting Information section 4.3) with a calculated axial zero field-splitting D value at the NEVPT2 level of +16.7 cm^{-1}, achieving easy-plane anisotropy as expected for a pseudo-octahedral Co^{II} complex.[44] Thus, single-molecule magnet complexes are in principle good candidates to show appealing transport properties, such as magnetoresistance effects in single-molecule devices.

Spin Texture of the Gold Surface. After the relation is established between the electronic configuration of the molecule and the development of magnetoresistance in our devices, it is necessary to investigate why spin-dependent transport develops on the Au surface only, while platinum and copper junctions do not present such behavior. To this aim, we carried out an analysis of the electronic structure of one slab of the three materials to analyze their differences and, consequently, to explain the singular properties of the gold junctions. The goal will be to check if there are surface levels that can efficiently interact with the t_{2g} molecular orbitals of the Co^{II} (or Fe^{II} complexes) through the π orbitals of $SeCN^-$ ligand in such way that the different α and β occupancies in these two metal complexes could induce a different magnetic polarization of the metal surface.

We highlight the main features of the Au(111) DFT band structure related to the problem of molecule surface mixing (Figure 6, PBE functional including spin−orbit effects, see Computational Details section): (i) The hybridization of the 6s and $6p_z$ levels (red and green lines, respectively, in Figure 6a, L band) shows the characteristic Rashba spin-dependent splitting due the SOC of the surface state of gold (see point A in Figure 6a). (ii) An sp band inversion at an energy larger than the Fermi level (point B) is observed in the Γ → M path. (iii) A second band crossing involving p and d orbitals appears close to the Fermi level at the M point (C in Figure 6a). The k-dependent band diagram (Figures 6b,c) also shows the L band splitting near Γ, and despite strong k-dependent spin polarization of the d- and p-type orbitals (blue and green lines, respectively in Figure 6a under −2 eV), there is a null net spin contribution along the whole Brillouin zone. Furthermore, point C presents a complex structure at the merging point of several bands with different spin polarization.

Considering that the orbitals responsible for the interaction between molecule and metal surface are the π orbitals of the

DOI: 10.1021/jacs.6b11166
J. Am. Chem. Soc. XXXX, XXX, XXX−XXX

axial $SeCN^-$ ligand, we must search for bands that can match this symmetry. We then performed spin-polarized calculations (without SOC coupling) of a 2 × 2 Au(111) supercell (see details of the choice of the unit cell in Supporting Information section 7). Under this perspective, the L band at Γ is not adequate for mixing, as it is composed by the hybridization of the 6s and $6p_z$ gold orbitals (see Figure S12), and will form a σ-bond with respect to the molecule. The L band at the M point (π/a, 0, 0) would offer a suitable orbital for mixing, as wave functions in neighbor atoms will present alternating signs of their wave function (a more detailed discussion of this surface orbitals is included in section S7). The participation of such surface orbitals is corroborated with the analysis of the main transmission eigenfunctions obtained with the ATK code[36] for the two transmission peaks corresponding to the two t_{2g} orbitals (d_{xz} and d_{yz}) of the Co^{II} complex close to the Fermi level (see Figure 4). In the case of the Co^{II} complex, the transport mechanism is mainly due to the transmission peak corresponding to the transmission eigenstate depicted in the right panel of Figure 7 (associated with the empty t_{2g} orbital), while that for Fe^{II}, with one fewer β electron, is in the left panel of Figure 7. Thus, a similar magnetoresistance behavior should be expected for these two complexes while, with the other studied transition metal atoms, the complexes do not have the appropriate electronic structure; only d^1 and d^2 complexes would be equivalent to the Fe^{II} and Co^{II} cases but with opposite spin carriers.

Analogous calculations to analyze the surface states were performed for Pt(111) and Cu(111) surfaces (see Figure 8). In the case of Cu, we observe a band structure resembling the gold case (see Figure 8), with a surface band related to valence $4s^1$ electron and sp band inversion in the Γ → M (π/a, 0, 0) path. As in the Au case, the d-based orbitals form a dense block of states that remain occupied along the Brillouin zone. This analogy is expected, as copper and gold belong to the same group of the periodic table and present the same valence configuration. We associate the lack of a magnetoresistance effect on Cu surfaces to the low atomic number of copper, which prevents the appearance of strong spin−orbit coupling effects in comparison to heavier elements, such as Au. Pt is just the opposite case: a heavy element with a different electronic configuration, as it has one fewer electron than gold. The Pt band structure shows the "surface band" associated with the 6s electron above the Fermi level (unoccupied orbital) in the complete Γ → M (π/a, 0, 0) path. In this way, the sp band inversion does not cross the Fermi energy, preventing the rich spin texture observed in Au from appearing.[43]

■ CONCLUSIONS

The present work provides the main ingredients to achieve large magnetoresistance at room temperature in a single-molecule device by exploiting metal complexes. The magnetic nature of the molecule is not the unique requirement to observe the magnetoresistance effect, and in fact, the specific electronic configuration plays a key role. In addition to the top ferromagnetic Ni electrode in the junction, the Au/molecule *spinterface* is an essential ingredient in the manifestation of the observed single-molecule magnetoresistance, as deduced from the study on the different metal surfaces, namely, Au, Cu, and Pt. The interplay of the surface potential and spin−orbit coupling at the metal surface is of utmost importance to create the magnetoresistance. The studied spin-dependent transport on single-molecule devices with the metal complex series $[M(tzpy)_2(NCSe)_2]$ (M = Mn, Co, and Ni) shows that the Co^{II} system is the only one presenting magnetoresistance effects in accord with the DFT+NEGF calculations that evidence Au/Co complex hybridized spin-polarized orbitals energetically close to the metal Fermi levels. Overall, these results demonstrate the crucial role of the spinterface[42,47] defined by the molecule (its electronic structure as spin filter) and the gold surface (spin texture triggered by spin−orbit effects) to provide a rational design of single-molecule spintronics.

■ EXPERIMENTAL METHODS

Sample Preparation. A Au(111) single crystal substrate (10 mm × 1 mm) of 99.9999% purity and orientation accuracy <0.1° (Mateck, Germany) was surface-functionalized with the $[M(tzpy)_2(NCSe)_2]$ complexes (M = Mn, Co, and Ni) (basic information on the synthesis and characterization can be found in Supporting Information section 1) by immersion in a micromolar ethanolic solution of the target compound for periods longer than 6 h. Pt (111) and Cu(111) single crystal substrates (10 mm × 1 mm), both of 99.999% purity and orientation accuracy <0.1° (Mateck, Germany), were surface-functionalized only with the $[Co(tzpy)_2(NCS)_2]$ complex by immersion in a micromolar ethanolic solution of the target compound for periods longer than 6 h (see section 1 for a more detailed preparation). All glassware and PTFE-STM cells were cleaned with piranha solution (3:1 H_2SO_4/H_2O_2 by volume) before usage, followed by rinsing with 18 MΩ cm^{-1} Milli-Q water (Millipore).

Conductance Measurements. An STM-BJ method was employed to build and characterize charge transport through single-molecule wires built with the different metal complexes studied in this work (Mn^{II}, Ni^{II}, and Co^{II}). The two biased electrodes of the molecular junction, a Au(111) single crystal (99.9999% Mateck, Germany) and a mechanically cut polycrystalline Ni wire (99.99%, Godfellow, UK), were used as the support and the STM top electrodes, respectively. In a regular STM-BJ experiment, the Ni tip was repeatedly driven onto the Au surface while the current flowing between them was simultaneously monitored. Several thousand (~5000) retraction curves were then stored and used to build the conductance histogram of the single-molecule device. Because not every curve displayed plateau features corresponding to the molecular quantum conductance of the single-molecule bridge, we designed an automatic algorithm that can identify and select curves containing such single-molecule features. The exact same selection criteria were applied throughout all measured series. To avoid the Ni wire oxidation under ambient conditions, the prepared Ni electrode was magnetically polarized and stored under anaerobic conditions before use, as we report in previous studies.[21] All experiments were conducted in an organic solvent (mesitylene) with very low oxygen and water solubility.

Technical Details of the Dynamic Break-Junction Experiments. Details about the STM-break-junction technique are published elsewhere.[30] All experiments were carried out with a homemade PTFE-STM cell and a PicoSPM II microscope head controlled using PicoScan 2500 electronics, all from Agilent. The STM head was mechanically and electronically isolated. Data was acquired using a NI-DAQmx/BNC-2110 National Instruments (LabVIEW data acquisition system) system and analyzed with our own LabVIEW code. In a typical break-junction experiment, the STM tip is first brought to a tunneling distance over a flat clean metallic surface area. The STM feedback is then turned off, and the tip is driven in and out of contact with the substrate at a speed of 1−2 V/s. This 2-point feedback loop is used to collect thousands of current decays (5000−6000) during the tip pulling cycles. In order to minimize possible mechanical disruption of the tip and sample surfaces, the reached maximum current in the 2-point feedback loop was set to a low value well below saturation, which prevented the STM tip crashing against the substrate electrode. 10−15% of the collected current decays display steps or plateaus, and are used to determine the single-molecule conductance using the expression $G = I_{step}/U_{bias}$ where G is the conductance, I the current, and U the potential difference between the tip and substrate

DOI: 10.1021/jacs.6b11166
J. Am. Chem. Soc. XXXX, XXX, XXX−XXX

electrodes. The current decays are accumulated to form linear conductance histograms. The observed peaks in the conductance histograms correspond to the observed plateaus in the current decays and provide averaged single-molecule conductance values. An automated selection process designed by own LabVIEW code was used to select the decays that showed plateaus from the ones that did not. The user defines the initial selection criteria that are fixed throughout all the experimental series.

Technical Details of the Static Blinking Experiments. The blinking captures (tens of curves) were accumulated into 2D maps during a total time of 6 h for each experiment.[34,48] No selection procedures were applied at this time, and so all blinking events are used to build the 2D histograms. In order to compare the lifetimes of the blinks in the 2D maps, all the samples were set into a common time origin and baseline. The final STM tip pulling after the blinking was performed by externally controlling the piezo Z-position (see Supporting Information section 5).

Computational Details. Electron transport calculations were carried out with the molecule sandwiched between five gold layers with a 4 × 3 surface unit cell using the ATK code[36,37] (version 2016.1) with the PBE functional,[49] a numerical single-ζ basis set, and an 11e$^-$ pseudopotential for the gold atoms,[50] while a double-ζ basis set with polarization was used for the other elements. The coherent transport properties were calculated using the nonequilibrium Green function procedure combined with the density functionl theory (DFT) calculations. NEVPT2 calculations with quasidegenerate perturbation theory to include spin−orbit effects[51] were employed to determine the zero-field splitting parameter D for the Co^{II} complex using Orca 3.0.3 code[52] and a def2-TZVPP basis set[53] with an active space considering the seven d electrons of Co^{II} center and the five d orbitals. Zero bias transmission curves were calculated using the Artaios 1.9 code,[54,55] while the Fock and Overlap matrices necessary for the transport calculations were obtained from unrestricted DFT calculations (B3LYP functional,[56] D95 V basis for H, C, and N, and LANL2DZ ECP basis set for heavier atoms[57−60]) by means of the Gaussian09 package.[61] Model systems were constructed from previously optimized molecules, setting the Se ends with Se−Au distances of 2.5 Å (hollow position). Each electrode consisted of 19 gold atoms. Slab calculations including spin−orbit coupling for the Au(111), Cu(111), and Pt(111) surfaces were performed using the green code[62] and its interface to the SIESTA package.[38] The PBE functional[49] was employed, and all atoms were described by a double-ζ basis set with polarization. Bulk cell parameters were used to build the slabs, without further geometry relaxation. Cell parameters for 1 × 1 surfaces were the following: (2.8837, 0.0) Å and (−1.4419, 2.4974) Å for Au(111), (2.5562, 0.0) and (−1.2781, 2.2137) for Cu(111), and (2.7744, 0.0) and (−1.3872, 2.4027) for Pt(111).

■ ASSOCIATED CONTENT

Supporting Information

The Supporting Information is available free of charge on the ACS Publications website at DOI: 10.1021/jacs.6b11166.

Chemical compound information, sample preparation information, and computational details (PDF)

Crystallographic details (CIF)

■ AUTHOR INFORMATION

Corresponding Authors

*ismadiezperez@gmail.com

*eliseo.ruiz@qi.ub.es

ORCID

Daniel Aravena: 0000-0003-3140-4852

Eliseo Ruiz: 0000-0001-9097-8499

Notes

The authors declare no competing financial interest.

■ ACKNOWLEDGMENTS

The research reported here was supported by the Spanish Ministerio de Economía y Competitividad (MINECO) (Grants CTQ2015-64579-C3-1-P, CTQ2015-64579-C3-3-P, CTQ2013-46275-P, CTQ2015-71406-ERC, and CTQ2016-78341-P, and Unidad de Excelencia María de Maeztu MDM-2015-0538) and Generalitat Valenciana (GVPROMETEO/2016/147). E.R. thanks Generalitat de Catalunya for an ICREA Academia award. F.J.V.-M. thanks the Spanish MINECO for a graduate FPI fellowship. I. D.-P. thanks the Ramon y Cajal program (MINECO) for financial support. D.A. thanks CONICYT + PAI "Concurso nacional de apoyo al retorno de investigadores/as desde el extranjero, convocatoria 2014 82140014" for financial support. D.A. thanks Centers of Excellence with Basal/CONICYT financing, Grant FB0807, CEDENNA. Powered@NLHPC: This research was partially supported by the supercomputing infrastructure of the NLHPC (ECM-02). The authors acknowledge the general facilities of the University of Barcelona (CCiT-UB) and the computer resources, technical expertise, and assistance provided by the Barcelona Supercomputing Centre.

■ REFERENCES

(1) Sinova, J.; Valenzuela, S. O.; Wunderlich, J.; Back, C. H.; Jungwirth, T. *Rev. Mod. Phys.* **2015**, *87*, 1213−1260.

(2) Hirohata, A.; Takanashi, K. *J. Phys. D: Appl. Phys.* **2014**, *47*, 193001.

(3) Fusil, S.; Garcia, V.; Barthelemy, A.; Bibes, M. Magnetoelectric Devices for Spintronics. In *Annual Review of Materials Research*; Clarke, D. R., Ed.; Annual Reviews: Palo Alto, CA, 2014; Vol. 44, pp 91−116.

(4) Sanvito, S. *Chem. Soc. Rev.* **2011**, *40*, 3336−3355.

(5) Bogani, L.; Wernsdorfer, W. *Nat. Mater.* **2008**, *7*, 179−186.

(6) Mannini, M.; Pineider, F.; Sainctavit, P.; Danieli, C.; Otero, E.; Sciancalepore, C.; Talarico, A. M.; Arrio, M.-A.; Cornia, A.; Gatteschi, D.; Sessoli, R. *Nat. Mater.* **2009**, *8*, 194−197.

(7) Urdampilleta, M.; Klyatskaya, S.; Cleuziou, J. P.; Ruben, M.; Wernsdorfer, W. *Nat. Mater.* **2011**, *10*, 502−506.

(8) Vincent, R.; Klyatskaya, S.; Ruben, M.; Wernsdorfer, W.; Balestro, F. *Nature* **2012**, *488*, 357−360.

(9) Ganzhorn, M.; Klyatskaya, S.; Ruben, M.; Wernsdorfer, W. *Nat. Nanotechnol.* **2013**, *8*, 165−169.

(10) Bagrets, A.; Schmaus, S.; Jaafar, A.; Kramczynski, D.; Yamada, T. K.; Alouani, M.; Wulfhekel, W.; Evers, F. *Nano Lett.* **2012**, *12*, 5131−5136.

(11) Schmaus, S.; Bagrets, A.; Nahas, Y.; Yamada, T. K.; Bork, A.; Bowen, M.; Beauerepaire, E.; Evers, F.; Wulfhekel, W. *Nat. Nanotechnol.* **2011**, *6*, 185−189.

(12) Xie, Z.; Markus, T. Z.; Cohen, S. R.; Vager, Z.; Gutierrez, R.; Naaman, R. *Nano Lett.* **2011**, *11*, 4652−4655.

(13) Naaman, R.; Waldeck, D. H., Spintronics and Chirality: Spin Selectivity in Electron Transport Through Chiral Molecules. In *Annual Review of Physical Chemistry*; Johnson, M. A., Martinez, T. J., Eds.; Annual Reviews: Palo Alto, CA, 2015; Vol. 66, pp 263−281.

(14) Yeganeh, S.; Ratner, M. A.; Medina, E.; Mujica, V. *J. Chem. Phys.* **2009**, *131*, 014707.

(15) Göhler, B.; Hamelbeck, V.; Markus, T. Z.; Kettner, M.; Hanne, G. F.; Vager, Z.; Naaman, R.; Zacharias, H. *Science* **2011**, *331*, 894−897.

(16) Carmeli, I.; Leitus, G.; Naaman, R.; Reich, S.; Vager, Z. *J. Chem. Phys.* **2003**, *118*, 10372−10375.

(17) Vager, Z.; Naaman, R. *Chem. Phys.* **2002**, *281*, 305−309.

(18) Michaeli, K.; Kantor-Uriel, N.; Naaman, R.; Waldeck, D. H. *Chem. Soc. Rev.* **2016**, *45*, 6478−6487.

(19) Mondal, P. C.; Fontanesi, C.; Waldeck, D. H.; Naaman, R. *Acc. Chem. Res.* **2016**, *49*, 2560−2568.

DOI: 10.1021/jacs.6b11166
J. Am. Chem. Soc. XXXX, XXX, XXX−XXX

(20) Aragonès, A. C.; Medina, E.; Ferrer-Huerta, M.; Gimeno, N.; Teixidó, M.; Palma, J. L.; Tao, N.; Ugalde, J. M.; Giralt, E.; Díez-Pérez, I.; Mujica, V. *Small* **2017**, *13*, 1602519.
(21) Aragonès, A. C.; Aravena, D.; Cerdá, J. I.; Acís-Castillo, Z.; Li, H.; Real, J. A.; Sanz, F.; Hihath, J.; Ruiz, E.; Díez-Pérez, I. *Nano Lett.* **2016**, *16*, 218−226.
(22) Aravena, D.; Ruiz, E. *J. Am. Chem. Soc.* **2012**, *134*, 777−779.
(23) Baadji, N.; Sanvito, S. *Phys. Rev. Lett.* **2012**, *108*, 217201.
(24) Bychkov, Y. A.; Rashba, E. I. *J. Phys. C: Solid State Phys.* **1984**, *17*, 6039−6045.
(25) Koga, T.; Nitta, J.; Takayanagi, H.; Datta, S. *Phys. Rev. Lett.* **2002**, *88*, 126201.
(26) Ting, D. Z. Y.; Cartoixa, X. *Appl. Phys. Lett.* **2002**, *81*, 4198−4200.
(27) Bercioux, D.; Lucignano, P. *Rep. Prog. Phys.* **2015**, *78*, 106001.
(28) Xu, B.; Tao, N. J. *Science* **2003**, *301*, 1221−1223.
(29) Hybertsen, M. S.; Venkataraman, L. *Acc. Chem. Res.* **2016**, *49*, 452−460.
(30) Xia, J. L.; Diez-Perez, I.; Tao, N. J. *Nano Lett.* **2008**, *8*, 1960−1964.
(31) Chen, F.; Li, X.; Hihath, J.; Huang, Z.; Tao, N. *J. Am. Chem. Soc.* **2006**, *128*, 15874−15881.
(32) Osorio, H. M.; Catarelli, S.; Cea, P.; Gluyas, J. B. G.; Hartl, F.; Higgins, S. J.; Leary, E.; Low, P. J.; Martín, S.; Nichols, R. J.; Tory, J.; Ulstrup, J.; Vezzoli, A.; Milan, D. C.; Zeng, Q. *J. Am. Chem. Soc.* **2015**, *137*, 14319−14328.
(33) Vardimon, R.; Klionsky, M.; Tal, O. *Nano Lett.* **2015**, *15*, 3894−3898.
(34) Aragonès, A. C.; Haworth, N. L.; Ciampi, S.; Bloomfield, N. J.; Wallace, G. G.; Coote, M. L.; Diez-Perez, I.; Darwish, N. *Nature* **2016**, *531*, 88−91.
(35) Haiss, W.; Wang, C.; Grace, I.; Batsanov, A. S.; Schiffrin, D. J.; Higgins, S. J.; Bryce, M. R.; Lambert, C. J.; Nichols, R. J. *Nat. Mater.* **2006**, *5*, 995−1002.
(36) QuantumWise A/S. *Atomistix ToolKit version 2014.2*; Copenhagen, Denmark, 2014.
(37) Brandbyge, M.; Mozos, J. L.; Ordejon, P.; Taylor, J.; Stokbro, K. *Phys. Rev. B: Condens. Matter Mater. Phys.* **2002**, *65*, 165401.
(38) Soler, J. M.; Artacho, E.; Gale, J. D.; Garcia, A.; Junquera, J.; Ordejon, P.; Sanchez-Portal, D. *J. Phys.: Condens. Matter* **2002**, *14*, 2745−2779.
(39) Johnson, M. *Handbook of Spin Transport and Magnetism*; Chapman and Hall/CRC, 2011.
(40) Gueddida, S.; Gruber, M.; Miyamachi, T.; Beaurepaire, E.; Wulfhekel, W.; Alouani, M. *J. Phys. Chem. Lett.* **2016**, *7*, 900−904.
(41) Galbiati, M.; Tatay, S.; Barraud, C.; Dediu, A. V.; Petroff, F.; Mattana, R.; Seneor, P. *MRS Bull.* **2014**, *39*, 602−607.
(42) Sanvito, S. *Nat. Phys.* **2010**, *6*, 562−564.
(43) Yan, B.; Stadtmuller, B.; Haag, N.; Jakobs, S.; Seidel, J.; Jungkenn, D.; Mathias, S.; Cinchetti, M.; Aeschlimann, M.; Felser, C. *Nat. Commun.* **2015**, *6*, 10167.
(44) Gomez-Coca, S.; Cremades, E.; Aliaga-Alcalde, N.; Ruiz, E. *J. Am. Chem. Soc.* **2013**, *135*, 7010−7018.
(45) Gomez-Coca, S.; Aravena, D.; Morales, R.; Ruiz, E. *Coord. Chem. Rev.* **2015**, *289*, 379−392.
(46) Gomez-Coca, S.; Urtizberea, A.; Cremades, E.; Alonso, P. J.; Camon, A.; Ruiz, E.; Luis, F. *Nat. Commun.* **2014**, *5*, 4300.
(47) Barraud, C.; Seneor, P.; Mattana, R.; Fusil, S.; Bouzehouane, K.; Deranlot, C.; Graziosi, P.; Hueso, L.; Bergenti, I.; Dediu, V.; Petroff, F.; Fert, A. *Nat. Phys.* **2010**, *6*, 615−620.
(48) Haiss, W.; Nichols, R. J.; van Zalinge, H.; Higgins, S. J.; Bethell, D.; Schiffrin, D. J. *Phys. Chem. Chem. Phys.* **2004**, *6*, 4330−4337.
(49) Perdew, J. P.; Burke, K.; Ernzerhof, M. *Phys. Rev. Lett.* **1996**, *77*, 3865−3868.
(50) Toher, C.; Sanvito, S. *Phys. Rev. B: Condens. Matter Mater. Phys.* **2008**, *77*, 155402.
(51) Atanasov, M.; Aravena, D.; Suturina, E.; Bill, E.; Maganas, D.; Neese, F. *Coord. Chem. Rev.* **2015**, *289*, 177−214.
(52) Neese, F. *Wiley Interdiscip. Rev. Comput. Mol. Sci.* **2012**, *2*, 73−78.
(53) Weigend, F.; Ahlrichs, R. *Phys. Chem. Chem. Phys.* **2005**, *7*, 3297−3305.
(54) Herrmann, C.; Groß, L.; Steenbock, T.; Solomon, G. C. *Artaios—A Code for Postprocessing Electronic Structure Calculations, 1.9*; 2015.
(55) Herrmann, C.; Solomon, G. C.; Ratner, M. A. *J. Phys. Chem. C* **2010**, *114*, 20813−20820.
(56) Becke, A. D. *J. Chem. Phys.* **1993**, *98*, 5648−5652.
(57) Dunning, T. H. J.; Hay, P. J. Gaussian basis sets for molecular calculations. In *Modern Theoretical Chemistry*; Schaefer, H. F., III, Ed.; Plenum: New York, 1977; pp 1−28.
(58) Hay, P. J.; Wadt, W. R. *J. Chem. Phys.* **1985**, *82*, 270−283.
(59) Hay, P. J.; Wadt, W. R. *J. Chem. Phys.* **1985**, *82*, 299−310.
(60) Wadt, W. R.; Hay, P. J. *J. Chem. Phys.* **1985**, *82*, 284−298.
(61) Frisch, M. J.; Trucks, G. W.; Schlegel, H. B.; Scuseria, G. E.; Robb, M. A.; Cheeseman, J. R.; Scalmani, G.; Barone, V.; Mennucci, B.; Petersson, G. A.; Nakatsuji, H.; Caricato, M.; Li, X.; Hratchian, H. P.; Izmaylov, A. F.; Bloino, J.; Zheng, G.; Sonnenberg, J. L.; Hada, M.; Ehara, M.; Toyota, K.; Fukuda, R.; Hasegawa, J.; Ishida, M.; Nakajima, T.; Honda, Y.; Kitao, O.; Nakai, H.; Vreven, T.; Montgomery, J.; Peralta, J. E.; Ogliaro, F.; Bearpark, M.; Heyd, J. J.; Brothers, E.; Kudin, K. N.; Staroverov, V. N.; Kobayashi, R.; Normand, J.; Raghavachari, K.; Rendell, A.; Burant, J. C.; Iyengar, S. S.; Tomasi, J.; Cossi, M.; Rega, N.; Millam, N. J.; Klene, M.; Knox, J. E.; Cross, J. B.; Bakken, V.; Adamo, C.; Jaramillo, J.; Gomperts, R.; Stratmann, R. E.; Yazyev, O.; Austin, A. J.; Cammi, R.; Pomelli, C.; Ochterski, J. W.; Martin, R. L.; Morokuma, K.; Zakrzewski, V. G.; Voth, G. A.; Salvador, P.; Dannenberg, J. J.; Dapprich, S.; Daniels, A. D.; Farkas, Ö.; Foresman, J. B.; Ortiz, J. V.; Cioslowski, J.; Fox, D. J. *Gaussian 09 (Revision D.01)*; Wallingford, CT, 2009.
(62) Cerdá, J.; Van Hove, M. A.; Sautet, P.; Salmeron, M. *Phys. Rev. B: Condens. Matter Mater. Phys.* **1997**, *56*, 15885−15899.

DOI: 10.1021/jacs.6b11166
J. Am. Chem. Soc. XXXX, XXX, XXX−XXX

Supporting Information

Metal-Controlled Magnetoresistance at Room Temperature in Single-Molecule Devices

Albert C. Aragonès,[†,§,‡] Daniel Aravena,[#,¥] Francisco J. Valverde-Muñoz,[⊥] José Antonio Real,[⊥] Fausto Sanz,[†,§], Ismael Díez-Pérez[†,§,‡*], Eliseo Ruiz,[◊,‡*]

[†] Departament de Ciència de Materials i Química Física, Universitat de Barcelona, Martí i Franquès 1 and Institut de Bioenginyeria de Catalunya (IBEC) Baldiri Reixac 15-21, Barcelona 08028 Spain

[§] Centro Investigación Biomédica en Red (CIBER-BBN). Campus Río Ebro-Edificio I+D, Poeta Mariano Esquillor s/n, 50018 Zaragoza, Spain.

[#] Departamento de Química de los Materiales, Facultad de Química y Biología, Universidad de Santiago de Chile (USACH), Casilla 40, Correo 33, Chile

[¥] Centro Para El Desarrollo de Nanociencias y Nanotecnología, CEDENNA, Santiago, Chile

[⊥] Institut de Ciència Molecular (ICMol), Universitat de València, 46980 Paterna, València, Spain

[◊] Departament de Química Inorgànica i Orgànica, Diagonal 645, 08028 Barcelona, Spain

[‡] Institut de Química Teòrica i Computacional, Universitat de Barcelona, Diagonal 645, 08028 Barcelona, Spain

1. Platinum and Copper surface characterization

Pt(111) surface was annealed with a H_2 flame to orientate the surface and eliminate possible residual contamination, and then was cooled down under a stream of $Ar+H_2$.[1–3] The surfaces were immediately immersed in an argon-purged μM ethanolic solution of the target compound for periods longer than 6 h under argon atmosphere.

Figure S1 left corresponds to a large topographical view of a freshly prepared Pt(111) surface taken by Atomic Force Microscope (AFM). The surface displays a very low roughness (RMS values of few nm) and atomically flat terraces as wide as 1 micron in length. In a single-molecule junction experiment, the tip is typically brought to a flat terrace where the single-molecule electrical contact is established.

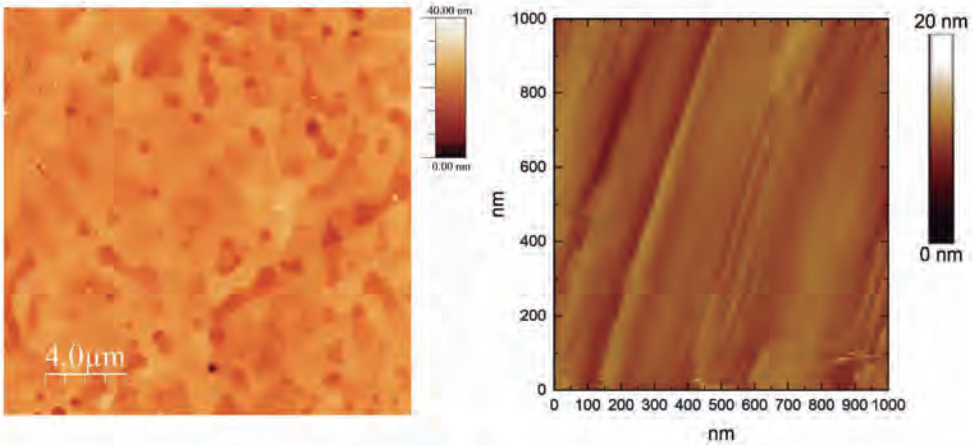

Figure S1. (left) A 20x20 μm^2 AFM image taking in tapping mode of a freshly prepared Pt(111) surface. (right) STM image of a Cu(111) surface in mesitylene using a freshly cut Ni tip. The image was recorded at 5nA set point current and 500 mV bias.

Cu(111) surface was electropolished to eliminate possible residual contamination in 75% orthophosphoric acid solution for 3 min at 1.80 V vs a Cu counter. Then the surface was washed with argon-purged 18 $M\Omega\ cm^{-1}$ Milli-Q water (Millipore) and a reductive treatment was applied under electrochemical control during 1.5 hours at -1.2 V (vs Ag/AgCl) in absolute EtOH. Finally, the Cu substrate was washed again with argon-purged Milli-Q water and immediately immersed in a μM argon-purged ethanolic solution of the target compound for periods of 12h under argon atmosphere.

In Fig S1 right the showed STM image surface displays atomically flat terraces where the single-molecule electrical contact is established.

2. Single-Molecule STM experiments of Co^{II} complex at lower conductance ranges

The used single-molecule experimental setup like many other similar STM-based instruments[4,5] is based on linear current amplification. The employed current amplifiers present a practical current wide of ca. 2 orders of magnitude. For this reason, in order to cover a substantial wide conductance range, the measurements were repeated under the same experimental conditions but using different amplifications and bias voltages. In Figure S2 are shown these control experiments presenting no current signatures for the $[Co(tzpy)_2(NCSe)_2]$ for the α-up polarized Ni electrode, performed at different amplifications covering a total conductance range from 10^{-3} G_0 to our detection limit of 10^{-6} G_0.

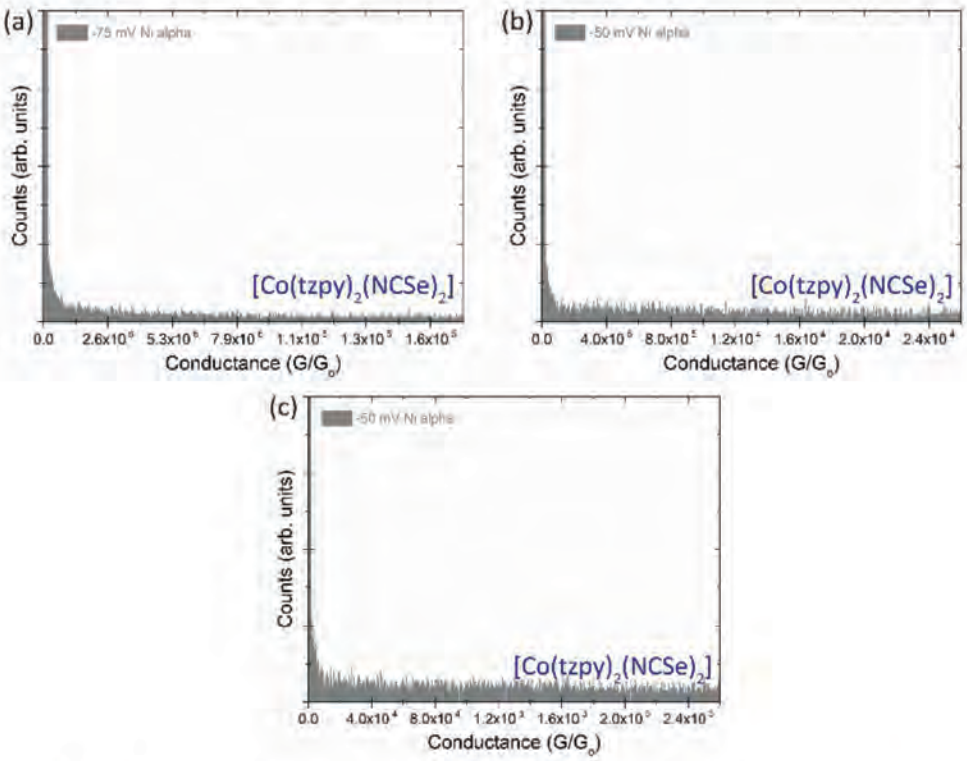

Figure S2. Single-molecule conductance histogram for the metal complex $[Co(tzpy)_2(NCSe)_2]$ bridging between Au and α-up magnetically polarized Ni electrode. The three histograms differ on the amplification used (a) 0.01nA/V, (b) 0.1nA/V and (c) 1nA/V. The applied bias was set to -75 mV in (c) and -50 mV in (b) and (c) as indicated in the figure.

3. Dynamic STM break-junctions of Co^{II} on a Cu surface

The suppression of the observed magnetoresistance effect presented by the $[Co(tzpy)_2(NCSe)_2]$ single-molecule wire built on Cu substrates (Figure 3 of the main text) was also confirmed using the STM break-junction approach (see Fig S3).

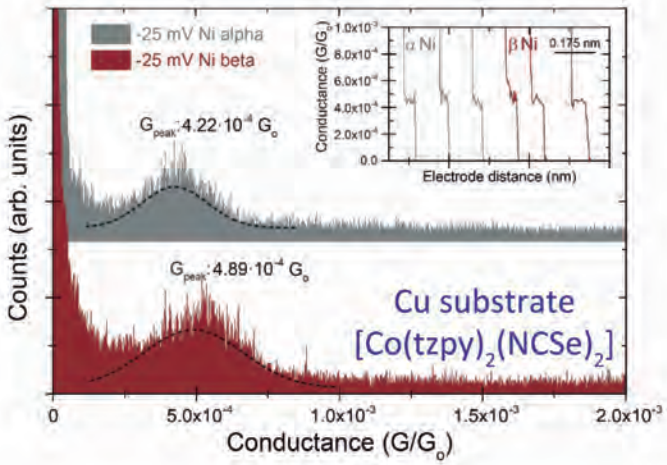

Fig S3. Conductance histograms for the $[Co(tzpy)_2(NCSe)_2]$ complex using a Cu substrate instead of Au and both α-up polarized (gray) and β-down polarized (maroon) Ni tip electrodes. The two histograms have been vertically offset. All conductance values have been extracted from Gaussian fits of the peaks. Insets show representative individual current versus pulling traces for the α-up polarized (left) and the β-down polarized (right) Ni electrodes used to build the conductance histograms. The applied bias was set to -25 mV as indicated in the figure legends.

The general procedure to analyze the experimental STM data assumes a Gaussian distribution of the tunneling current flowing from a tip as a pointlike electron source[6-8] the captured current histograms were studied using a Gaussian fitting. This fitting was employed to determine the most probably molecular conductances for the measured systems. The Gaussian fits were performed without any kind of background subtraction,[9] using the background as a baseline. The most probable conductance obtained by the peaks maximum of the Gaussian fitting match with the qualitative assigned current major counts maximum,[9] which can be obtained without any fitting.[10]

4. Single-Molecule STM measurements with positive bias

The following conductance histograms correspond to the $(Mn(tzpy)_2(NCSe)_2]$, $[Co(tzpy)_2(NCSe)_2]$, $[Ni(tzpy)_2(NCSe)_2$ complexes on Au surfaces and $[Co(tzpy)_2(NCSe)_2]$ complex using a Cu substrate instead of Au, all of them under a positive bias voltage (injection of the electrons from the Ni tip electrode). For negative biases see Fig. 2 in the main text.

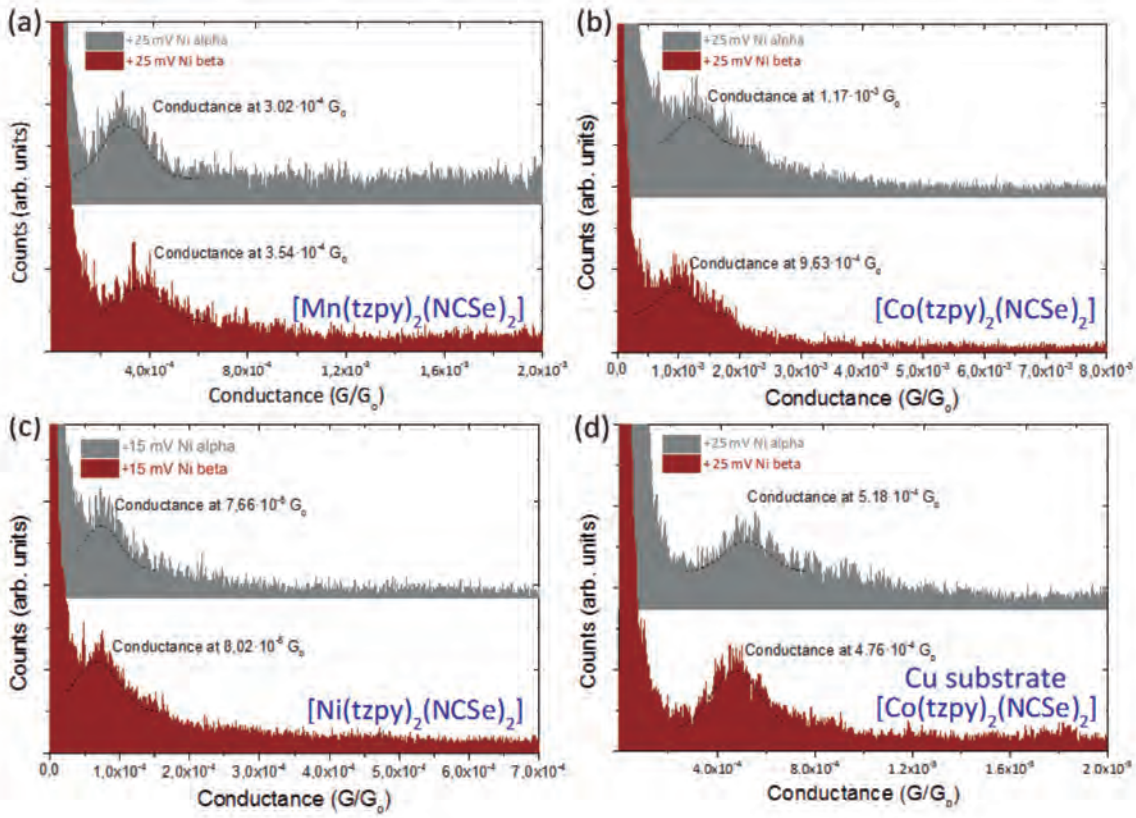

Figure S4. Single-molecule conductance histogram for the metal complexes: (a) S=5/2 $[Mn(tzpy)_2(NCSe)_2]$, (b) S=3/2 $[Co(tzpy)_2(NCSe)_2]$, (c) S=1 $[Ni(tzpy)_2(NCSe)_2]$ and (d) $[Co(tzpy)_2(NCSe)_2]$ using a Cu substrate instead of Au, bridging between Au and both α-up polarized (gray) and β-down (maroon) magnetically polarized Ni electrodes. The two histograms of all the panels have been vertically offset for clarity. All conductance values have been extracted from Gaussian fits of the peaks. The applied bias was set to +15 mV in (c) and +25 mV in (a), (b) and (d) as indicated in the figure.

5. Pulling STM experiments

In order to univocally ascertain the establishment of a single-molecule connection between the two electrodes in the captured *blinking* traces, we concatenate a pulling stage at the end of the blinking event and look for molecular breakdown features that identify the molecular bridge was effectively formed. Figure S5a-c shows pulling traces for single-molecule junctions established between the Ni STM tip electrode and either the Au, Pt or Cu substrates, respectively. The inset Figures show the actual *blinking* event followed by the pulling process (shadowed area) where the Ni tip electrode is retracted few nanometers away from the surface resulting in the molecular junction breakdown. In all studied cases, the pulling curves (Fig. S5a-c) showed a small plateau that survives more than an Å of the pulling stage, followed by a sudden drop of the current, which indicates the moment the molecular junction finally breaks.[11,12] When the STM junction does not contain a molecular bridge, a fast exponential decay starting at zero is observed in the pulling curve (Fig. S5d).

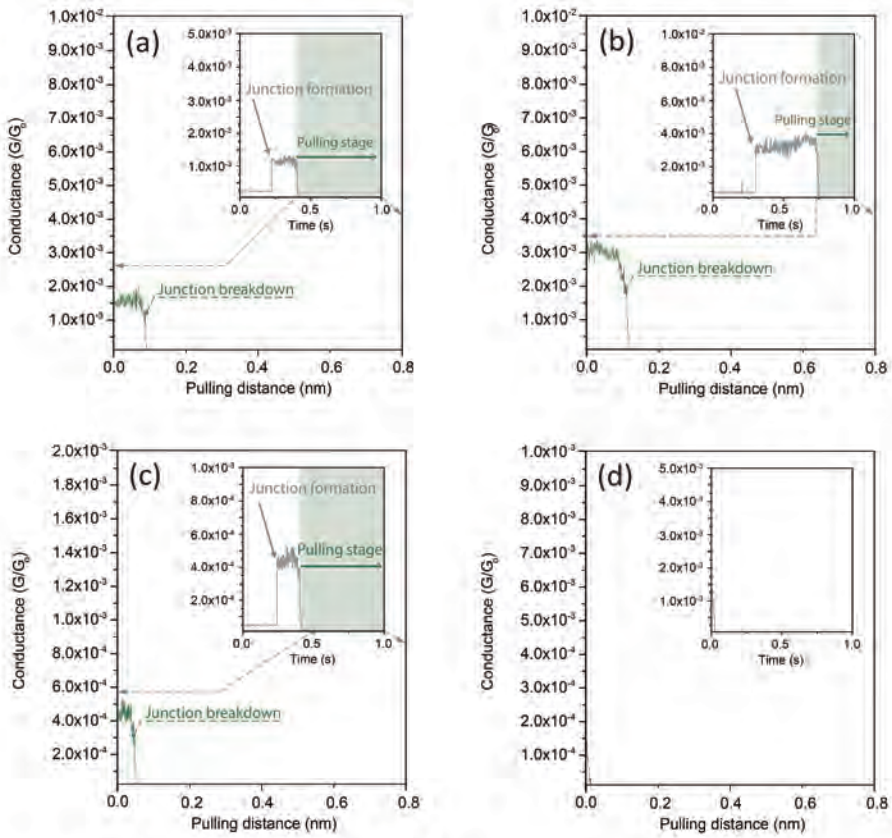

Figure S5. Pulling curves taking during a *blinking* process in the static single-molecule junction approach (see also main manuscript) built between the Ni STM tip electrode and

either Au (a), Pt (b) and Cu (c). A pulling curve in the absence of a molecular bridge ins shown in (d). The applied bias was set to -10 mV.

6. Transition metal complexes synthesis and characterization

6.1 Synthesis of the metal complexes

Synthesis of [M(tzpy)$_2$(NCSe)$_2$] (M = Ni^{II}, Co^{II}): The synthetic procedure for the Ni^{II} and Co^{II} derivatives was carried out using H-type vessels (total volume 30 mL). $MSO_4 \cdot nH_2O$ (0.125 mmol, 35.5 mg [n = 6 (Ni^{II})], 35.8 mg [n = 7 (Co^{II})] and KNCSe (36.7 mg, 0.25 mmol) were mixed in the solid state and placed at the bottom of one side of the H-type vessel while the opposite side contained the ligand tzpy (50 mg, 0.25 mg). The H-type tube was carefully filled with MeOH and sealed to avoid evaporation. Crystalline sample of [M(tzpy)$_2$(NCSe)$_2$] (M = Ni^{II}, Co^{II}) were obtained in three weeks. Yield ca. 70%

Synthesis of [Mn(tzpy)$_2$(NCSe)$_2$]: The synthetic procedure was modified due to the larger solubility of the Mn^{II} derivative. It was obtained by liquid-liquid diffusion technique (layering). A solution of $MnSO_4 \cdot 4H_2O$ [35.5 mg (0.21 mmol)] in 3 mL of H_2O was poured into a test tube (bottom layer). Then, a 1:1 mixture of H_2O:MeOH (30 mL) was slowly added (middle layer). Finally, a 1:1 mixture containing KNCSe (60.6 mg, 0.42 mmol) and tzpy (82.4 mg, 0.42 mmol) in MeOH (3 mL) was added (top layer). Crystalline samples of the title compound were obtained in 3 weeks.

Elemental Analysis: **[Mn(tzpy)$_2$(NCSe)$_2$]**: Calculated (%): C, 43.85; H, 2.45; N, 21.31. Found: C, 43.17; H, 2.23; N, 20.78; **[Co(tzpy)$_2$(NCSe)$_2$]**: Calculated (%): C, 43.59; H, 2.44; N, 21.18. Found: C, 43.38; H, 2.31; N, 20.81; **[Ni(tzpy)$_2$(NCSe)$_2$]**: Calculated (%): C, 43.61; H, 2.44; N, 21.19. Found: C, 43.29; H, 2.39; N, 20.76

6.2 IR spectra of the paramagnetic compounds

A single strong stretching C-N mode centered at 2060 cm^{-1} (Mn), 2070 cm^{-1} (Co) and 2090 cm^{-1} (Ni) suggests the coordination of the NCSe- groups in *trans* configuration. Characteristic aromatic bands appear within the 3120-3040 cm^{-1} range. Very complex spectra appear within the 1500-400 cm^{-1} range, but it is possible to distinguish the characteristic C=C and C=N stretching modes of the aromatic rings in the 1600-1500 cm^{-1} range.

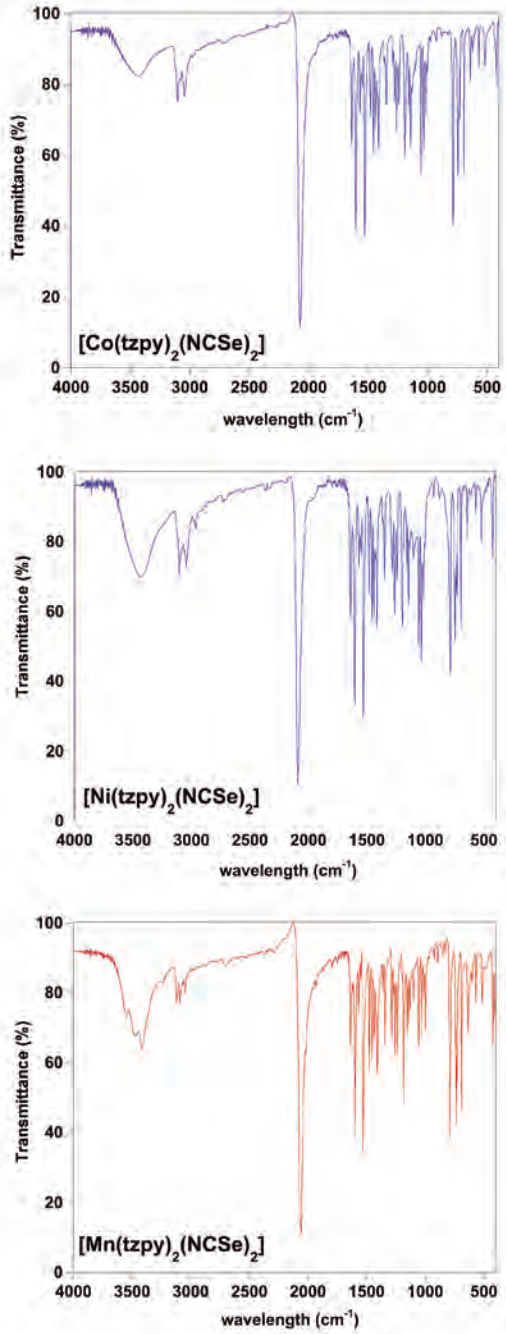

Figure S6. IR spectra of $[M(tzpy)_2(NCSe)_2]$ M= Co, Ni, and Mn.

6.3 Magnetic characterization of the single-molecule magnet behavior of [Co(tzpy)$_2$(NCSe)$_2$]

The Co^{II} complex shows dependence of the imaginary part of the susceptibility with the frequency (Fig. S8 right) and consequently is a mononuclear SMM.

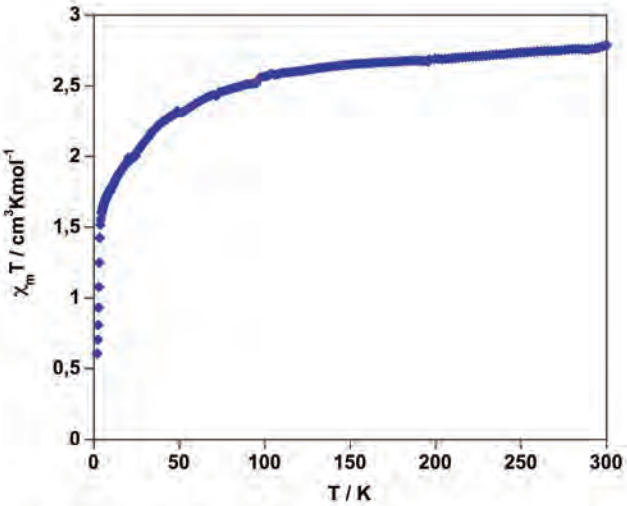

Figure S7. χT vs. temperature data for the [Co(tzpy)$_2$(NCSe)$_2$].

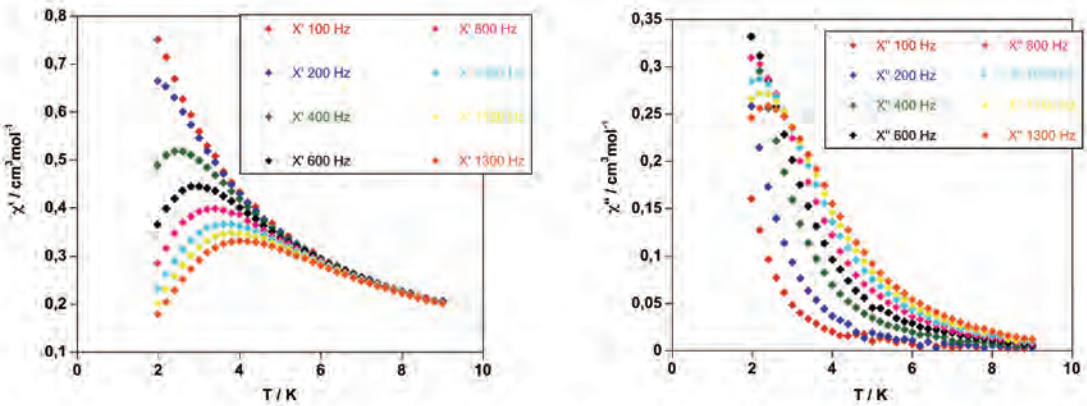

Figure S8. Real (left) and imaginary (right) contributions of the magnetic susceptibility vs. temperature data extracted from AC SQUID measurements for the [Co(tzpy)$_2$(NCSe)$_2$].

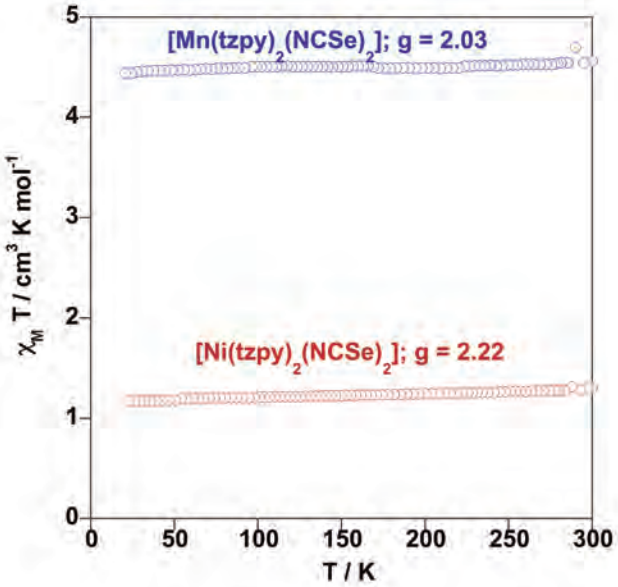

Figure S9. χT vs. temperature data for the $[Mn(tzpy)_2(NCSe)_2]$ and $[Nitzpy)_2(NCSe)_2]$ complexes.

6.4 Structural characterization of the [M(tzpy)$_2$(NCSe)$_2$] compounds

Single crystal X-ray diffraction has been carried out with success for [Co(tzpy)$_2$(NCSe)$_2$]. This compound crystallizes in the triclinic P-1 space group and is isostructural with the homologous [Fe(tzpy)$_2$(NCSe)$_2$].[13] Tables S1 and S2 gather relevant crystallographic data and bond length and angles, respectively. Figure S10 displays an ORTEP representation of the molecule with thermal ellipsoids at 50% probability level together with the atom numbering of the asymmetric unit. The Co^{II} ion lies on an inversion center generating a slightly distorted [CoN_6] octahedral site with slightly compressed axial positions occupied by the N atom of the $NCSe^-$ groups [Co-N(5) = 2.097(3) Å]. The equatorial positions of the octahedron are occupied by the N atoms of the tzpy ligands [Co-N(1) = 2.144(3) Å and Co-N(2) = 2.121(2) Å]. The two equatorial tzpy ligands are essentially coplanar, and the Fe-N(5) bonds belonging to the *trans* $NCSe^-$ groups are practically perpendicular to the equatorial plane (the separation of 90° degrees of the N(5)-Co-N(1) and N(5)-Co-N(2) angles is -3.49(10)° and 0.58(10)°, respectively. The selenocyanate groups are practically linear, they separate 1.6(3)° from 180°. A13.2° off-axis tilt of the Co-N(5)-C(12)-Se bond system is also observed.

Very thin needles of the homologous [Ni(tzpy)$_2$(NCSe)$_2$] complex were obtained. However, no full crystallographic analysis could be accomplished due to the quality of the crystals. We have tentatively assigned to these crystals the *Cmca* orthorhombic space group with a = 11.9055(12) Å, b = 30.623(3) Å, c = 13.6744(11) Å and V = 4985.4(8) Å^3. The fact that this volume is ca 8 times larger than that of the Co and Fe derivatives, may indicate that the analyzed crystals were twinned. Although great disorder was observed in the tzpy ligands the approximate solutions clearly shows them occupying the equatorial plane while the selenocyanate groups are coordinated in *trans* configuration.

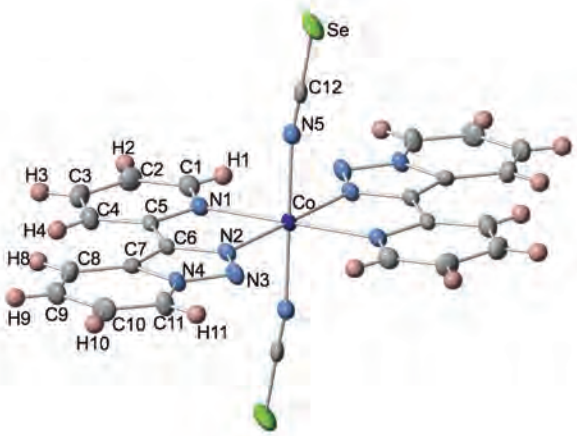

Figure S10. ORTEP representation of the $[Co(tzpy)_2(NCSe)_2]$ and atom numbering of the asymmetric unit.

Table S1. Crystal data of $[Co(tzpy)_2(NCSe)_2]$

Empirical formula	$C_{24}H_{16}N_{10}Se_2Co$
Mr	661.32
Crystal system	triclinic
Space group	*P*-1
a (Å)	8.0891(5)
b (Å)	8.6468(8)
c (Å)	9.3489(6)
α (Å)	81.292(7)
β (Å)	72.583(6)
γ (Å)	76.509(7)
V (Å^3)	604.36(9)
Z	1
D_c (mg cm^{-3})	1.817
F(000)	325
μ (Mo-K$_\alpha$)(mm^{-1})	3.758
Crystal size (mm)	0.04 x 0.06 x 0.06
Temperature (K)	120(1)
No. of total reflections	3026
No. of reflections [$I>2\sigma(I)$]	2368
R_1 [$I>2\sigma(I)$]	0.0401
wR [$I>2\sigma(I)$]	0.0879
S	0.871

$R_1 = \Sigma\ ||F_o| - |F_c|| \ / \ \Sigma\ |F_o|$; $wR = [\ \Sigma\ [w(F_o^2 - F_c^2)^2] \ / \ \Sigma\ [w(F_o^2)^2]]^{1/2}$.

$w = 1/\ [\sigma^2(F_o^2) + (m\ P)^2 + n\ P]$ where $P = (F_o^2 + 2F_c^2) \ / \ 3$; m = 0.0501; n = 0.8943

Table S2. Selected bond lengths (Å) and angles(°) of $[Co(tzpy)_2(NCSe)_2]$

Co-N(1)	2.144(3)
Co-N(2)	2.121(2)
Co-N(5)	2.097(3)
Se-C(12)	1.792(3)
N(1)-Co-N(2)	77.14(10)
N(1)-Co-N(5)	86.51(10)
N(2)-Co-N(5)	90.58(10)
N(5)-C(12)-Se	178.4(3)

7. Electronic Structure calculations

To interpret the topology of the surface states present in point C, we aimed to obtain real orbitals for these levels. In this way, we performed spin polarized calculations (without SOC coupling) of a 2x2 Au(111) supercell to fold the band structure and get rid of the imaginary part for the orbitals at C. we repeated the former calculation with a thinner slab (just 3 layers). In this way, we avoid analyzing a large number of orbitals belonging to inner layers, focusing on the relevant surface states. The price to pay is including a spurious interaction between top and bottom layers, which introduces artificial splittings in the band diagram. Despite the latter, we can observe that the general structure of the band diagram is maintained in the smaller calculation (see Figure S11).

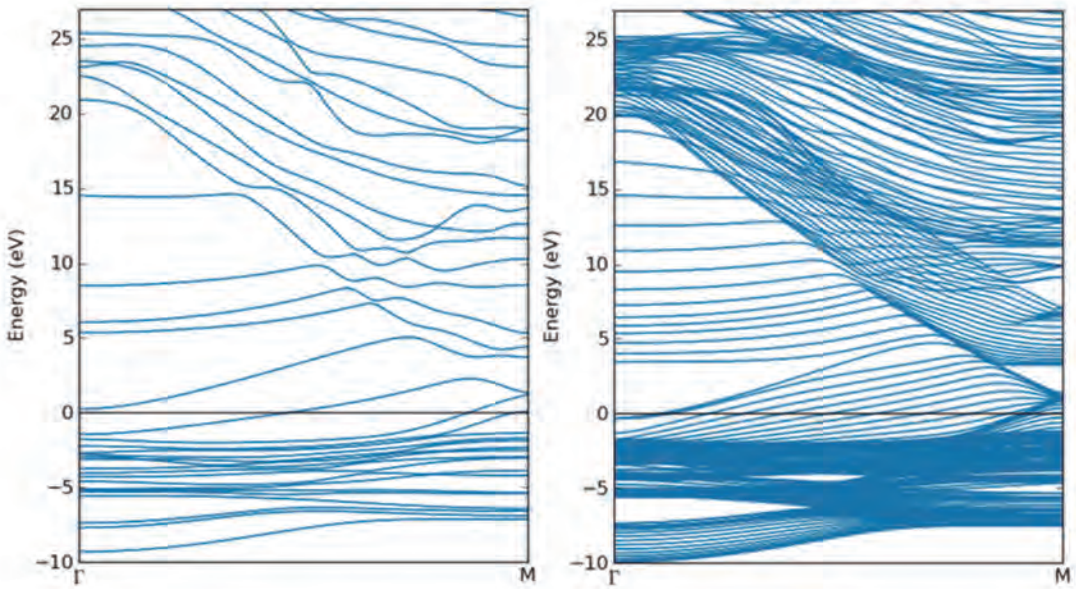

Figure S11 Band diagram along the Γ → M path for the 3 Au(111) (left) and 18 Au(111) layers (right). (Both surfaces are 1x1). The Fermi level is indicated by a horizontal black line.

From the analysis of the orbitals involved in the gold surfaces at different k points, we can extract some insights about the molecule-surface interaction. Besides of the surface state corresponding to the L-band at 0.63 eV over the Fermi level at Γ point (see Fig. S12 left), we observe nine orbitals, grouped in sets of three at energies 0.29 eV, 2.44 eV and 2.87 eV at the M point (see Fig. S12 right. Only one orbital per energy is represented). Six of them present important contribution from both surfaces and three are mainly described by the middle layer (see one orbital of each set in Fig. S12 right). Since the mixing between top and bottom layers of the slab is an artefact of the model, we expect three states for each surface.

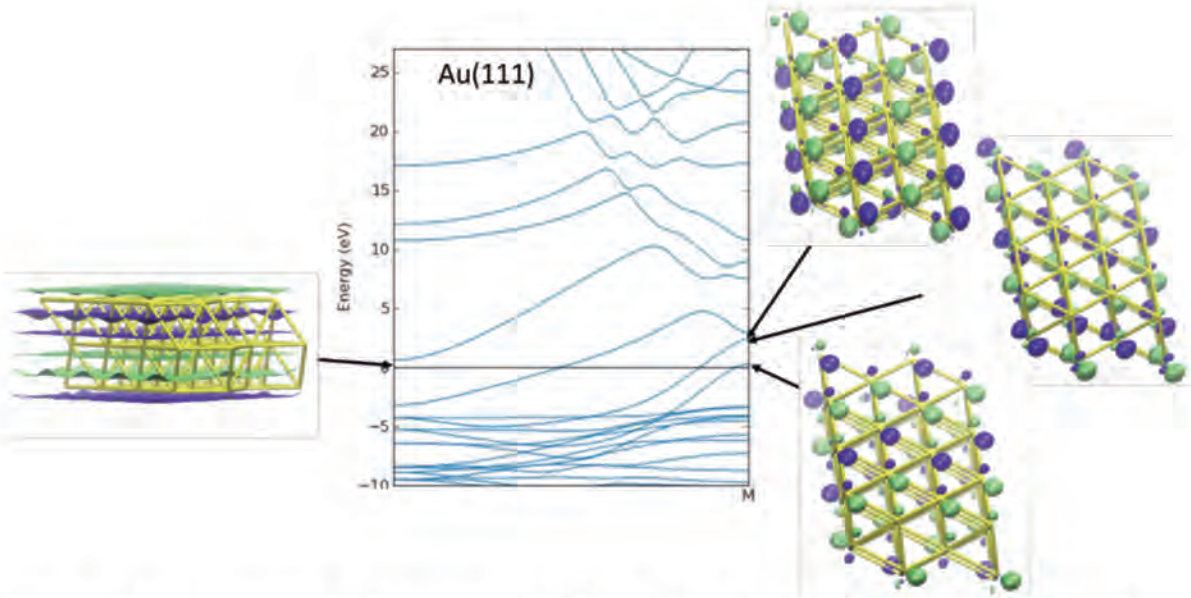

Figure S12 Wavefunctions of selected states at Γ and M points. Orbitals were obtained from a spin polarized calculation of a Au(111) 3-layer slab considering a 2x2 surface. For consistency, the band diagram corresponds to the same calculation performed using a Au(111) 1x1 surface.

The local shape of the three orbitals at 0.29 eV in the M point is interesting as they appear to be 120° rotations of the same motif (see Figure S13). At each atom, there is a major lobe pointing to the centre of the equilateral triangle formed by three gold atoms, and a much smaller lobe of the same sign points in the opposite direction. The second contribution in importance is of opposite sign and points outside the surface, being asymmetrical with respect to the up-down direction. After combined with effect of the spin-orbit coupling, this asymmetry in these three wavefunctions will allow an effective mixture to the molecular orbitals (with large differences between alpha and beta orbitals) resulting in a spin polarization of the surface. This fact brings an explanation to the mechanism associated with the magnetoresistance effect presented in this work.

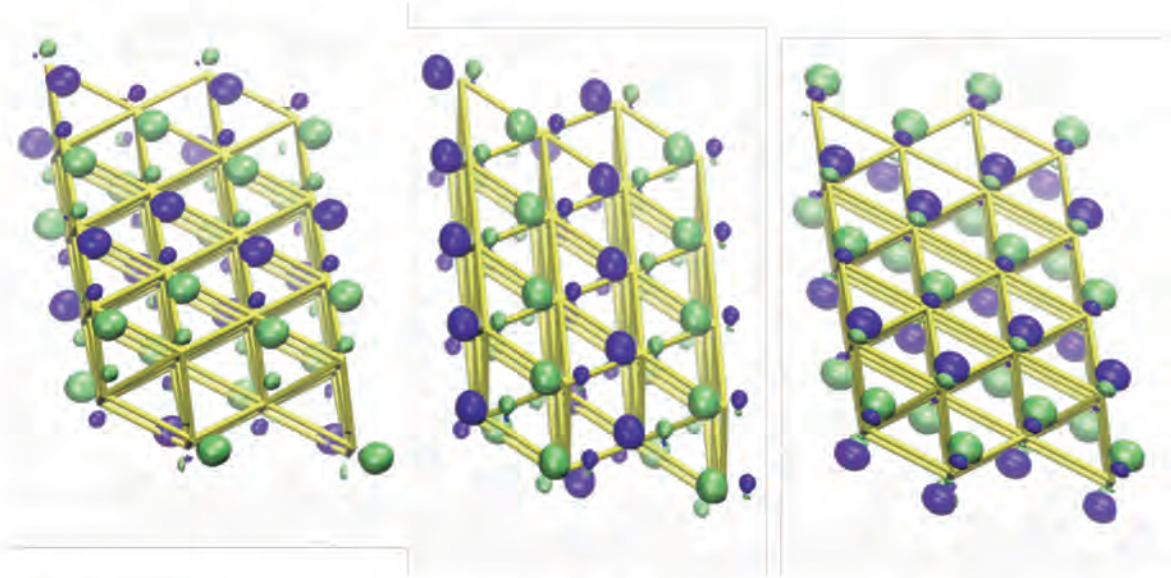

Figure S13 Wave functions for three bands at 0.29 eV (the first one is represented in Fig. S12 right-down to indicate the corresponding point in the band diagram) over the Fermi Level for the spin polarized calculation of a 3-layer Au(111) slab.

8. References

1. Rodes, A., Zamakhchari, M. A., El Achi, K. & Clavilier, J. *J. Electroanal. Chem. Interfacial Electrochem.* **1991**, *305*, 115.
2. Orts, J. M.; Gómez, R.; Feliu, J. M.; Aldaz, A.; Clavilier, J., *The Journal of Physical Chemistry* **1996,** *100*, 2334.
3. Rodes, A. & Clavilier, J. *J. Electroanal. Chem.* **1993**, *344*, **344,** 269.
4. Bruot, C.; Hihath, J.; Tao, N. *Nat. Nanotechnol.* **2011**, *7*, 35.
5. Haiss, W.; Wang, C.; Grace, I.; Batsanov, A. S.; Schiffrin, D. J.; Higgins, S. J.; Bryce, M. R.; Lambert, C. J.; Nichols, R. J. *Nat. Mater.* **2006**, *5*, 995.
6. Bracher, C.; Riza, M.; Kleber, M. *Phys. Rev. B* **1997**, *56*, 7704.
7. Lucas, A. A.; Morawitz, H.; Henry, G. R.; Vigneron, J.-P.; Lambin, P.; Cutler, P. H.; Feuchtwang, T. E. *Phys. Rev. B* **1988**, *37*, 10708.
8. Stoll, E.; Baratoff, A.; Selloni, A.; Carnevali, P. *J. Phys. C Solid State Phys.* **1984**, *17*, 3073.

9. Ponce, J.; Arroyo, C. R.; Tatay, S.; Frisenda, R.; Gaviña, P.; Aravena, D.; Ruiz, E.; van der Zant, H. S. J.; Coronado, E. *J. Am. Chem. Soc.* **2014**, *136*, 8314.

10. Li, X.; He, J.; Hihath, J.; Xu, B.; Lindsay, S. M.; Tao, N. *J. Am. Chem. Soc.* **2006**, *128*, 2135.

11. Aragonès, A. C.; Haworth, N. L.; Ciampi, S.; Bloomfield, N. J.; Wallace, G. G.; Coote, M. L.; Diez-Perez, I.; Darwish, N., *Nature* **2016,** *531*, 88.

12. Aragonès, A. C.; Haworth, N. L.; Ciampi, S.; Bloomfield, N. J.; Wallace, G. G.; Coote, M. L.; Diez-Perez, I.; Darwish, N., *Protoc. Exch.* (2016). doi:10.1038/protex.2016.013

13. Arcis-Castillo, Z.; Pineiro-Lopez, L.; Muñoz, M. C.; Ballesteros, R.; Abarca, B.; Real, J. A., *CrystEngComm* **2013,** *15*, 3455.

2.1.3 Findings and Discussion

— *The main findings of this study were the following:*

- Ni-[M(tzpy)$_2$(NCSe)$_2$]-Au junctions stability fits with the usual values observed on typical STM-BJ experiments.[97,111,322–324]

- Only the Co(II) complex on Au substrate under *substrate-to-Ni tip* current sense showed spin-dependent current to the α-↑Ni and β-↓Ni tip polarization, the observed conductance change is at least 100-fold under opposite Ni magnetic polarization conditions. Oppositely, under *Ni tip-to-Au substrate* current sense, the same Cu(II) complex did not show any kind of spin-dependent current. Ni(II) and Mn(II) complexes did not show dependence on the Ni tip polarization under any experimental condition, and present reduced molecular conductances respect Co(II) of a order of magnitude and a factor of ca. 3.5, respectively.

- Single-molecule conductance measurements using the [Co(tzpy)$_2$(NCSe)$_2$] and the Ni tip electrode and Cu or Pt substrate electrodes did not show any kind of conductance dependence on the Ni tip polarization for both current senses. The observed effects were the changes in the molecular conductance values and the junction stability compared to the observed lifetime employing Au substrate, for Cu case slightly reduced and for Pt extremely increased (ca. 2-fold).

- Pulling curves collected over the blinks showed plateaus. Contrary, the exerted on the tunneling current showed a sharp exponential current decay immediately after the application.

- The obtained calculations under non-polarized current or electrodes, show the following results for each metal complex. Co(II) complexes show one occupied and one empty t_{2g} β orbitals close to the Au electrode ε_F in comparison with the α channel orbitals that display the highest occupied orbitals ca. 1.0 eV above Au electrode ε_F. Ni(II) complexes despite presenting delocalized e_g orbitals close to the ε_F for both α and β electrons with a higher β contribution,[294,325] the narrow transmission peaks are manifesting the very weak mixing of orbitals of the complex to the π nature of axial -SeCN orbitals that interacts with the Au surface levels. Finally, Mn(II) complexes present the highest occupied α e_g orbitals and the lowest empty β t_{2g} orbitals far from the Au ε_F, around 0.5 eV below and 1.8 eV above in the DOS, however the latter present a a higher contribution.

— *The discussion of the results is summarized below:*

- From the obtained calculations, is proved that all the studied complexes show different effective channels for α and β electrons, accordingly such complexes

were suitable for spin-filtering functions under injected polarized current. But experimentally have been demonstrated that MR do not depends only on the (open-shell) electronic structure as well as the merely presence of the polarized electron channels of the molecules, because from all the presented metal complexes only the Co(II) complex showed MR effects. As DFT+NEGF transmissions shown, two new critical requirements related with the molecular orbitals of the metal center emerged: they must interact with the junction metal electrodes enough strongly through the extended electronic states and also they have to present close energy values to the ε_F for one of the electronic spins allowing its transport. Only the empty highly t_{2g} β orbitals of Co(II) complexes gather the explained conditions, unlike the other two complexes thus do not show MR effects. Ni(II) complexes have a very weak mixing of orbitals, causing also the significant reduced molecular conductance and Mn(II) complexes present a huge energy gap respect the Au ε_F respectively, reducing lightly its conductance respect the Co(II) complex. The highly coupling (broad transmission peaks) of Co(II) complexes' empty t_{2g} β orbital causes the conduction through (β-polarized) electron carriers.

- Despite the understanding of the crucial function of the metal center and its requirements to obtain spin-dependent transport, this parameter can not explain all the observed effects and their phenomenology, therefore several questions need to be resolved emerged from the two unexpected MR suppression effects due the *current sense inversion* and the *metal substrate material modification.*

  1. The *Ni tip-to-Au substrate* current sense do not show the intuitive MR behavior for the Au-[$Co(tzpy)_2(NCSe)_2$]-Ni junction, contrary what was expected. Surprisingly only under the opposite current *Au substrate-to-Ni tip* current sense the MR effect is effective. From this unexpected phenomena can be deduced that the single-molecule device only behaves as spin-filter when the current is injected from the Au substrate and not from the Ni tip, replacing necessarily the latter by the former as polarized electronic source. The discussion of this double asymmetric behavior is presented below.

     The *Ni tip-to-Au substrate* MR suppression can be easily explained by a Ni tip–molecule magnetic polarization alignment. The resulting calculated energy involved in the flipping of the molecular spin for the Co(II) complex, is about 90^{-1} cm, a favorable value to allow Ni tip–molecule alignment. As a consequence of the effective alignment, the MR behavior can be suppressed under a *Ni tip-to-Au substrate* current sense because the molecule will permanently receive the same favored (or unfavored) spin-carriers, causing a kind of "spintronic diode" effect. Furthermore, assuming the new role of the Au substrate as the polarized electronic source due the polarizing interfacial effects, the Ni tip should be treat as the magnetic stimuli to switch the spin-filter behavior via its polarization direction, therefore attesting the required **paramagnetic** response of the

open-shell central molecules for the spin-filtering mechanism.
The most reasonable explanation to justify the MR behavior from a current *Au substrate-to-Ni tip*, assumes that such injected current suffers a previous pre-polarization effect on the Au surface. Since Au is a diamagnetic material requires a surface polarization and its origin can only be consequence of the attachment of molecules to the Au surface. From the obtained results of previous studies which analyzed similar scenarios to ours, was conclude that a strongly directional polarizing nature of the S-Au bond[326–329] can generate a directional magnetization to the interface.[330] Combining such idea with the presented single-molecule device, a pre-polarization of the current on the Au surface can be justified as a consequence of the superficial magnetization effect originated on the molecule-surface interface where some spin-polarized bands of the surface induce the spin-polarization[151,330,331] of the emitted electrons. The effects of surface polarization and the emitted polarized current opens the door to a new scenario which need the further validation presented in the next Section of the thesis.

2. The role of the metal substrate's surface is essential for the observed MR effect in the studied asymmetric junctions, setting aside the material electrode effect over the molecular conductance.[62,332–335] Control experiments performed on Cu and Pt substrate show an electron transport insensitive to the magnetic polarization of the Ni tip electrode. Employing the computational results can be assumed that Cu and Pt surface levels cannot efficiently interact with the molecular orbitals of the Co(II) complexes through the π-orbitals of -SeCN ligand with different α and β occupancy. Cu substrate as a consequence of its low atomic number lacks on a strong SOC, in comparison of Au or Pt. Besides that, Pt substrate presents a dense block of *d bands* crossing the ε_F and *6s* associated *bands* above it, representing a completely different scenario from the presented by Au which can be related with the MR absence too. These arguments reinforce the crucial contribution of the molecule-metal interface to the spin-dependent current, since the materials should affect to the originated polarized current due their different electronic structures according to the proposed hypothesis where only the Au substrate electrode can be used as polarized electronic source.

The combination of the proposed two asymmetric *key-parameters* to build a single-molecule device with MR effects has been developed. Although the achieved MR, the lack of the comprehension of the mechanisms and phenomenology of the spin-polarized current origins need complementary research to be completely understood. At this point the origin of the polarized current on the molecule-surface interface is assumed to be due the molecule-surface polarizing effects. The implications of this new phenomenon and the new essential role taken by the molecule-surface interface will represent the new focus of study in the following Section. For this reason will be introduced as a new *key-parameter* along with the previous two.

2.2 The role of the Spinterface

As a consequence of the results of the single-molecule device presented in the previous Section, where the device only behaves as a spin-filter when the current is injected from the Au substrate is concluded that such current should be polarized to allow the observed spin-filter effects. As has been discussed, Au is not a magnetizable electrode due its diamagnetism emits or accepts electrons of both orientations equally well,([116]) so it leads to believe that the injected current from the Au substrate suffers a sort of pre-polarization or pre-selection superficial effect because of the attached molecules. Is known that in some cases as a direct consequence of the molecular attachment on Au surfaces and depending its bond polarity strength, can appear some molecule-Au interface polarizing effects manifested as superficial induced magnetism.[330] Despite such effects have been reported since some decades ago,[326,327,336] the association of this interfacial effect to a spintronics phenomenology is very recent,[120,132,337] in fact is still being developed an emerging field of research and new applications calling to this effect, the "Spinterface" mixing both fundamental concepts *Spin(tronics)* and *Interface*.

The concept of Spinterface[120,132] was born due an apparent *ex-nihilo* (from the Latin "out of nothing") magnetization effect experimentally observed for the first time on both Au surfaces and nanoparticles modified with thiolated molecules,[327,338] which present magnetic response in the direction of the S-Au bond as a consequence of its fairly strongly polarizing nature,[326,328,329] arising as an inherent interfacial directional magnetization due to the two dimensional organization of the adsorbed molecules on the metal substrate. All the cited works are few examples of precedents which studied or employed the Spinterface effect, the amount of such studies is vast, but the ones focused on spintronics at the molecular or monolayer scale are extremely reduced excepting the pioneering works developed by Naaman and coworkers. Their research was based on spin-dependent transport experiments using polarized photoelectrons from a metal surface transported through a Self-Assembled Monolayers (SAM) of chiral structures. All the observed phenomena related with the variation of the chirality of the molecules and the polarization of the photoelectrons are founded on a well-defined combined two effects as a consequence of the SOC. *(i)* The Chiral Induced Spin Selectivity effect (CISS), directly dependent on the molecular chirality due the electron interaction with an asymmetric molecular structures[224,339,340] and the *(ii)* Spinterface due a *induced S-Au bond magnetization* effect at the molecule-metal.[326,336,341] Despite the latter is the subject of study of this Chapter, the CISS effect is added as the fundamental part to building a single-molecule device based on chiral peptides presented on this thesis in Chapter 4 on Page 218 for the *EMFs on molecules* part.

The Spinterface origin is still under discussion and exists especially extensive theoretical studies about how it is originated by the surface Rashba spin-splitting at the bare Au surface.[120,153,154,201,287,290] Rashba spin-splitting is caused by the SOC (see *Section "Spintronic surface effects: SOC and Rashba splitting"*, Page 47) interaction of the free electron on Au surfaces,[342] which generates an anisotropic magnetiza-

tion due unbalanced topological surface states, known as spin-texture, phenomenon detectable using photoemission spectroscopic techniques like ARPES.[208–210,212,213] Under an scenario like the above described where molecules are linked to Au and the orbitals are mixed through the long polarized molecule-Au bond, the Rashba spin-splitting effect is amplified through the generated SOC by the bond which stresses the spin-unbalance (and defines the spin-texture) creating some spin-polarized bands at the surface that interact with the molecular levels favoring one spin-polarization from the possible two. Adapting this new concepts to our single-molecule device where electrons will be transported through a molecule-Au Spinterface,[343] the mentioned spin-unbalance will impose a preferential electron polarization because the molecular levels of a specific spin-polarization will be more accessible to hybridize, favoring the emission of this specific electron spin-polarization. This spin-preference, is an *asymmetry* because defines an interfacial current polarization effect[153,153,154,290] being the fundamental reason to employ the ***Spinterface*** as the new third asymmetric *key-parameter* on the presented spin-filter device. On this interface the electron spin orientation can be pre-selected from an injected non-polarized current acting as an effective polarized electronic source, justifying the observed spin-filtering effect of the previous Section.

On this Section the ***Spinterface*** as a asymmetric *key-parameter* is introduced to the tested single-molecule spin-filter device along with the other two preceding proved *key-parameters*, the ***open-shell/paramagnetism*** of the central molecule and the Ni electrode's ***magnetic polarization***. The three *key-parameters* are combined and each one ascribes a specific functionality to the device, defining the following proposed model. Mainly, the molecule-Au ***Spinterface***[151,330,331] allows the interaction of some spin-polarized bands of the surface with the molecular levels of the molecule, the resulting spin-polarized states are responsible of the current pre-polarization. This polarized current emitted from the functionalized surface of Au substrate (source) is injected to the ***paramagnetic molecule*** which acts as a tunable spin-filter, through its spin-selective channels the transmitted electrons suffer energy penalties depending the molecular magnetic moment alignment according to the Ni electrode's ***magnetic polarization***.[121] The best physically way to combine the three *key-parameters* way is through the STM microscope, like in the previous experiment. Below is detailed how this tool and different combined *ingredients* were employed to conduct the single-molecule current experiments study the spin-filtering effect of the proposed single-molecule device.

2.2.1 The experimental research

In this second step for the study and development of a single-molecule spin-filter device at RT, via a *set-up* based on an STM microscope were gathered different *ingredients* associated to the three essential asymmetric *key-parameters*. Despite the employed *set-up* (Figure 2.3) was close to the used in the previous one (Figure 2.2) the main differences were reflected on the experimental controls and the kind of supporting computational calculations.

Mainly, as a first *ingredient* were used two hexacoordinate Fe(II) complexes molecules (*i*) $[Fe(tzpy)_2(NCS)_2]$ and $[Fe(tzpy)_2(NCSe)_2]$ based on the previous studied $[M(tzpy)_2(NCSe)_2]$ complexes, and also synthesized on purpose[313–315]) to be employed as model molecules for the same reasons such as neutral charge, diamagnetic ligands, stability, symmetry[43] magnetizable and potential spin-filtering capabilities thanks to the metal center, as was before theoretically confirmed like previous works.[288,299] Both Fe(II) complexes are SCO (see the explanation on previous Page 59) and present switchable character depending on the working temperature, between the diamagnetic S=0 *low-spin* $t_2g^6e_g^0$ electron configuration and the paramagnetic S=2 *high-spin* $t_2g^4e_g^2$ electron configuration, both compounds present the latter electronic configuration due the experimental conditions performed at RT because the T_{CTC} values are 160K and 250K for $[Fe(tzpy)_2(NCS)_2]$ and $[Fe(tzpy)_2(NCSe)_2]$, respectively. Unlike the $[Co(tzpy)_2(NCSe)_2]$ complex, such Fe(II) complexes present an achievable *low-spin* electronic configuration at LT regimes, fact that was be used to switch such complexes to the diamagnetic state suppressing their susceptibility to an external magnetic stimuli allowing the study of the effects over the SOC, Spinterface and MR behavior. In the other hand, at RT were performed the target single-molecule current measurements since the ***open-shell/paramagnetism*** of the Fe(II) complexes allowed the spin-dependent transport under magnetic stimuli. The two different complexes present the already tested -SeCN and the never-used-before -SCN axial ligands acting as *anchoring groups* thanks to the presented affinity to the metal electrodes.[316,317,344] The differences on the MR effect given by the employed *anchoring groups* were aimed to study their effects on the Spinterface as reinforcement to elucidate the interfacial molecule-Au surface magnetization effects. Analogous to the procedure previously used, the second *ingredient* was again a ferromagnetic Ni STM tip(*ii*) *ex-situ* magnetized in the two α-↑Ni and β-↓Ni ***magnetic polarizations*** to tune the spin-dependent transport; besides, according the previous results has to be used as a drain electrode to obtain MR behavior. Finally, the last *ingredient* is the Au(111) substrate electrode(*iii*). Also following the previous results, the Au electrode was chosen because from all the already studied materials was the only one that allows the MR effect on the studied asymmetric junctions if it is used as source electrode as is showed in the previous Section. The other complement that needs the Au substrates' surface to create the ***Spinterface*** allowing a pre-polarization stage, are the -SeCN and -SCN *anchoring groups* the former was chosen due the described superficial spin-polarization effects and the latter due the its close electronic structure to the former.

With the aim to further deepen the study of the Spinterface, a part from carry out the single-molecule spin-dependent transport measurements the presented research was specially focused in performing different control experiments which involved the essential new role taken by the molecule-surface interface, for this reason different variables were changed to modify the characteristics of this interface. Despite the details of the control experiments are specified in the next Section, the fundamental reasons of such experiments follows. Two different *anchoring groups* were used to compare their possible effects over the spin-dependent transport due the inherent dissimilar electronic structure and the affinity for Au substrate, because such differences affect the molecule-Au bond interfacial polarization and the spin-unbalancing. Also, since the spin-splitting can be affected by the interplay of attached paramagnetic structures on the surface due its SOC interaction,,[188,189,192,193,345] were employed the also synthesized on purpose[313–315] S=0 diamagnetic molecules ($[Fe(L)^{A}(NCS)_2]$)) structurally close to the target molecules as a control. For the same reason, since such target molecules are SCO they were transited also to the diamagnetic S=0 *low-spin* electronic configuration working at LT regimes. The last performed control was the replacement of the Au substrate by Cu, because it is an element enough lighter to minimize the Spinterface's effects due its lack of large or significant SOC contribution, as was previously argued in *Section "Spintronic surface effects: SOC and Rashba splitting"* (Page 47).

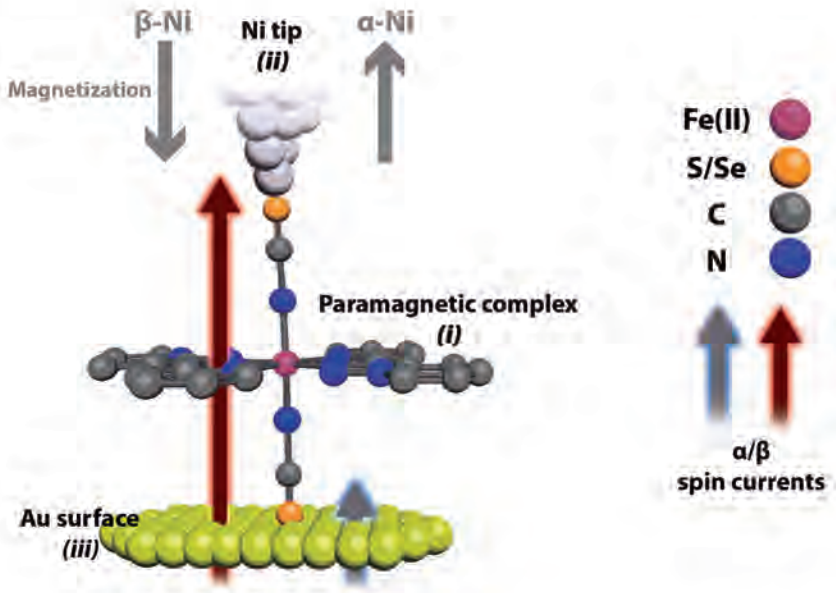

Figure 2.3: Schematic representation of the single-molecule device showing spin-filtering capabilities with the three "ingredients" labeled.

Thanks to the three described *ingredients*, was possible to develop a single-molecule device with spin-filtering capabilities and find out the polarized current origin and the ***Spinterface*** *key-parameter's* role on the device as well as the fully

understanding of its phenomenology. Figure 2.3 pretends to illustrate the proposed single-molecule device and the spin-dependent transport by means of the representation of the STM main components and such *ingredients*, showing the two different scenarios under both Ni tip magnetic polarizations.

In the performed experiments, the employed procedure was the STM-BJ (see *Section "STM Break-Junction Technique"*, on Page 26) into its the dynamic *tapping* approach (see *Appendix C.1*, Page 325) with the objectives to capturing thousands of currents decays from *Tip electrode*-molecule-*Substrate electrode* junctions under the different experimental conditions detailed in this subsection. A detailed description of the sample, substrate and tip preparation can be found from Page 328 (*Appendix C.2*). For the experimental details related with the LT-STM see *Appendix C.3*, Page 335. The experiments were carried out employing polycrystalline Ni wire to obtain the STM tips electrodes and Au(111) or Cu(111) monocrystals were utilized as substrate electrodes, mesitylene organic solvent was used as a medium. The performed single-molecule conductance measurements were supported by computational DFT calculations performed with *GREEN Code63* and its DFT-based interface *SIESTA* package64 including fully relativistic pseudo-potential formalism, in order to account SOC contribution; that took in account the three asymmetric *key-parameters* to corroborate the spin-dependence of the current focusing on the study of the electronic structure of the molecule-surface Spinterface. They included the Ni tip magnetic polarization, the material of the electrode (Au or Cu) and the diamagnetic or paramagnetic character with spin state of the bridging molecules. *CASSCF-RASSI* calculations were conducted to calculate magnetic anisotropies.

2.2.2 Objectives and Summary of the experimental work

- To study the spin-dependent current response on the established singe-molecule device for both $[Fe(tzpy)_2(NCS)_2]$ and $[Fe(tzpy)_2(NCSe)_2]$ complexes, the experiments were done at RT employing both Ni tip α-$\uparrow$ and β-$\downarrow$ magnetic polarizations and a bias voltage between the -10 mV and -25 mV for the*Au substrate-to-Ni tip* current sense. Also was studied the current response inverting source and drain roles of the electrodes, the same single-current measurements were conducted under the *Ni tip-to-Au substrate* current sense applying a bias voltage range between the +10 mV and +25 mV.

- The use of both -SCN and -SeCN axial ligands were performed with the aim to compare the presented affinity to the electrodes and the possible variation of the GM effects due different influence on the Spinterface.

- To evaluate the relevance of the magnetized electrode were used diamagnetic Au tip and non-magnetized Ni tip electrodes to conduct single-current measurements for both paramagnetic Fe(II) complexes with -SCN and -SeCN axial ligands due the possible SOC effect on the Spinterface with different bias voltages magnitudes and both current senses ($\pm$10 mV and $\pm$25 mV).

- With the objective to evaluate the dependence of the SOC and Spinterface with the metal substrate material, $[Fe(tzpy)_2(NCSe)_2]$ complex was measured replacing the Au substrate electrode by another one made by Cu under the experimental *set-up* that presents MR effect, in order to modify the molecule-surface interaction.

- To assess the effects over spin-dependent transport of the paramagnetic state of the metal complexes, were performed junctions under the diamagnetic state using the diamagnetic $[Fe(L)^A(NCS)_2]$ S=0 and also decreasing the working temperature well below the T_{CTC} to transit the $[Fe(tzpy)_2(NCSe)_2]$ complex to its diamagnetic state (S=0) under the experimental *set-up* that presents MR effect.

In the following pages is shown the summarized research as a published paper and its Supplementary Information:

"Albert C. Aragonès, Daniel Aravena, Jorge I. Cerdá, Zulema Acís-Castillo, Haipeng Li, José Antonio Real, Fausto Sanz, Joshua Hihath, Eliseo Ruiz, and Ismael Díez-Pérez. Large Conductance Switching in a Single-Molecule Device through Room Temperature Spin-Dependent Transport. *Nano Letters*, 16(1):218–226, jan 2016".

NANO LETTERS
Letter
pubs.acs.org/NanoLett

Large Conductance Switching in a Single-Molecule Device through Room Temperature Spin-Dependent Transport

Albert C. Aragonès,[†,‡,§] Daniel Aravena,[∥,⊥] Jorge I. Cerdá,[#] Zulema Acís-Castillo,[▽] Haipeng Li,[○] José Antonio Real,[▽] Fausto Sanz,[†,‡,§] Josh Hihath,[*,○] Eliseo Ruiz,[*,∥] and Ismael Díez-Pérez[*,†,‡,§]

[†]Departament de Química Física, Universitat de Barcelona, Martí i Franquès 1, 08028 Barcelona, Spain

[‡]Institute for Bioengineering of Catalonia (IBEC), Baldiri Reixac 15-21, 08028 Barcelona, Spain

[§]Centro Investigación Biomédica en Red (CIBER-BBN), Campus Río Ebro-Edificio I+D, Poeta Mariano Esquillor s/n, 50018 Zaragoza, Spain

[∥]Departament de Química Inorgànica and Institut de Química Teòrica i Computacional, Universitat de Barcelona, Diagonal 645, 08028 Barcelona, Spain

[⊥]Departamento de Química de los Materiales, Facultad de Química y Biología, Universidad de Santiago de Chile (USACH), Casilla 40, Correo 33, Santiago, Chile

[#]Instituto de Ciencia de Materiales de Madrid, CSIC, Cantoblanco, 28049 Madrid, Spain

[▽]Institut de Ciència Molecular (ICMol), Universitat de València, 46980 Paterna, València, Spain

[○]Department of Electrical and Computing Engineering, University of California-Davis, 2064 Kemper Hall, Davis, California 95616, United States

S *Supporting Information*

ABSTRACT: Controlling the spin of electrons in nanoscale electronic devices is one of the most promising topics aiming at developing devices with rapid and high density information storage capabilities. The interface magnetism or *spinterface* resulting from the interaction between a magnetic molecule and a metal surface, or *vice versa*, has become a key ingredient in creating nanoscale molecular devices with novel functionalities. Here, we present a single-molecule wire that displays large (>10000%) conductance switching by controlling the spin-dependent transport under ambient conditions (room temperature in a liquid cell). The molecular wire is built by trapping individual spin crossover Fe^{II} complexes between one Au electrode and one ferromagnetic Ni electrode in an organic liquid medium. Large changes in the single-molecule conductance (>100-fold) are measured when the electrons flow from the Au electrode to either an α-up or a β-down spin-polarized Ni electrode. Our calculations show that the current flowing through such an interface appears to be strongly spin-polarized, thus resulting in the observed switching of the single-molecule wire conductance. The observation of such a high spin-dependent conductance switching in a single-molecule wire opens up a new door for the design and control of spin-polarized transport in nanoscale molecular devices at room temperature.

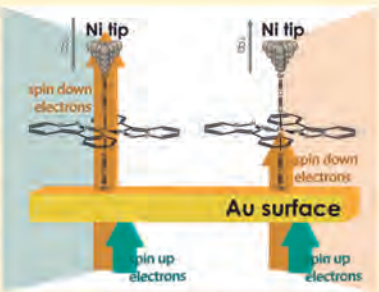

KEYWORDS: *Single-molecule junctions, spin-crossover complexes, magnetoresistance, STM break-junction, density functional calculations, spinterface, spin orbit coupling*

Controlling the spin of electrons has become one of the major challenges in the emerging field of Spintronics.[1,2] Electron spin offers an attractive extra degree of freedom, beyond the electron charge, which opens up a range of possibilities in the future design of electronic devices with new functionalities and larger bandwidths.[3] To fulfill today's technological needs, miniaturization is a requirement that must be pursued in the field of Spintronics, just as it has been in conventional electronics. Single-molecule devices promise to function both as a test-bench for fundamental studies in Spintronics and as a means to explore new routes for the design of organic, nanoscale, spin devices.[4] Spin-polarized scanning tunneling microscopy (SP-STM) has brought with it an extended realm of fundamental knowledge of the spin-dependent electronic structure of single magnetic molecules adsorbed on a metallic substrate.[5,6] SP-STM profits from the injection of spin-polarized currents into the STM junction to achieve spin mapping at subangstrom spatial resolutions.[7] Such experiments have allowed the visualization of a variety of hybridized spin-polarized states between a molecule and a

Received: September 4, 2015
Revised: November 13, 2015
Published: December 16, 2015

DOI: 10.1021/acs.nanolett.5b03571
Nano Lett. 2016, 16, 218−226

metal surface, giving rise to interfacial magnetism.[5,6,8−12] In this Letter, we explore this molecule−metal interfacial magnetism to design a new quantum nanoscale device that exploits the spin information.

A few examples of single-molecule spintronic devices have been presented,[13−15] and most that have, have resulted from the development of single-molecule transport approaches using nonmagnetic systems. Individual transition metal complexes displaying high-spin electronic configurations have been trapped between two nonmagnetic metal beads at low temperatures and the transport properties characterized at the single-molecule level.[16−18] In order to add spin-dependent functionalities to such single-molecule wires, magnetic Ni beads have been introduced into a junction formed with diamagnetic molecules,[5,19,20] resulting in observed changes in the single-molecule magnetoresistance. These results demonstrate the potential of nanoscale spin-selective transport, the performance of which might reach device application requirements by introducing metal complexes with much higher spin−orbit coupling.[21] Examples of this possibility include the characterization of magnetoresistive supramolecular nanoscale devices based on terbium^{III} complexes resulting in a number of spin functionalities such as spin valves,[22] spin transistors,[23] or spin resonators.[24] Such phtalocyaninate Tb^{III} molecules have become a reference in the metal/molecule interface studies, either with gold[25] or magnetic nickel surfaces.[26]

The fundamental studies mentioned above were performed far from practical operating conditions, such as ultrahigh vacuum (UHV) and low temperatures. However, room-temperature, spin-dependent transport has also been demonstrated through chiral structures such as DNA in a nanoscale device.[27] The mechanism has been well described for self-assembled monolayers (SAMs) as a combined effect of spin−orbit interaction in the chiral molecular structure[28,29] and the induced Au−S bond magnetization at the molecule−metal interface.[30−32] The latter effect has been experimentally observed on both gold surfaces and nanoparticles modified with thiolated molecules.[33,34] Although still under discussion, it originates in an amplification of the surface Rashba spin splitting at the bare metal surface[35] by the highly polarized metal-S bond.[30] Extensive theoretical studies support a spin-filter effect based on such interfacial Rashba effect.[36,37]

Spin crossover (SCO) complexes, most of them Fe^{II} complexes, have remarkable magnetic properties based on ground-state spin switching (for Fe^{II} systems, between the diamagnetic $S = 0$ low-spin $t_{2g}^6e_g^0$ and paramagnetic $S = 2$ high-spin $t_{2g}^4e_g^2$ electron configurations) controlled by means of an external stimulus, i.e., temperature, light, pressure, solvent interactions, or electric field.[38,39] This switching behavior makes them a target for Spintronics because the high-spin magnetic state usually presents higher conductance than the diamagnetic low-spin state.[12,40−46] The difference in the transport properties between the two states is due to the change in the electron configuration; the structural changes (larger metal−ligand bond distances in the high-spin state) play a minor role.[40,41]

In this study, we combine all of the above ingredients to design a single-molecule electrical wire that exhibits room-temperature conductance modulation of several orders of magnitude through spin-dependent transport. The junction is built by bridging individual Fe^{II} SCO complexes with high- and low-spin states between a gold electrode and a magnetically polarized nickel electrode. This is a fundamental difference from other experiments mentioned above that use two magnetic electrodes. The Fe^{II} complexes were designed with two axial −SCN (or −SeCN) chemical groups that served as the metal−molecule anchoring points (Figure 1).[47,48] Trans-

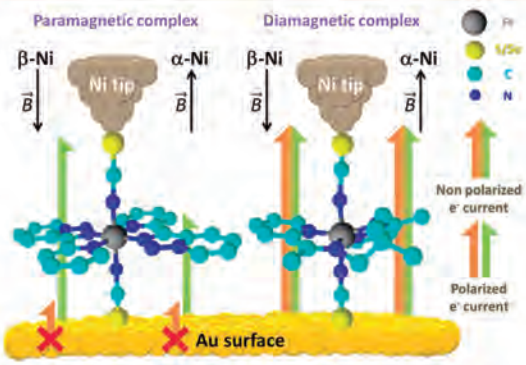

Figure 1. Schematic representation of the single-molecule junctions studied under two opposite Ni magnetic polarizations (labeled α and β). The paramagnetic $[Fe(tzpy)_2(NCS)_2]$ complex shows a high conductance switching which depend on the Ni tip spin polarizations (see arrows), while the transport in the diamagnetic $[FeL^A(NCS)_2]$ complex remains invariable.

port experiments with the high-spin complex show a single-molecule conductance change of at least 100-fold under opposite Ni magnetic polarization conditions. This large magnetoresistance switching is achieved at a near-zero bias voltage, which implies the use of very small currents and low power consumption. This change in conductance is observed when the electrons are injected from the gold to the magnetic nickel electrode, and the nickel electrode is magnetically polarized in opposite directions along the junction main axis. Our theoretical model suggests that the observed conductance change is the combined result of three consecutive stages. First, spin selection occurs at the molecule−gold interface as a result of new hybridized spin-polarized states. Second, the spin-polarized current generated at such interface by spin−orbit coupling (SOC) is enhanced by the high-spin $S = 2$ Fe^{II} complex that favors the transport of minority spin (α-up) carriers.[40] And third, the direction of the nickel magnetic polarization controls the final device conductance because the transport of minority spin carriers is also more efficient in the magnetically polarized tip.[49] The proposed model is supported by two control experiments: (i) the gold substrate is replaced by a copper one, which minimizes the spin surface effects due to the lack of large spin−orbit contributions, thereby canceling the first stage, and (ii) the paramagnetic high-spin complex is substituted by a homologous diamagnetic low-spin $S = 0$ Fe^{II} complex, whose molecule/metal interface cannot induce spin polarization in the carriers, thus eliminating the second stage of the mechanism.

Results and Discussion. *Single-Molecule Transport in Ambient Conditions.* Single-molecule conductance experiments under different Ni magnetic polarizations (Figure 1) were conducted on high-spin $[Fe(tzpy)_2(NCS)_2]$ and $[Fe(tzpy)_2(NCSe)_2]$[47] single-molecule contacts under ambient conditions using an STM break-junction approach.[15] Briefly, a freshly cut Ni tip was magnetically polarized ex situ by placing it in close proximity to a 1 T NdFeB magnet for a period of 2 h. After the magnetization, the Ni tip was placed into the STM tip

DOI: 10.1021/acs.nanolett.5b03571
Nano Lett. 2016, 16, 218−226

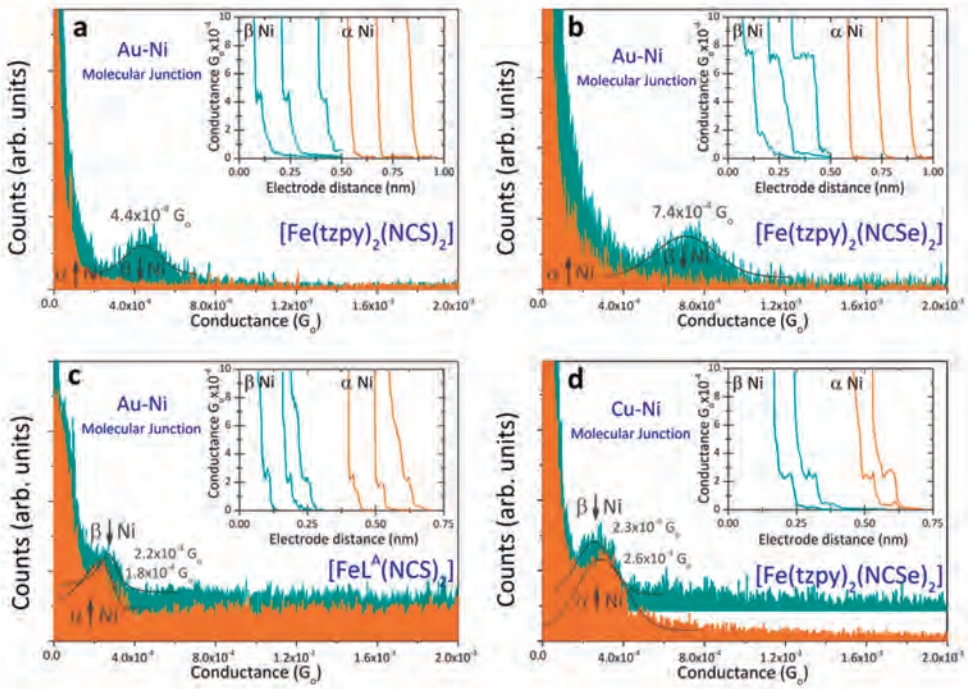

Figure 2. Conductance histograms for the single-molecule transport of Fe^{II} complexes under ambient conditions: (a) paramagnetic $[Fe(tzpy)_2(NCS)_2]$, (b) paramagnetic $[Fe(tzpy)_2(NCSe)_2]$, and (c) diamagnetic $[FeL^A(NCS)_2]$ complexes obtained with Au and both α-up polarized (orange) and β-down polarized (green) Ni electrodes. (d) Single-molecule conductance histograms for the $[Fe(tzpy)_2(NCSe)_2]$ complex obtained with Cu and both α-up polarized (orange) and β-down polarized (green) Ni electrodes. The two histograms have been vertically offset for clarity. All conductance values have been extracted from Gaussian fits of the peaks. Insets show representative current versus pulling traces used to build the conductance histograms for the α-up polarized (orange) and the β-down polarized (green) Ni electrodes. The applied bias was set to −10 mV.

holder. To avoid Ni oxidation during the magnetization stage, the Ni tip was kept under anaerobic conditions (see experimental details in Supporting Information (SI) sections 2.1 and 2.2). The magnitude and direction of the magnetic polarization of the Ni tip were characterized before and after the STM break-junction experiment using SQUID magnetometry to ensure that the Ni magnetization persisted over the entire time frame of the experiments (see SI section 2.3). The magnetized STM Ni probe was then driven toward the surface and pulled back again in successive cycles, using a 2-point feedback loop on the tunneling current flowing between the two electrodes under a constant bias voltage.[15,50]

Some representative current traces obtained during the pulling stage of the above successive cycles are shown in the insets of Figures 2a,b for the compounds in the high-spin state, $[Fe(tzpy)_2(NCS)_2]$ and $[Fe(tzpy)_2(NCSe)_2]$, respectively. When a molecule bridges between the two electrodes, a plateau appears in the current trace at the specific molecular conductance.[15,50] The −SCN group for molecular anchor purposes has been previously demonstrated in single-molecule contacts.[51] The absence of other exposed interacting groups in these compounds as well as the single plateau features in the decay curves[52,53] suggests the axial −S(Se)CN as the only anchoring points. In order to study spin-dependent transport across the single-molecule junctions, the conductance measurements were performed by magnetically polarizing the Ni electrode in the two opposite directions perpendicular to the surface (insets of Figure 2a,b). The α and β labels correspond to the magnetic polarization of the Ni electrode pointing upward and downward, respectively, from the SQUID characterization (SI section 2.3).

Two different charge transport behaviors are observed for the junction of the high spin Fe^{II} complex when the Ni electrode is magnetically polarized along either the α-up or the β-down directions and the electrons are injected from the Au to the Ni electrode (see Figure 1, left panel). When the Ni electrode is in the β-down polarization, both compounds, $[Fe(tzpy)_2(NCS)_2]$ and $[Fe(tzpy)_2(NCSe)_2]$, display current plateaus in the individual traces around characteristic conductance values (green curves in Figure 2a,b insets). Hundreds of these individual traces are accumulated into the corresponding conductance histogram where the peak maxima represent the most probable conductance values of the single-molecule contact (green histograms in Figure 2a,b). The $[Fe(tzpy)_2(NCSe)_2]$ displays a conductance of $7.4 \times 10^{-4} G_0$, roughly twice that of the $[Fe(tzpy)_2(NCS)_2]$, $4.4 \times 10^{-4} G_0$, which indicates higher electrical coupling in the former. This stronger Au−SeCN affinity also results in a longer average plateau length of 0.09 nm compared to 0.04 nm obtained for the SCN derivative (see SI section 4.5). These results also suggest that the molecules are anchored to the electrodes through Au−SCN/SeCN and Ni−SCN/SeCN bonds on each

DOI: 10.1021/acs.nanolett.5b03571
Nano Lett. 2016, 16, 218−226

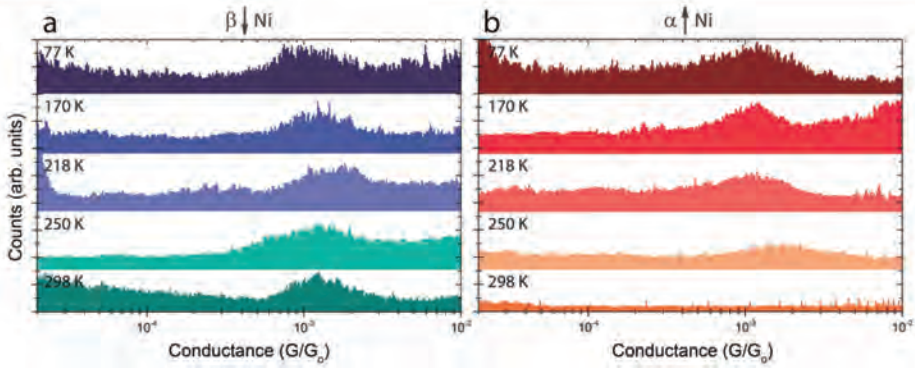

Figure 3. Temperature-dependent conductance histograms for the paramagnetic $[Fe(tzpy)_2(NCSe)_2]$ compound in vacuum under β-down (a) and α-up (b) Ni magnetic polarizations. The histograms have been vertically offset for clarity. The applied bias was set to −10 mV.

side of the junction, respectively. In contrast, no current plateaus were observed in the individual pulling traces for the α-up polarized Ni electrodes for either compound (orange curves in Figure 2a,b insets). The single-molecule conductance is in this case below the detection limit of our current amplifiers ($<10^{-6}G_0$, see orange histograms in Figure 2a,b). Note that single-molecule conductance switching is not observed when nonpolarized Ni electrodes are employed (see SI sections 4.3 and 4.4), where both molecules displays similar conductances.

To corroborate the role of the paramagnetic molecule in the observed spin-dependent transport experiment, single-molecule transport was also studied in a homologous diamagnetic low-spin $[FeL^A(NCS)_2]$ (L^A = *N,N'*-bis(1-pyridin-2-ylethylidene)-2,2-dimethylpropane-1,3-diamine) compound[52] (Figure 1). Similar conductance values were obtained under both α-up and β-down Ni magnetic polarizations (see Figure 2c), thus confirming that the spin-dependent conductance in the single-molecule contact stems from the paramagnetic nature of the compound, and that the formation of the single-molecule bridge is not affected by the magnetic polarization of the Ni electrode. Direct comparison of the single-molecule transport results in Figure 2 suggests a strong spin-dependent conductance switching for the high-spin Fe^{II} junction, i.e., the conductance of the paramagnetic single-molecule wire is suppressed in one of the Ni magnetic polarization directions. If a Cu substrate is used instead of Au, the observed spin-dependent transport for the $[Fe(tzpy)_2(NCSe)_2]$ compound is also suppressed (see Figure 2d).

Considering the small applied bias, the lack of magnetoresistance when the electrons are injected into the molecule from the spin polarized nickel electrode (see SI section 4.6, Figure S14) suggests that the spin polarized character of the current coming from the tip is responsible for the magnetoresistance suppression. In this scenario, magnetoresistance would be suppressed if the polarized current could modify the molecule's magnetic moment when both are antialigned. Transport in this case is due to minority carriers in the Ni tip with a spin opposite to the molecule, which is aligned with the magnetization of the tip. Spin-transfer torque mechanisms, well established in layered systems, could apply to our molecular bridge if, for instance, one assumes the magnetic interaction between the exchange field at the molecule and at the magnetization of the transient electron.[54−56] Further studies are needed to clarify such mechanism.

Temperature-Dependent Single-Molecule Transport. To further demonstrate that the observed single-molecule spin-dependent transport depends on the paramagnetic properties of the molecule, we also examined the conductance switching of the single-molecule Fe^{II} complex $[Fe(tzpy)_2(NCSe)_2]$ device as a function of temperature. This compound transits from a high-spin state at room temperature ($t_{2g}^4e_g^2$), to a low-spin state below ~250 K, so the current blockage under α-up Ni electrode magnetization should not be observed at low temperatures. To test this hypothesis, single-molecule wires were characterized in a vacuum STM break-junction system (see experimental details in SI section 4.9). Figure 3a,b shows comparable conductance histograms for the two β-down and α-up Ni electrode magnetic polarizations respectively as a function of the sample temperature. At low temperatures (well below the spin transition at ~250 K), a single-molecule feature is observed, which is independent of the magnetic polarization (α-up, β-down) of the Ni tip, comparable to what we observe in the low-spin $[FeL^A(NCS)_2]$ at room temperature (Figure 2c). The observed ~5-fold difference in conductance between both low-spin scenarios ($[FeL^A(NCS)_2]$ at room temperature and $[Fe(tzpy)_2(NCSe)_2]$ at low temperature) can be ascribed to the different ligand field for the Fe center in both complexes as well as the different anchoring group, going from the more −SCN to the less resistive −SeCN. In the α-up case, a monotonic decrease of the peak height in the single-molecule conductance histograms is observed as the temperature crosses the transition point (~250 K) of the spin-crossover compound from the low to the high electronic spin configuration (see SI section 3.2). At temperatures close to room temperature, the conductance histogram displays no maximum under this α-up Ni electrode polarization in analogy to the one presented in Figure 2b (orange) for the same compound measured under ambient conditions. Likewise, a single-molecule feature is observed at 298 K under β-down Ni polarization (Figure 3a), which is similar to the measurements under same polarization in ambient conditions (Figure 2b). The slight <2-fold observed difference in conductance is likely due to the different environments (vacuum versus organic medium, see Experimental Section) Note that the conductance values for the low-spin and the high-spin molecular wires are statistically indistinguishable, and they are also similar, within the experimental error, to both β-down and nonpolarized Ni electrodes. The same results were also found for the

DOI: 10.1021/acs.nanolett.5b03571
Nano Lett. 2016, 16, 218−226

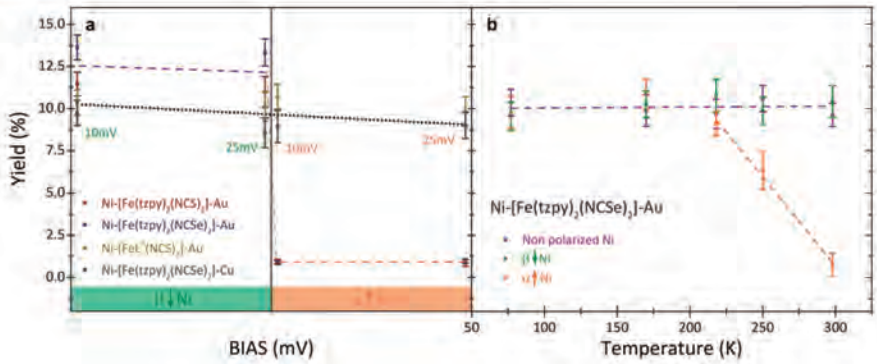

Figure 4. Yield values (%) of current plateau appearance in single-molecule experiments. The β-down and α-up Ni polarizations are in green and orange, respectively. (a) The three different complexes $[Fe(tzpy)_2(NCS)_2]$, $[Fe(tzpy)_2(NCSe)_2]$, and diamagnetic $[FeL^A(NCS)_2]$ are showed in red, blue, and yellow, respectively. Transport measurements with the Cu electrode are showed in gray. Different points correspond to different bias voltages and the error bars denote the standard deviation from different experiments. (b) The paramagnetic $[Fe(tzpy)_2(NCSe)_2]$ was also measured as a function of temperature under both Ni polarizations showing the spin transition under the α-up Ni polarization. The dotted lines connect the average points as a visual guide.

experiments performed under ambient conditions (see Figures 2b and SI12). These observations suggest that one of the spin-polarized channels (the α channel) at the molecule/Au interface fundamentally dominates the conducting state of the paramagnetic spin-crossover molecular junction in all cases.

The results in Figures 2 and 3 can be also analyzed in terms of the frequency of the observed single-molecule events in the experimental curves, named molecular junction yield (%). Because the spin-polarization effect can be also subjected to statistical variations even under a fixed Ni magnetic polarization (not every electron crossing the junction will be spin-polarized), the single-molecule yield will bring a more statistically meaningful picture to the observed spin-dependent single-molecule conductance behavior. The yield in single-molecule experiments represents the percentage of individual traces that display current plateaus over the total number of curves acquired. When this number is low (below 1%), no peaks in the conductance histogram are observed, meaning that the measured conductance of any formed molecular junction between the electrodes is statistically outside the experimentally accessible current range. Figure 4a summarizes the experimental yield of the single-molecule transport experiments in ambient conditions for all studied Fe compounds under the two Ni magnetic polarizations.

All three compounds, the paramagnetic $[Fe(tzpy)_2(NCS)_2]$ and $[Fe(tzpy)_2(NCSe)_2]$ as well as the diamagnetic $[FeL^A(NCS)_2]$, present yields above 10% for the junctions formed between the β-polarized Ni and Au electrodes, with the yield usually being larger for the $[Fe(tzpy)_2(NCSe)_2]$ complex due to its stronger binding affinity. Yields between 5% and 20% are currently obtained in well-established single-molecule contacts with dithiolated backbones (see SI section 4.7).[57,58] In contrast, when the Ni polarization is inverted, the yield for the two paramagnetic compounds drop to values below 1%, whereas the yield for the diamagnetic complex remains constant. A comparable behavior of the yield is observed as a function of the sample temperature (Figure 4b). With the α-Ni polarization, the measured yield changes from the standard values (>10%) to low values (<1%) when the increasing temperature crosses the transition temperature for this SCO compound (SI section 3.2). The observed transition occurs over a fairly wide temperature range around the bulk transition temperature, in agreement with recent spectroscopic studies of similar SCO compounds on a 2D Au nanoparticles film.[47,59] Such shallow transition is the reflection of the progressive change of the high-spin to low-spin population ratio as the temperature crosses the transition point. All together, the above result demonstrates the transition of a single-molecule wire from a high-spin (room temperature) to a low-spin state (low temperature), displaying large room temperature conductance switching (<10 000%).

Theoretical Calculations. We have considered two possible scenarios in order to explain the magnetoresistance effect when the transport is going from the Au surface to the Ni tip. The first one considers that the magnetic anisotropy of the molecule−surface ensemble is large enough to keep the molecular spin aligned in a preferent direction, and, consequently, it will result in a different transport of α and β electrons through the molecule. Alternatively, the second scenario assumes that the spin of the molecule remains aligned with the magnetization of the nickel tip, and it is the interaction of the molecular levels with some spin polarized bands of the gold surface that induce the observed spin filter behavior.

In order to check the magnitude of the magnetic anisotropy of the system, we performed theoretical CASSCF calculations using an accurate procedure to include spin−orbit effects (RASSI method, see SI section 5.2). Single-determinant methods, such as those based on DFT, fail for systems with large magnetic anisotropy. CASSCF multireference approach properly introduces the spin−orbit effect, but it is limited to nonperiodic small systems. The calculation of the isolated high spin Fe^{II} complex and such molecule deposited on small Au_4 cluster to model the structure gives in both cases moderate magnetic anisotropy (barriers around 20 K). This fact suggests the unlikeliness of the first scenario that would require a very high magnetic anisotropy to explain the observed magneto-resistance effect at room temperature.

To understand the origin of the observed spin-polarization differences in the electron currents traversing the molecular junctions and address the interplay between the changing molecule's magnetic moment (second scenario described above) and the surface states, we performed density functional theory (DFT) based calculations including SOC and modeled

DOI: 10.1021/acs.nanolett.5b03571
Nano Lett. 2016, 16, 218−226

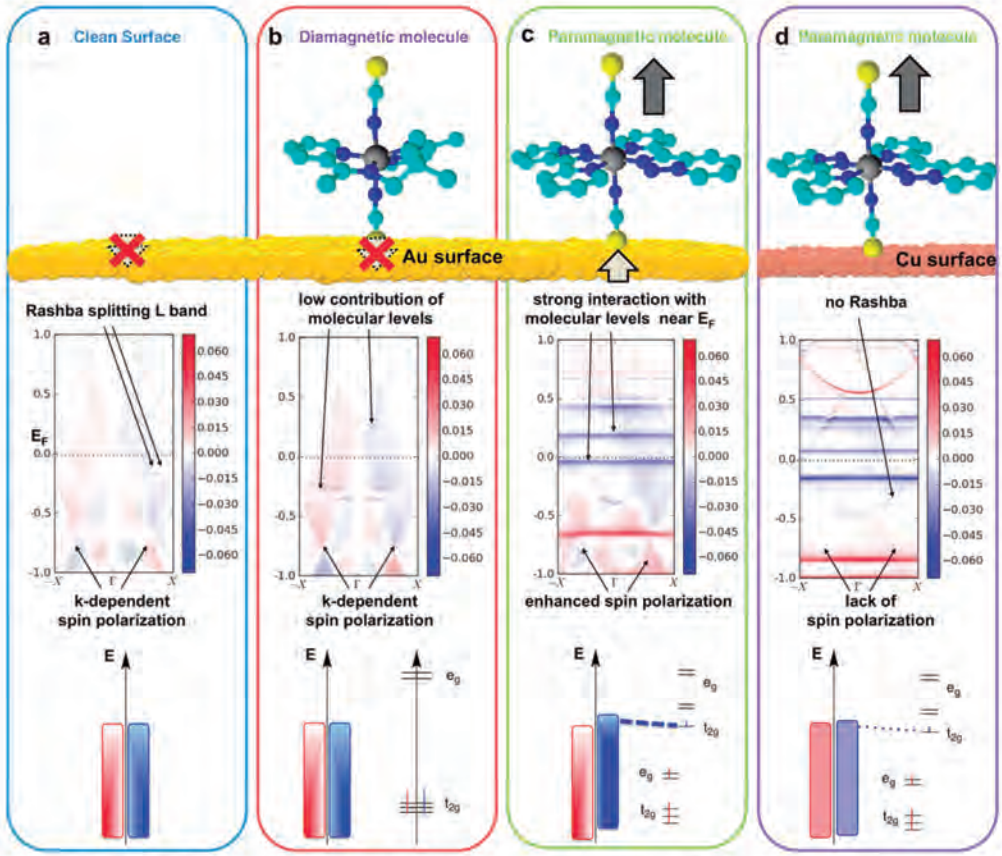

Figure 5. Calculated out of plane spin texture for the clean and covered Au(111) surface: DFT calculated logarithm of the z component of the magnetization for the DOS(α)-DOS(β) difference (central panel) and a schematic DOS representation (bottom panel) for the clean and covered Au(111) surfaces. The usual splitting of L-band and a k-dependent spin-polarization (Rashba effect) is found in the DFT calculations for the gold surface systems (a–c), also indicated with a nonuniform filling in the schematic DOS of the surface bands as opposed to the copper surface. (d) Symmetric spin-polarized levels will vanish for panels a and b when summing over the Brillouin zone. Horizontal lines correspond to the hybridized molecular levels for the high-spin Fe^{II} complex adsorbed to the electrode surface (c,d). Moreover, relative high spin polarization of the gold surface (k-dependent spin polarization) occurs when a high-spin Fe^{II} complex is strongly adsorbed through its single β t_{2g} electron (c). This effect is small when absorbed on the copper surface (d).

the surfaces as true semi-infinite systems (see SI section 5.1). We considered the four different cases employed in the nanoscale transport experiments (Figure 5a–d): (i) a clean Au(111) surface; (ii) a diamagnetic $[FeL^{A}(NCS)_2]$ molecule deposited on the same gold surface, and (iii) the paramagnetic $[Fe(tzpy)_2(NCS)_2]$ complex deposited on both Au(111) and (iv) Cu(111) surfaces. k-Resolved magnetization maps along the surface normal, $S\_z(E,k)$, projected on the surface atoms attached to the anchoring S are presented in the Figure 5a-d central panel. As expected from a strong SOC, the characteristic L-band splitting and a rich k-dependent spin texture is obtained for all gold systems, while absent in the copper surface (see also Figure S17), confirming that the Rashba effect is accurately taken into account in our calculations by the inclusion of the large spin–orbit contributions of the gold surface.[60,61] In the presence of absorbed paramagnetic molecule (Figure 5c-d), up to five minority spin molecular levels (horizontal blue lines) hybridize with the metal and become transport-dominant around the Fermi level.

In Figure 5a–c, we present the density of states (DOS, majority-α colored in red and minority-β in blue) of the studied interfaces (see calculations in SI section 5). Indeed, for the nonmagnetic cases (Figure 5a,b), the DOS of the gold electrodes has a k-dependent spin polarization due to the large spin–orbit effects (red versus blue regions in Figure 5), but cancels out when summing over the Brillouin zone (strong symmetry in the k-dependent spin-polarized DOS in Figures 5a,b). For the paramagnetic molecule absorbed on a Au surface (Figure 5c), there is a fairly strong interaction of the single spin molecular levels with the metal energy levels around the Fermi energy. It is worth noting the small hybridization of the molecular orbitals in the $[FeL^{A}(NCS)_2]$ complex with the surface due to the nonbonding nature of the t_{2g} orbitals (see Figure 5b and also Figure S17b). The paramagnetic $[Fe(tzpy)_2(NCS)_2]$ complex induces a small spin delocalization[62]

DOI: 10.1021/acs.nanolett.5b03571
Nano Lett. 2016, 16, 218–226

(same sign as that of the molecule) in the three gold atoms directly bonded to the anchoring sulfur atom (0.004 e^- with same sign as that of the molecule, Figure 5c), which is not fully compensated by an opposite spin density of 0.002 e^- found for the rest of the gold surface layer (see Table S1). The results for the Cu/paramagnetic molecule scenario reveal a very low increase of the spin polarization of the surface (Figure 5d) after the interaction with the high spin Fe^{II} complex, in contrast to the Au/paramagnetic molecule case (Figure 5c).

The above theoretical analysis reveals the key ingredients that determine the spin-dependent transport measured in the single-molecule experiments (Figure 2); the effective SOC and its interplay with the induced spin polarization at the metallic surface is responsible for the spin-polarization of the electrons traversing the Au electrode/paramagnetic compound interface. This spin-polarized current crosses the single-molecule bridge and translates into different conductances values depending on the particular α- or β-magnetization of the Ni electrode, and results in the observed overall conductance switching of the single-molecule device.

The experimental results are also in agreement with previous DFT transport calculations showing a large preference for the minority carriers in the high-spin d^6 Fe^{II} complexes, i.e., $[Fe(tzpy)_2(NCS)_2]$ and $[Fe(tzpy)_2(NCSe)_2]$ S = 2 complexes.[40] Assuming five α and one β electrons, the highest occupied (HOMO) and lowest unoccupied (LUMO) β-molecular orbital levels lie very close to the electrode Fermi levels (Figure 5c) and they are responsible for the spin-polarized transport. In addition, there is an enhancement of the spin polarization of the gold surface due to the interaction with the magnetic molecule (Figure 5c). This spin polarization of the gold levels results in a favorable interaction with one of the two molecular channels that explains the observed conductance change as a function of the Ni electrode magnetization direction. The t_{2g} and e_g levels for the diamagnetic $[FeL^A(NCS)_2]$ complex are identically occupied, therefore, α and β channels are equivalent and, consequently, no spin-dependent transport is observed. The spin-polarized Au electrode/paramagnetic molecule interface (also present in carbon nanotube based devices)[22−24] is the critical effect that allows the spin-polarized current, and it is both experimentally and theoretically corroborated by the lack of such an effect in the homologous copper device (Figures 2d and 5d).

It is noted here that the proposed calculation corresponds to an analysis of the electronic structure of the molecule−surface interface aimed for the identification of key points that consistently explain the observed dependence of the current on (i) the tip magnetization direction, (ii) the material of the electrode (Au or Cu), and (iii) the spin state of the bridging molecule. The accurate calculation of the transmission function would correspond to the bias-dependent current that is beyond the two-channel model and out of reach for current computational methodologies.

Experimental Section. Relevant methodological details are included in this section. For further details, an extended version is available in the SI file linked to this work.

Surface Preparation. A Au(111) single crystal (Matek, Germany) was surface-functionalized with either $[Fe(tzpy)_2(NCS)_2]$ or $[Fe(tzpy)_2(NCSe)_2]$ compounds (basic information on the synthesis and characterization can be found in the SI sections 3.1 and 3.2)[47] by immersion in a μM ethanolic solution of the target compound for periods longer than 6 h. XPS measurements of the resulting SAMs confirmed the presence of the Fe complex on the Au surface as well as the formation of an Au−S/Au-Se bond (see SI sections 1.2). In order to avoid formation of molecular aggregates in solution during the absorption of the target compounds onto the Au surface, we used concentrations within the low Lambert−Beer range (see SI section 1.1). The last point is determinant to get clean single-molecule transport results.

Conductance Measurements. An STM-BJ method[15] was employed to build and characterize charge transport through single-molecule wires built with the different Fe^{II} complexes studied in this work. The two biased (−10 mV) electrodes in the molecular junction, a Au(111) single crystal (99.99% Matek, Germany) and a mechanically cut polycrystalline Ni wire (99.99%, Godfellow, UK) were used as the support and the STM top electrodes, respectively. In a regular STM-BJ experiment (see manuscript), the Ni tip was repeatedly driven onto the Au surface in the presence of molecules (unless indicated), while simultaneously monitoring the current flowing between them. Several thousands (~5000) retraction curves were then stored and used to build the conductance histogram of the single-molecule device. Because not every curve displayed plateau features corresponding to the molecular quantum conductance of the single-molecule bridge, we designed an automatic algorithm that identifies and selects curves containing such single-molecule features. The exact same selection criteria were applied throughout all measured series. To avoid the Ni wire oxidation under ambient conditions, the prepared Ni electrode was magnetically polarized and stored under in anaerobic conditions before use. All experiments were conducted in an organic solvent mesitylene (unless otherwise indicated) with very low oxygen and water solubility. The Ni tip oxidation was monitored during use by ex situ SEM-EDS electron microscopy (see SI section 2.2).

Computational Calculations. DFT calculations were performed with the GREEN code[63] and its interface to the DFT-based SIESTA package[64] including the recently implemented fully relativistic pseudopotential (PP) formalism, in order to account for spin−orbit coupling (SOC) contributions[65] (see SI section 5.1 for more details). CASSCF-RASSI calculations were conducted to determine the magnetic anisotropy of the Fe^{II} complex and the molecule deposited on Au_4 cluster (see SI section 5.2 for more details).

Conclusion. We present an example of large room temperature conductance switching based on spin-dependent transport in a single-molecule device that results upon the strong interaction of a paramagnetic molecule with heavy-metal surface atoms. This finding represents a new form of generating large magnetoresistance effects in a single-molecule device in the absence of an applied external magnetic field. Our qualitative theoretical model sets the key ingredients to account for the observed large spin-dependent conductance switching in the single-molecule device: (i) Engineering a hybrid electrode/molecule interface that results in spin-polarized states. This spinterface is responsible for the polarization of the current flowing through the single-molecule contact. (ii) Selecting a paramagnetic molecule with appropriate electronic structure, as the high-spin Fe^{II} complexes, to favor transport through one of the spin channels. (iii) Using a spin-polarized ferromagnetic electrode on one side of the single-molecule junction that acts as the spin-polarized electron *drain*. Imposing different directions of the top electrode's magnetic polarization then controls the observed magnetoresistance.

DOI: 10.1021/acs.nanolett.5b03571
Nano Lett. 2016, 16, 218−226

These experiments demonstrate the crucial role that the molecule–surface magnetic interactions, the spinterface,[66] have on the design of the next generation of nanoscale spintronic devices and set the basis for future design of nanoscale magnetic molecular circuits.

■ ASSOCIATED CONTENT

Supporting Information

The Supporting Information is available free of charge on the ACS Publications website at DOI: 10.1021/acs.nanolett.5b03571.

Sample characterization (section S1), Ni electrodes characterization (section S2), preparation and magnetic characterization of the molecular system SAMs (section S3), single-molecule transport measurements (section S4), and computational details (section S5) (PDF)

■ AUTHOR INFORMATION

Corresponding Authors

*E-mail: isma_diez@ub.edu.
*E-mail: eliseo.ruiz@qi.ub.es.
*E-mail: jhihath@ucdavis.edu.

Notes

The authors declare no competing financial interest.

■ ACKNOWLEDGMENTS

This research was supported by the Spanish *Ministerio de Economía y Competitividad* (Grants CTQ2012-36090, CTQ2011-23862-C02-01, MAT2013-47878-C2-R and CTQ2010-18414 and *Generalitat Valenciana* (GVPROMETEO2012-049) as well as the United States National Science Foundation (J.H. and H.L. ECCS-1231915). D.A. thanks *Conicyt-Chile* for a predoctoral fellowship. A.C.A. and Z.A.-C. thank the Spanish *Ministerio de Educación, Cultura y Deporte* for graduate FPU fellowships. I.D.-P. thanks the Ramon y Cajal program (MINECO) and the EU Reintegration Grant (FP7-PEOPLE-2010-RG-277182) for financial support. E.R. thanks Generalitat de Catalunya for an ICREA academia award. The authors acknowledge the general facilities of the University of Barcelona (CCiT-UB) and the computer resources, technical expertise, and assistance provided by the Barcelona Supercomputing Centre.

■ REFERENCES

(1) Wolf, S. A.; Awschalom, D. D.; Buhrman, R. A.; Daughton, J. M.; von Molnar, S.; Roukes, M. L.; Chtchelkanova, A. Y.; Treger, D. M. *Science* **2001**, *294*, 1488.
(2) Zutic, I.; Fabian, J.; Das Sarma, S. *Rev. Mod. Phys.* **2004**, *76*, 323.
(3) Sinova, J.; Žutić, I. *Nat. Mater.* **2012**, *11*, 368.
(4) Sanvito, S. *Chem. Soc. Rev.* **2011**, *40*, 3336.
(5) Schmaus, S.; Bagrets, A.; Nahas, Y.; Yamada, T. K.; Bork, A.; Bowen, M.; Beaurepaire, E.; Evers, F.; Wulfhekel, W. *Nat. Nanotechnol.* **2011**, *6*, 185.
(6) Schwobel, J.; Fu, Y. S.; Brede, J.; Dilullo, A.; Hoffmann, G.; Klyatskaya, S.; Ruben, M.; Wiesendanger, R. *Nat. Commun.* **2012**, *3*, 953.
(7) Wiesendanger, R. *Rev. Mod. Phys.* **2009**, *81*, 1495.
(8) Mugarza, A.; Krull, C.; Robles, R.; Stepanow, S.; Ceballos, G.; Gambardella, P. *Nat. Commun.* **2011**, *2*, 490.
(9) Krull, C.; Robles, R.; Mugarza, A.; Gambardella, P. *Nat. Mater.* **2013**, *12*, 337.
(10) Alam, M. S.; Stocker, M.; Gieb, K.; Müller, P.; Haryono, M.; Student, K.; Grohmann, A. *Angew. Chem., Int. Ed.* **2010**, *49*, 1159.
(11) Mugarza, A.; Robles, R.; Krull, C.; Korytár, R.; Lorente, N.; Gambardella, P. *Phys. Rev. B: Condens. Matter Mater. Phys.* **2012**, *85*, 155437.
(12) Miyamachi, T.; Gruber, M.; Davesne, V.; Bowen, M.; Boukari, S.; Joly, L.; Scheurer, F.; Rogez, G.; Yamada, T. K.; Ohresser, P.; Beaurepaire, E.; Wulfhekel, W. *Nat. Commun.* **2012**, *3*, 938.
(13) Ramachandran, G. K.; Hopson, T. J.; Rawlett, A. M.; Nagahara, L. A.; Primak, A.; Lindsay, S. M. *Science* **2003**, *300*, 1413.
(14) Reed, M. A.; Zhou, C.; Muller, C. J.; Burgin, T. P.; Tour, J. M. *Science* **1997**, *278*, 252.
(15) Xu, B.; Tao, N. J. *Science* **2003**, *301*, 1221.
(16) Heersche, H. B.; de Groot, Z.; Folk, J. A.; van der Zant, H. S. J.; Romeike, C.; Wegewijs, M. R.; Zobbi, L.; Barreca, D.; Tondello, E.; Cornia, A. *Phys. Rev. Lett.* **2006**, *96*, 206801.
(17) Parks, J. J.; Champagne, A. R.; Costi, T. A.; Shum, W. W.; Pasupathy, A. N.; Neuscamman, E.; Flores-Torres, S.; Cornaglia, P. S.; Aligia, A. A.; Balseiro, C. A.; Chan, G. K.-L.; Abruña, H. D.; Ralph, D. C. *Science* **2010**, *328*, 1370.
(18) Burzurí, E.; Zyazin, A. S.; Cornia, A.; van der Zant, H. S. J. *Phys. Rev. Lett.* **2012**, *109*, 147203.
(19) Bagrets, A.; Schmaus, S.; Jaafar, A.; Kramczynski, D.; Yamada, T. K.; Alouani, M.; Wulfhekel, W.; Evers, F. *Nano Lett.* **2012**, *12*, 5131.
(20) Li, J.-J.; Bai, M.-L.; Chen, Z.-B.; Zhou, X.-S.; Shi, Z.; Zhang, M.; Ding, S.-Y.; Hou, S.-M.; Schwarzacher, W.; Nichols, R. J.; Mao, B.-W. *J. Am. Chem. Soc.* **2015**, *137*, 5923.
(21) Mannini, M.; Pineider, F.; Sainctavit, P.; Danieli, C.; Otero, E.; Sciancalepore, C.; Talarico, A. M.; Arrio, M.-A.; Cornia, A.; Gatteschi, D.; Sessoli, R. *Nat. Mater.* **2009**, *8*, 194.
(22) Urdampilleta, M.; Klyatskaya, S.; Cleuziou, J. P.; Ruben, M.; Wernsdorfer, W. *Nat. Mater.* **2011**, *10*, 502.
(23) Vincent, R.; Klyatskaya, S.; Ruben, M.; Wernsdorfer, W.; Balestro, F. *Nature* **2012**, *488*, 357.
(24) Ganzhorn, M.; Klyatskaya, S.; Ruben, M.; Wernsdorfer, W. *Nat. Nanotechnol.* **2013**, *8*, 165.
(25) Komeda, T.; Isshiki, H.; Liu, J.; Zhang, Y.-F.; Lorente, N.; Katoh, K.; Breedlove, B. K.; Yamashita, M. *Nat. Commun.* **2011**, *2*, 217.
(26) Lodi Rizzini, A.; Krull, C.; Balashov, T.; Kavich, J. J.; Mugarza, A.; Miedema, P. S.; Thakur, P. K.; Sessi, V.; Klyatskaya, S.; Ruben, M.; Stepanow, S.; Gambardella, P. *Phys. Rev. Lett.* **2011**, *107*, 177205.
(27) Xie, Z.; Markus, T. Z.; Cohen, S. R.; Vager, Z.; Gutierrez, R.; Naaman, R. *Nano Lett.* **2011**, *11*, 4652.
(28) Yeganeh, S.; Ratner, M. A.; Medina, E.; Mujica, V. *J. Chem. Phys.* **2009**, *131*, 014707.
(29) Göhler, B.; Hamelbeck, V.; Markus, T. Z.; Kettner, M.; Hanne, G. F.; Vager, Z.; Naaman, R.; Zacharias, H. *Science* **2011**, *331*, 894.
(30) Carmeli, I.; Leitus, G.; Naaman, R.; Reich, S.; Vager, Z. *J. Chem. Phys.* **2003**, *118*, 10372.
(31) Naaman, R.; Vager, Z. *Phys. Chem. Chem. Phys.* **2006**, *8*, 2217.
(32) Vager, Z.; Naaman, R. *Chem. Phys.* **2002**, *281*, 305.
(33) Nealon, G. L.; Donnio, B.; Greget, R.; Kappler, J. P.; Terazzi, E.; Gallani, J. L. *Nanoscale* **2012**, *4*, 5244.
(34) Hernando, A.; Crespo, P.; Garcia, M. A.; Pinel, E. F.; de la Venta, J.; Fernandez, A.; Penades, S. *Phys. Rev. B: Condens. Matter Mater. Phys.* **2006**, *74*, 052403.
(35) Bychkov, Y. A.; Rashba, E. I. *J. Phys. C: Solid State Phys.* **1984**, *17*, 6039.
(36) Koga, T.; Nitta, J.; Takayanagi, H.; Datta, S. *Phys. Rev. Lett.* **2002**, *88*, 126601.
(37) Ting, D. Z. Y.; Cartoixa, X. *Appl. Phys. Lett.* **2002**, *81*, 4198.
(38) Halcrow, M. A. *Spin-Crossover Materials: Properties and Applications*; Wiley: Chichester, U.K., 2013.
(39) Ruiz, E. *Phys. Chem. Chem. Phys.* **2014**, *16*, 14.
(40) Aravena, D.; Ruiz, E. *J. Am. Chem. Soc.* **2012**, *134*, 777.
(41) Baadji, N.; Sanvito, S. *Phys. Rev. Lett.* **2012**, *108*, 217201.
(42) Martinho, P. N.; Rajnak, C.; Ruben, M. In *Spin-Crossover Materials: Properties and Applications*; John Wiley & Sons, Ltd: Chichester, U.K., 2013; p 375.
(43) Meded, V.; Bagrets, A.; Fink, K.; Chandrasekar, R.; Ruben, M.; Evers, F.; Bernand-Mantel, A.; Seldenthuis, J. S.; Beukman, A.; van der

DOI: 10.1021/acs.nanolett.5b03571
Nano Lett. 2016, 16, 218−226

Zant, H. S. J. *Phys. Rev. B: Condens. Matter Mater. Phys.* **2011**, *83*, 245415.
(44) Wagner, S.; Kisslinger, F.; Ballmann, S.; Schramm, F.; Chandrasekar, R.; Bodenstein, T.; Fuhr, O.; Secker, D.; Fink, K.; Ruben, M.; Weber, H. B. *Nat. Nanotechnol.* **2013**, *8*, 575.
(45) Gopakumar, T. G.; Matino, F.; Naggert, H.; Bannwarth, A.; Tuczek, F.; Berndt, R. *Angew. Chem., Int. Ed.* **2012**, *51*, 6262.
(46) Prins, F.; Monrabal-Capilla, M.; Osorio, E. A.; Coronado, E.; van der Zant, H. S. J. *Adv. Mater.* **2011**, *23*, 1545.
(47) Niel, V.; Gaspar, A. B.; Munoz, M. C.; Abarca, B.; Ballesteros, R.; Real, J. A. *Inorg. Chem.* **2003**, *42*, 4782.
(48) Lissel, F.; Schwarz, F.; Blacque, O.; Riel, H.; Lörtscher, E.; Venkatesan, K.; Berke, H. *J. Am. Chem. Soc.* **2014**, *136*, 14560.
(49) Johnson, M. *Handbook of Spin Transport and Magnetism*; Chapman and Hall/CRC: Boca Raton, FL, 2011.
(50) Xia, J. L.; Diez-Perez, I.; Tao, N. J. *Nano Lett.* **2008**, *8*, 1960.
(51) Ko, C.-H.; Huang, M.-J.; Fu, M.-D.; Chen, C.-h. *J. Am. Chem. Soc.* **2010**, *132*, 756.
(52) Brefuel, N.; Vang, I.; Shova, S.; Dahan, F.; Costes, J. P.; Tuchagues, J. P. *Polyhedron* **2007**, *26*, 1745.
(53) Kiguchi, M.; Ohto, T.; Fujii, S.; Sugiyasu, K.; Nakajima, S.; Takeuchi, M.; Nakamura, H. *J. Am. Chem. Soc.* **2014**, *136*, 7327.
(54) Tserkovnyak, Y.; Brataas, A.; Bauer, G. E. W.; Halperin, B. I. *Rev. Mod. Phys.* **2005**, *77*, 1375.
(55) Haney, P. M.; et al. *Phys. Rev. B: Condens. Matter Mater. Phys.* **2007**, *76*, 024404.
(56) Jiang, L.; Liu, X.; Zhang, Z.; Wang, R. *Phys. Lett. A* **2014**, *378*, 426.
(57) Li; Hihath, J.; Chen, F.; Masuda, T.; Zang, L.; Tao. *J. Am. Chem. Soc.* **2007**, *129*, 11535.
(58) Hines, T.; Díez-Pérez, I.; Nakamura, H.; Shimazaki, T.; Asai, Y.; Tao, N. *J. Am. Chem. Soc.* **2013**, *135*, 3319.
(59) Devid, E. J.; Martinho, P. N.; Kamalakar, M. V.; Šalitroš, I.; Prendergast, Ú.; Dayen, J.-F.; Meded, V.; Lemma, T.; González-Prieto, R.; Evers, F.; Keyes, T. E.; Ruben, M.; Doudin, B.; van der Molen, S. J. *ACS Nano* **2015**, *9*, 4496.
(60) Mazzarello, R.; Corso, A. D.; Tosatti, E. *Surf. Sci.* **2008**, *602*, 893.
(61) Kosugi, T.; Miyake, T.; Ishibashi, S. *J. Phys. Soc. Jpn.* **2011**, *80*, 074713.
(62) Cano, J.; Ruiz, E.; Alvarez, S.; Verdaguer, M. *Comments Inorg. Chem.* **1998**, *20*, 27.
(63) Cerda, J.; Van Hove, M. A.; Sautet, P.; Salmeron, M. *Phys. Rev. B: Condens. Matter Mater. Phys.* **1997**, *56*, 15885.
(64) Soler, J. M.; Artacho, E.; Gale, J. D.; Garcia, A.; Junquera, J.; Ordejon, P.; Sanchez-Portal, D. *J. Phys.: Condens. Matter* **2002**, *14*, 2745.
(65) Cuadrado, R.; Cerda, J. I. *J. Phys.: Condens. Matter* **2012**, *24*, 086005.
(66) Sanvito, S. *Nat. Phys.* **2010**, *6*, 562.

DOI: 10.1021/acs.nanolett.5b03571
Nano Lett. 2016, 16, 218−226

Supporting information (SI)

Large Conductance Switching in a Single-Molecule Device through Room Temperature Spin-dependent Transport

Albert C. Aragonès, [†,§] Daniel Aravena,[‡,#] Jorge I. Cerdá,[∥] Zulema Acís-Castillo,[⊥] Haipeng Li[¶], José Antonio Real,[⊥] Fausto Sanz, [†,§], Josh Hihath,[¶*] Eliseo Ruiz,[‡*] Ismael Díez-Pérez [†,§*]

[†] Departament de Química Física, Universitat de Barcelona, Martí i Franquès 1, 08028 Barcelona, Spain and Institute for Bioengineering of Catalonia (IBEC) Baldiri Reixac 15-21, Barcelona 08028 Spain

[§] Centro Investigación Biomédica en Red (CIBER-BBN). Campus Río Ebro-Edificio I+D, Poeta Mariano Esquillor s/n, 50018 Zaragoza, Spain.

[‡] Departament de Química Inorgànica and Institut de Química Teòrica i Computacional, Universitat de Barcelona, Diagonal 645, 08028 Barcelona, Spain

[#] Departamento de Química de los Materiales, Facultad de Química y Biología, Universidad de Santiago de Chile (USACH), Casilla 40, Correo 33, Chile

[∥] Instituto de Ciencia de Materiales de Madrid, CSIC, Cantoblanco, 28049 Madrid, Spain

[⊥] Institut de Ciència Molecular (ICMol), Universitat de València, 46980 Paterna, València, Spain

[¶] Department of Electrical and Computing Engineering, University of California-Davis, 2064 Kemper Hall, Davis, CA 95616

1. Sample characterization

1.1. *UV-visible absorbance spectra of the paramagnetic compounds*

UV-visible spectra were recorded from μM ethanolic solutions of the paramagnetic compounds prior to SAM formation. All main absorbance peaks ranged between 400 and 470 nm (Figure S1). Comparison between Fe^{II}-complex solutions preserved under Ar atmosphere and the same solutions bubbled with pure O_2 shows that $[Fe(tzpy)_2(NCS)_2]$ can be oxidized in solution under ambient conditions (see peak shift in S1). Contrarily, $[Fe(tzpy)_2(NCSe)_2]$ show no evident signs of oxidation. The $[Fe(tzpy)_2(NCS)_2]$ solutions were kept under strict inert atmosphere and the oxidation degree of the compound monitored by UV-visible spectroscopy.

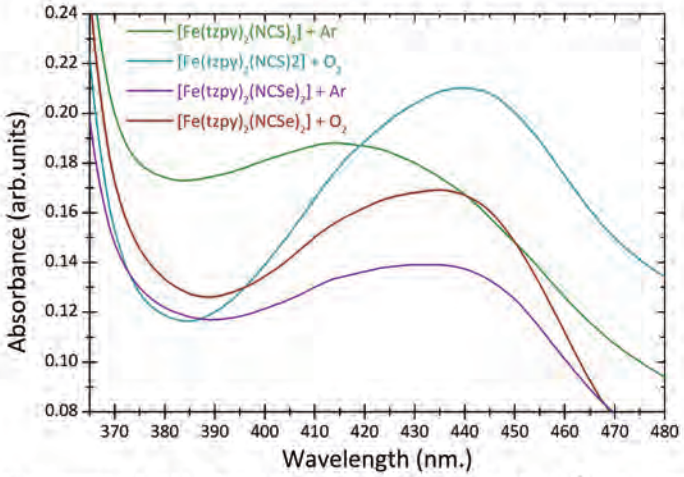

Figure S1. UV-visible spectra of μM ethanolic solutions of $[Fe(tzpy)_2(NCS)_2]$ and $[Fe(tzpy)_2(NCSe)_2]$ under different environmental conditions.

To avoid formation of aggregates in solution during the SAM preparation, we used concentrations within the Lambert-Beer range (Figure S2). The employed concentrations for the SAM preparation of both complexes were between 20 and 25 μM. Concentrations in the lower Lambert-Beer range were kept to avoid multilayer formations.

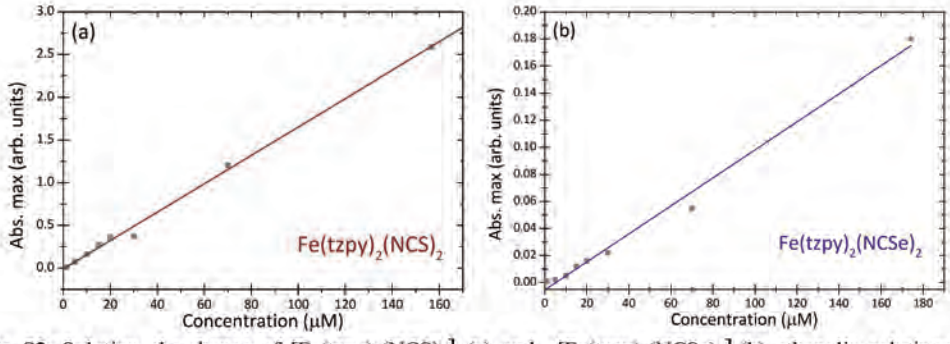

Figure S2. Solution absorbance of $[Fe(tzpy)_2(NCS)_2]$ (a) and $[Fe(tzpy)_2(NCSe)_2]$ (b) ethanolic solutions as a function of the compound concentration.

1.2. *XPS measurements*

X-Ray Photoelectron Spectroscopy (XPS) measurements were performed to confirm the absorption of the Fe-complex onto the Au surface electrode and the binding chemistry. Figure S3a shows the Fe 2p binding energy thus confirming the presence of the Fe-complex on the Au electrode surface. The 0.2-0.3 eV displacement for the Au 4f binding energy (Figure S3b) evidences the S/Se-Au bond formation[1-4].

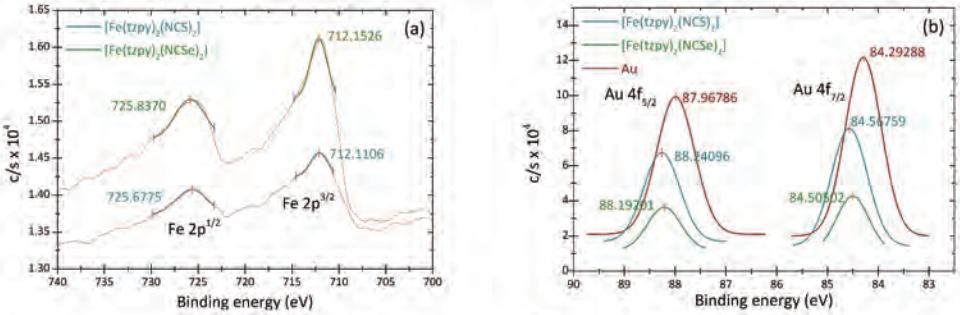

Figure S3. (a) XPS Fe2p signal of Au electrodes modified with $[Fe(tzpy)_2(NCS)_2]$ and $[Fe(tzpy)_2(NCSe)_2]$. (b) XPS Au 4f signal of a bare Au substrate (red), and a Au modified electrode with $[Fe(tzpy)_2(NCS)_2]$ (cyan) and $[Fe(tzpy)_2(NCSe)_2]$ SAMs (green).

2. Ni electrodes characterization

2.1. *Imaging Au(111) with Ni tips*

Figure S4 corresponds to STM images recorded with a freshly mechanically cut Ni tip stored under an Ar atmosphere. Typical steps and terraces of the Au(111) surface are observed (step height ~0.23 nm). Similar characteristic features from the Au(111) single crystal surface were observed in the images recorded before and after single-molecule transport experiments were performed in the working organic medium (Figures S4a and b, respectively) with the only appearance of extra steps/defects due to the sudden tip-surface interactions (in S4b). These results imply that the tip preserves its sharpness and metallic nature. We observed a decrease of the image quality or even complete image lost when using Ni tips that were exposed to ambient conditions for periods of minutes. The surface oxidation state of the Ni electrodes becomes a critical parameter for the reproducibility of the single-molecule transport measurements (see SI section 2.2).

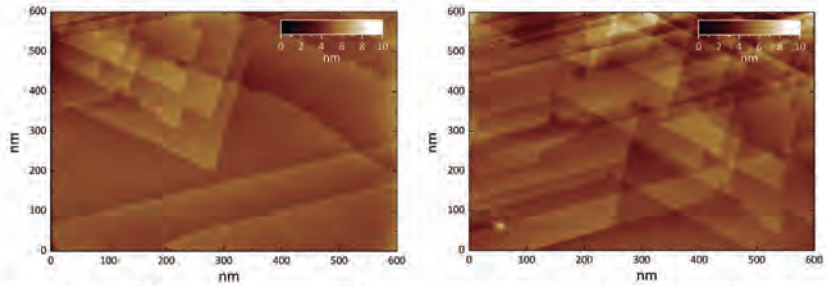

Figure S4. STM images of a bare Au(111) surface in mesetylene using a freshly cut Ni tip before (a) and after (b) single-molecule experiments. The images were recorded at 0.1 nA set point current and 30 mV bias.

2.2. *SEM-EDS measurements*

Ni tips oxidation was qualitatively monitored using Energy Dispersive Spectroscopy (EDS) in an electron microscope (SEM). In order to follow the surface Ni oxidation upon exposure to ambient conditions, three different Ni tips were analysed: a freshly cut tip, a tip exposed to the atmosphere for 120 minutes and a tip stored under Ar atmosphere for 120 minutes. Each Ni tip was analysed before and after performing single-molecule junction experiments. All measurements were done at the tip apex that was the active part in the single-molecule transport experiments. A point of the Ni wire away from the tip apex was also measured as a control (Figure S5 insets). Freshly cut Ni tips present the lowest oxygen content versus non-preserved tips under an inert atmosphere, which present the highest (Figure S5a-b). Note that due to the different total integration times among the different EDS recording, peak absolute values cannot be compared and so the O-to-Ni ratio is used instead for comparison between spectra. Tips preserved under an Ar atmosphere present a slightly higher surface oxidation compare to a freshly cut tip (Figure S5c). Importantly, only a slight increased oxidation of the Ni tip apex is observed after the single-molecule experiment is conducted (Figure S5a-c).

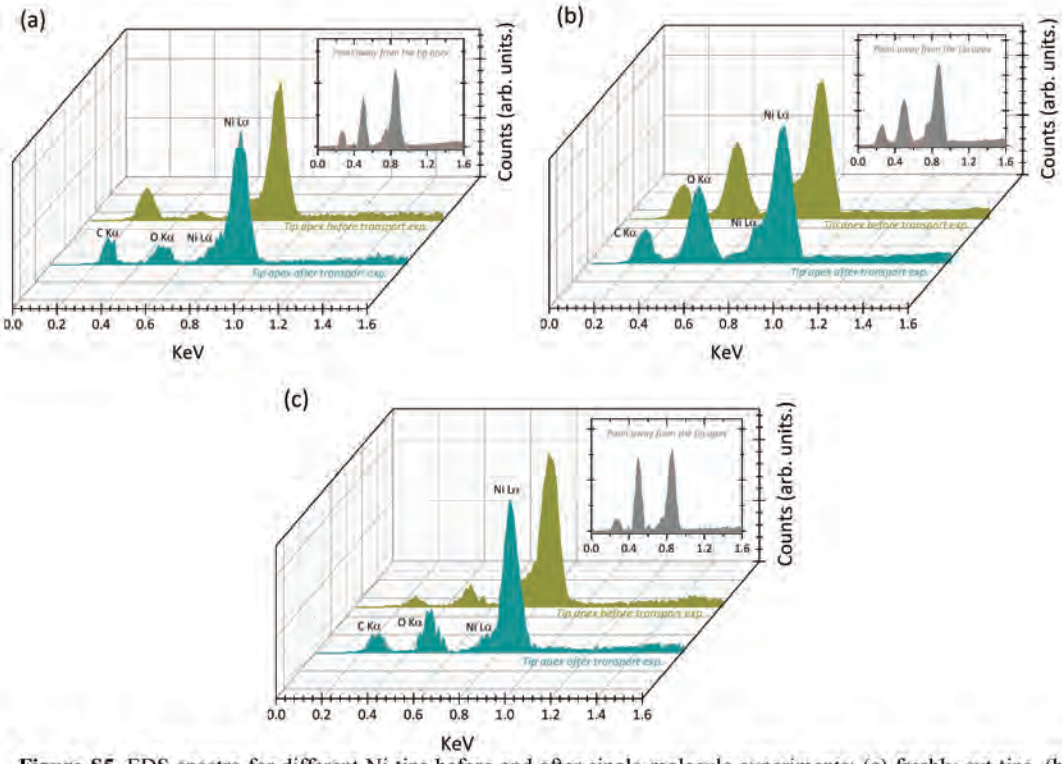

Figure S5. EDS spectra for different Ni tips before and after single-molecule experiments: (a) freshly cut tips, (b) non-preserved tips and (c) preserved tip under an Ar atmosphere. Figure insets are EDS in a point away from the tip apex.

2.3. *Characterization of the Ni tip magnetization*

Measurements of the Ni tips magnetization with SQUID were conducted to monitor the Ni tip magnetization before and after single-molecule transport experiments were performed. We magnetized the Ni tips by place them in a close proximity to a commercial 1T NdFeB magnet (see manuscript). The permanent Ni tip magnetization (at zero applied magnetic field) is indicated by arrows in the magnetization curves (Figure S6). Ni tips magnetized with opposite poles of the magnet display inverted magnetizations. Following the same convention used through all the manuscript, the Ni spin up (α) corresponds to negative magnetization obtained by polarizing the tip near the magnet north pole, and the Ni spin down (β) to positive magnetization obtained by polarizing the tip near the magnet south pole (Figure S6a). Increasing exposure times near the magnet results in progressively larger tip magnetizations (Figures S6a-c) until a saturation value of 30 emu·g^{-1} is reached at magnetization times over 2 hours. Magnetization times over this value were employed to magnetize the Ni electrodes for single-molecule transport experiments. Magnetizing the tip under larger magnetic fields using the SQUID magnet did not result in a larger initial Ni tip magnetization (Figure S6c). Roughly >80% of the initial Ni tip magnetization remained after single-molecule junction experiments were performed with the same tip. Differences in the M values obtained before and after the break-junction experiment are most likely due to slight differences in the tip tilting orientation at the SQUID sample holder.

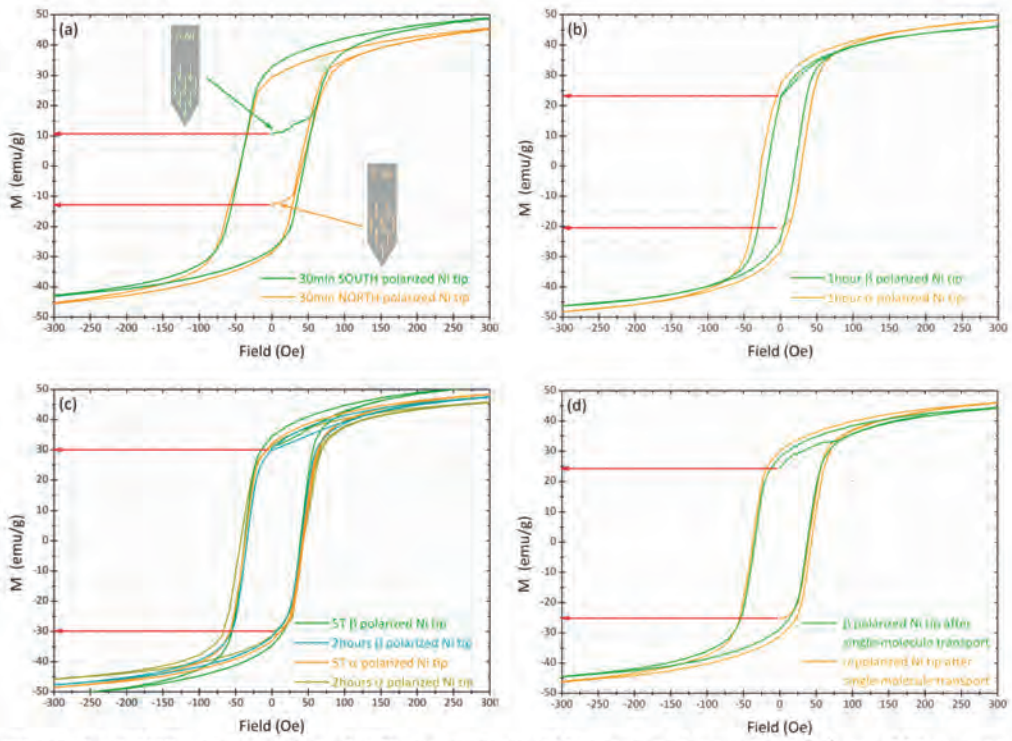

Figure S6. SQUID measurements of different magnetized Ni tips. (a-c) Magnetization times of 30 minutes, 1 hour and 2 hours, respectively. In (c), comparison with a 1h magnetized Ni tip under 5T magnetic field. (d) Measurements of 2 hours magnetized Ni tips after single-molecule transport experiments.

3. Preparation and magnetic characterization of the molecular systems SAMs

3.1 Synthesis

The organic ligands tzpy and L^A and crystalline samples of the corresponding complexes $[Fe(tzpy)_2(NCS)_2]$, $[Fe(tzpy)_2(NCSe)_2]$ (tzpy = 2-pyridyl[1,2,3]triazolo[1,5-α]pyridine) and $[FeL^A(NCS)_2]$ (L^A = N,N'-bis(1-pyridin-2-ylethylidene)-2,2-dimethylpropane-1,3-diamine) where synthesized according to methods published elsewhere.[5-7]

3.2 Thermal Spin Crossover of the Fe-complex crystals

Figures S7 and S8 shows magnetic susceptibility versus temperature curves for the $[Fe(tzpy)_2(NCS)_2]$ and $[Fe(tzpy)_2(NCSe)_2]$ crystals. Both complexes show a low (S = 0) to high (S = 2) spin electronic transition below room temperature. The low magnetic susceptibility measured at room temperature for compound $[FeL^A(NCS)_2]$ confirmed the diamagnetic (S = 0) ground state, a result consistent with its structural analysis performed at 293 K.[6]

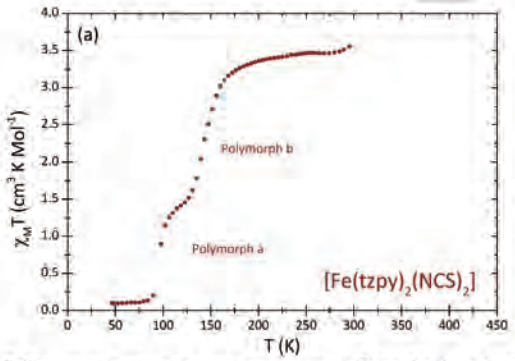

Figure S7. Magnetic susceptibility vs temperature measurements of the $[Fe(tzpy)_2(NCS)_2]$. Two different critical transition temperatures are observed due to occurrence of well-characterized crystalline polymorphs.

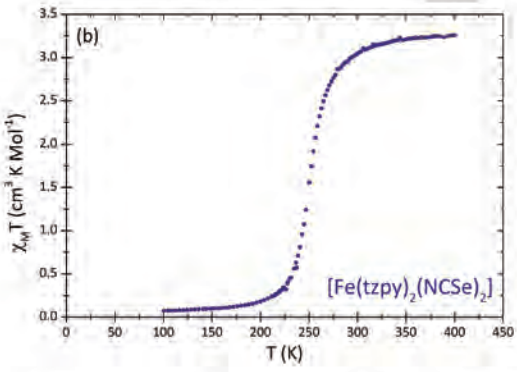

Figure S8. Magnetic susceptibility vs temperature measurements of the $[Fe(tzpy)_2(NCSe)_2]$ (b) crystals.

4. Single-molecule transport measurements

All histograms were built using an automatic algorithm that selects individual traces displaying plateaus. Same selection criteria were used through all experimental series to avoid the subjectivity in manual selection methods.

4.1. *Au-[Fe(tzpy)$_2$(NCS)$_2$]-Au junctions*

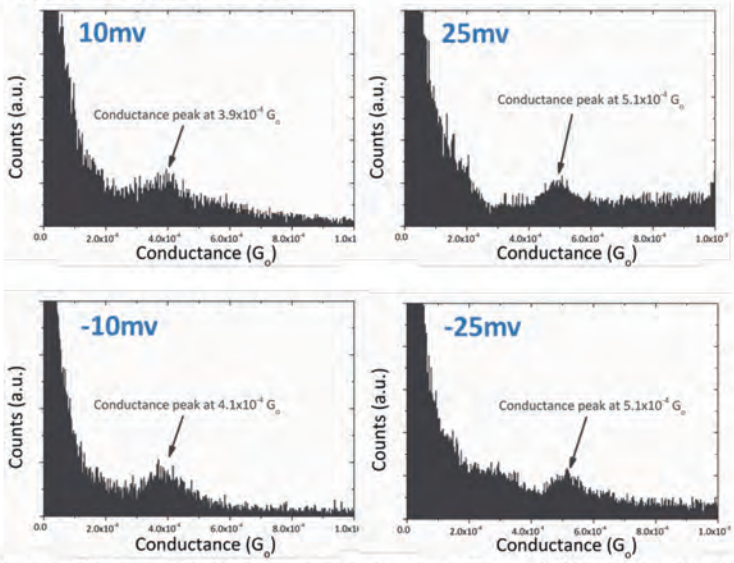

Figure S9. Conductance histograms built from thousands of Au-[Fe(tzpy)$_2$(NCS)$_2$]-Au junctions. Sample bias voltages are indicated.

4.2. *Au-[Fe(tzpy)$_2$(NCSe)$_2$]-Au junctions*

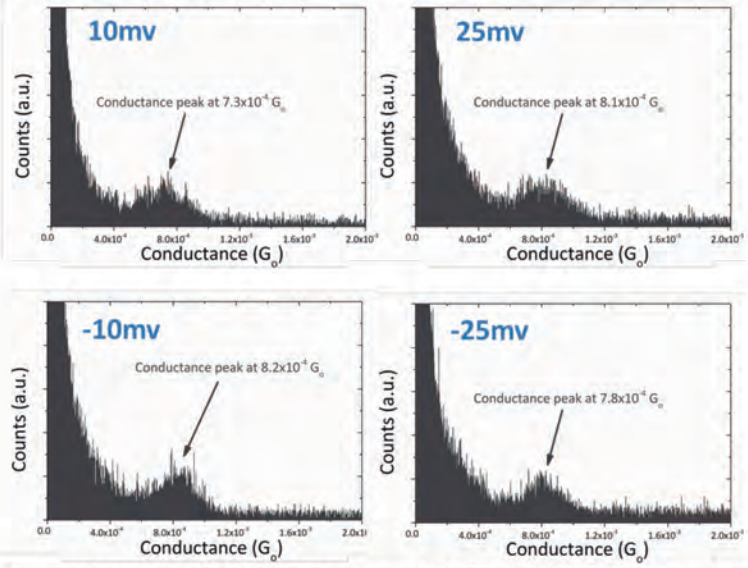

Figure S10. Conductance histograms built from thousands of Au-[Fe(tzpy)$_2$(NCSe)$_2$]-Au junctions. Sample bias voltages are indicated.

4.3. *Non-polarized Ni-[Fe(tzpy)$_2$(NCS)$_2$]-Au junctions*

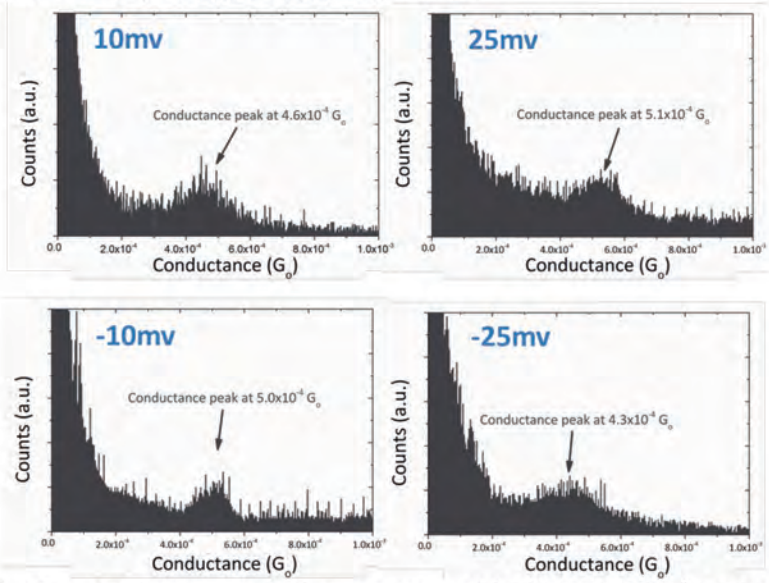

Figure S11. Conductance histograms built from thousands of Ni-[Fe(tzpy)$_2$(NCS)$_2$]-Au junctions using a non-polarized Ni electrode. Sample bias voltages are indicated.

4.4. *Non-polarized Ni-*[Fe(tzpy)$_2$(NCSe)$_2$]*-Au junctions*

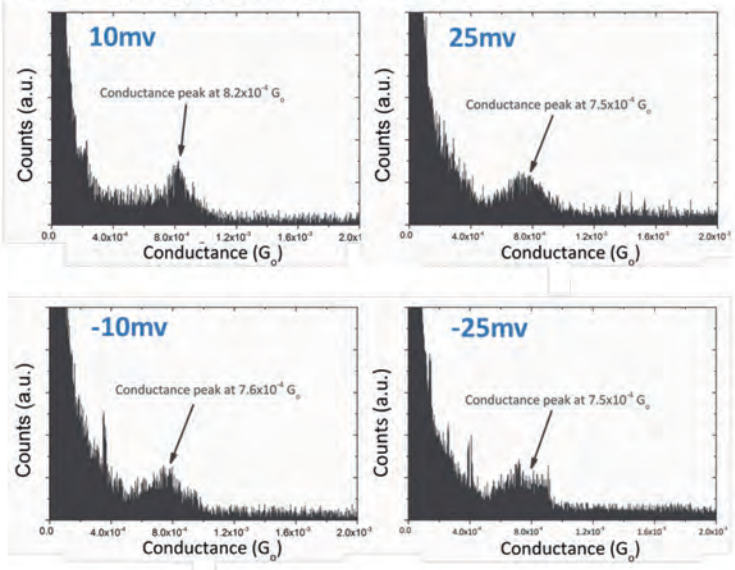

Figure S12. Conductance histograms built from thousands of Ni-[Fe(tzpy)$_2$(NCSe)$_2$]-Au junctions using a non-polarized Ni electrode. Sample bias voltages are indicated.

4.5. *1D & 2D conductance histograms of polarized the Ni-paramagnetic molecule-Au junction*

Figure S13 shows 1D conductance histograms and 2D maps built from several thousands of single-molecule traces collected for the -SeCN paramagnetic Fe^{II} complexes without any selection for both Ni tip magnetic polarizations. Single-molecule features are exclusively observed in the case of the β-down Ni polarization, which yields a prominent peak in the 1D histogram (Fig. S13a) and a bright spot around the molecular conductance value in the 2D maps with including all decay curves (Fig. SI13b, left panel). 2D-maps from selected traces for both –SCN and –SeCN derivatives. An average plateau length is extracted for each compound (see main manuscript), showing a longer values for the less resistive –SeCN anchoring group.

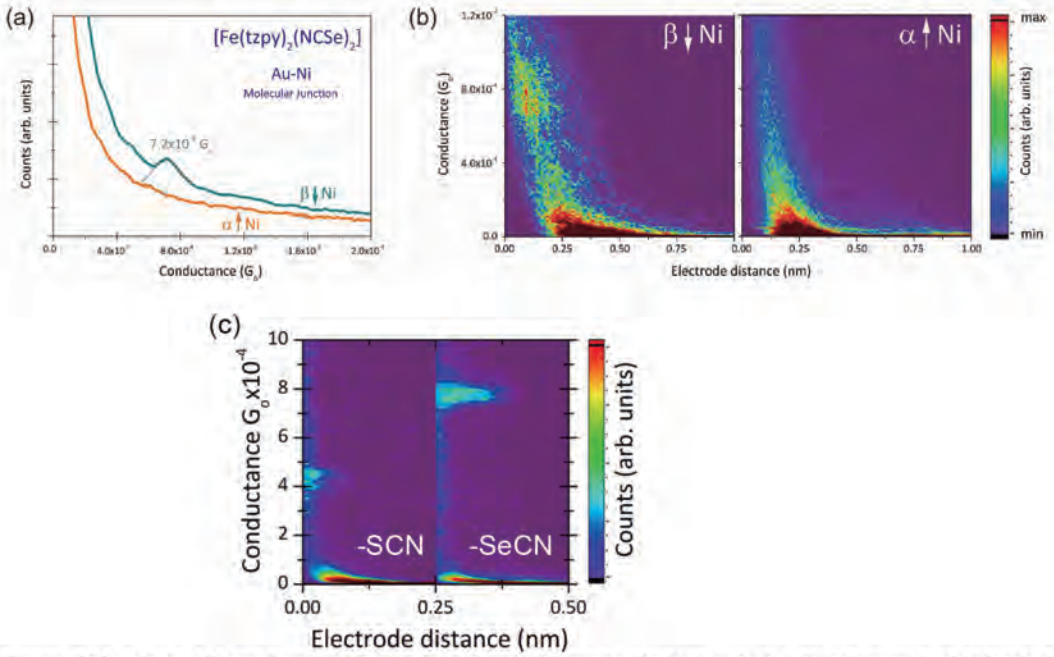

Figure S13. Linear 1D conductance histograms (a) and 2D maps (b) built out of a few thousand of individual single-molecule traces without any data selection for the -SeCN high-spin Fe^{II} complex under both directions of the Ni tip polarization. (c) 2D maps of both –SCN and –SeCN derivatives built out of selected traces displaying plateaus to measure an average plateau length for each compound.

4.6. *Injecting electrons from the magnetically polarized Ni electrode into the Ni-paramagnetic Fe^{II} molecules-Au junctions*

Figure S14 shows conductance histograms obtained from the Ni-molecule-Au junction with both $[Fe(tzpy)_2(NCS)_2]$ and $[Fe(tzpy)_2(NCSe)_2]$ molecules by injecting highly polarized electrons from the magnetically polarized Ni electrode.

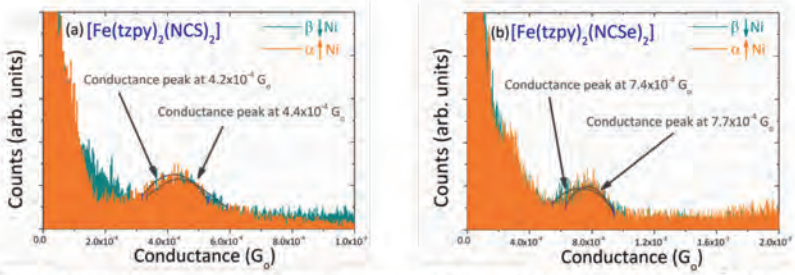

Figure S14. Conductance histograms built from thousands of polarized Ni-[$Fe(tzpy)_2(NCS)_2$]-Au and polarized Ni-$Fe(tzpy)_2(NCSe)_2$-Au junctions. Bias voltage is reversed as compared to Figures 2a-b of the manuscript.

4.7. *Ni-1,8-Octandithiol-Au junctions*

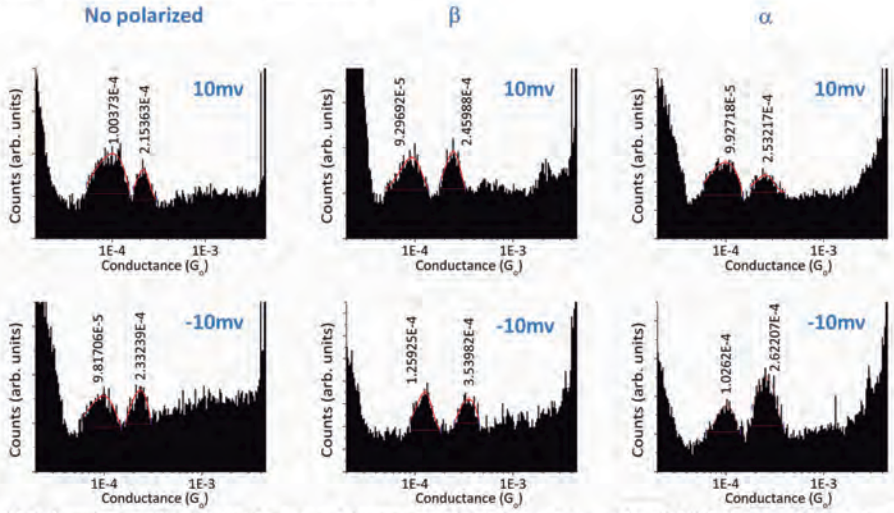

Figure S15. Semi-logarithmic conductance histograms built from thousands of Ni-1,8-octandithiol-Au junctions. Magnetization direction and sample bias voltages are indicated. The observed two sets of peaks are ascribed to previously reported low and high S-contact geometries.[11]

4.8. *Au Quantum Point Contacts formed at bare Ni-Au junctions*

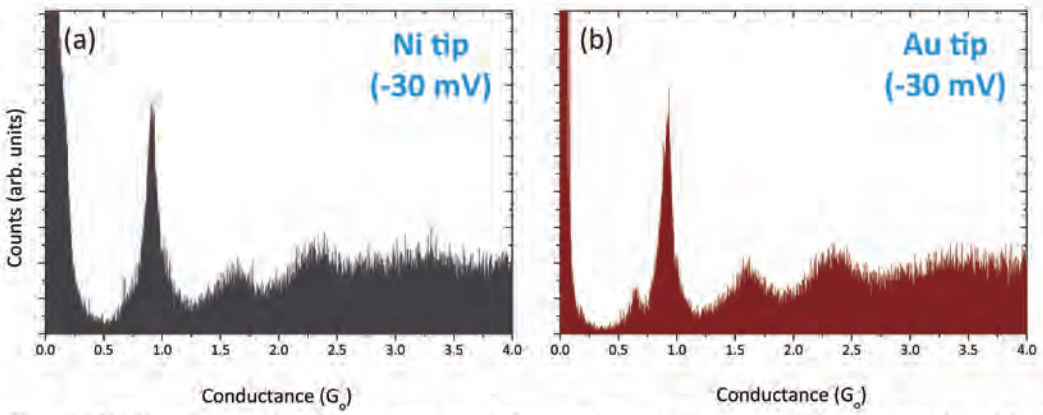

Figure S16. Comparison of conductance histograms showing the same quantum point contact formation at both Ni-Au (a) and Au-Au (b) junctions. The clean histogram obtained in (a) demonstrates that the Ni surface remains clean and oxide-free after the Ni tip preparation, magnetization and transport measurements under anaerobic conditions.

4.9. *Low temperature single-molecule transport measurements*

To perform systematic studies of the temperature dependence of the magnetoresistance SAMs were prepared as described above and mounted onto a home-made variable temperature STM assembly. The STM assembly was placed in a liquid helium cryostat (Janis Research Company) and placed under a vacuum of $2x10^{-6}$ Torr. The Dewar was then filled with liquid nitrogen and cooled to ~78K. Once the temperature of the system was stable the tip of the STM was brought into the proximity of the substrate and the break junction experiments were performed as described for the room temperature case. A homemade 10nA/V amplifier was used to record the current vs. distance traces. To obtain conductance measurements at different temperatures a 25W resistive heater was used to heat the STM head assembly while maintaining vacuum. A PID controller was used to control the current applied to the heater and maintain the temperature to +/- 0.5K. Measurements were performed at 78K, 175K, 225K, 250K, and room temperature.

5. Computational Details

5.1. *Details on DFT computational calculations*

All the calculations have been performed with the GREEN code[12] and its interface to the DFT based SIESTA package[13] including the recently implemented fully-relativistic pseudo-potential (PP) formalism in order to account for spin-orbit coupling (SOC) contributions.[14] For the PPs generation (including pseudo core-corrections[15] for the Au, Fe and Ni atoms) and the self-consistent DFT calculations we used the generalized gradient approximation (GGA) to the exchange-correlation energy as parametrized by Perdew at al.[16] The localized atomic orbital (AO) basis set employed by SIESTA were generated under the double-ζ polarized (DZP) scheme with confinement energies of 100 meV for all atoms, the 3D real space grid resolution (so called mesh-cutoff) was set to ~0.07 Å ^{3} while the Brillouin zone (BZ) was sampled with a (2×2)

k-grid. The surface systems were initially treated as 2D slabs with a rectangular $\begin{pmatrix} 6 & 0 \\ 4 & 8 \end{pmatrix}$ supercell (denoted as (6×8) hereafter) relative to the Au(111) (1×1) lattice and comprised five bulk-like gold layers with the $[Fe(tzpy)_2(NCS)_2]$ or $[FeL^A(NCS)_2]$ molecules adsorbed at a 3-fold hollow site at a S-Au bond distance of 2.5 Å. In order to address the role of the SOC, we calculated self-consistently the Hamiltonian[14] for the system with the gold slab and the adsorbed paramagnetic $[Fe(tzpy)_2(NCS)_2]$ complex with the magnetization axis always fixed along the surface normal z, either pointing away from the surface (↑Fe, also called α-up) or towards the surface (↓Fe, also called β-down), where ↑ (↓) refers to the magnetic moment along $+z$ or $-z$ (see Table S1). In Figure S16, the two components of the magnetization for the $[Fe(tzpy)_2(NCS)_2]$ molecule on the gold surface show the relatively large spin delocalization of the SCN ligands.

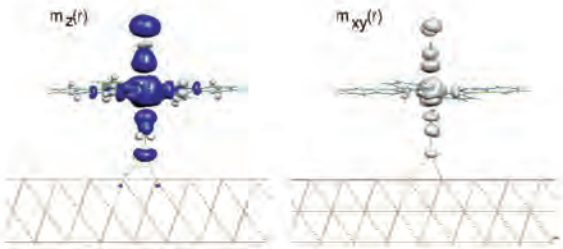

Figure S17. Magnetization density isosurfaces for the $[Fe(tzpy)_2(NCS)_2]$+Au(111) slab system in the ↓Fe configuration and for the out-of-plane and in-plane components, $m_z(r)$ and $m_{xy}(r)$, respectively. Blue (white) colors are used for negative (positive) isosurfaces, while the isosurface value in $m_{xy}(r)$ is ten times smaller than that in $m_z(r)$.

The spin resolved PDOS can be almost directly extracted from the GFs as:

$$PDOS^{\sigma}(\varepsilon,k) = -\frac{i}{\pi} Tr[G_{ss}^{\sigma\sigma}(\varepsilon,k)O_{ss}(k) + G_{sb}^{\sigma\sigma}(\varepsilon,k)O_{sb}(k)] \qquad (1)$$

where σ indexes the spin, $G_{ij}^{\sigma\sigma}(\varepsilon,k)$ the spin diagonal box of the GF linking principal layers i and j (here s and b refer to the surface and sub-surface layers, respectively) and $O_{ij}(k)$ is the overlap matrix between the two layers. For the $PDOS(\varepsilon,k,\sigma)$ plots along several lines in the BZ (Figure 4 of the manuscript) we increased the resolution for visual purposes by setting E_i=5 meV and a step along each line of just $\delta k = 0.008$ Å^{-1}.

Table S1. Spin populations in μB (electrons), for the two spin configurations considered for the Au(111)-$[Fe(tzpy)_2(NCS)_2]$ surface semi-infinite system (see text). Columns refer to projections on the molecule, the Au nearest neighbors to the S, Au_{NN}, and the rest of Au atoms in the first layer, Au_1.

	Spin populations		
	Molecule	Au_{NN}	Au_1
β-down↓Fe	-3.924	-0.004	+0.002
α-up↑Fe	+3.924	+0.004	-0.002

For the sake of completeness, we show in Figure S17 maps of the logarithm of the DOS(ε,*k*) along the main directions of the (6x8) Brillouin zone and projected on the molecule and the gold surface atoms. The molecular levels are essentially dispersionless with the majority spin component (α-up) presenting a gap so that, close to the Fermi level, only the minority spin (β-down, blue) effectively contributes to the transport properties. On the other hand, the projections on the gold atoms all show the characteristic dispersive *sp* bands with a clear Rashba split for the surface state (L-band). Although differences between both spin components are not visible in this scale, substracting one from the other reveals a rich spin structure (see Figure 5). It is worth noting the small hybridization of the molecular orbitals of the $[FeL^A(NCS)_2]$ complex with the surface due to the non-bonding nature of the t_{2g} orbitals (see Figure S17b).

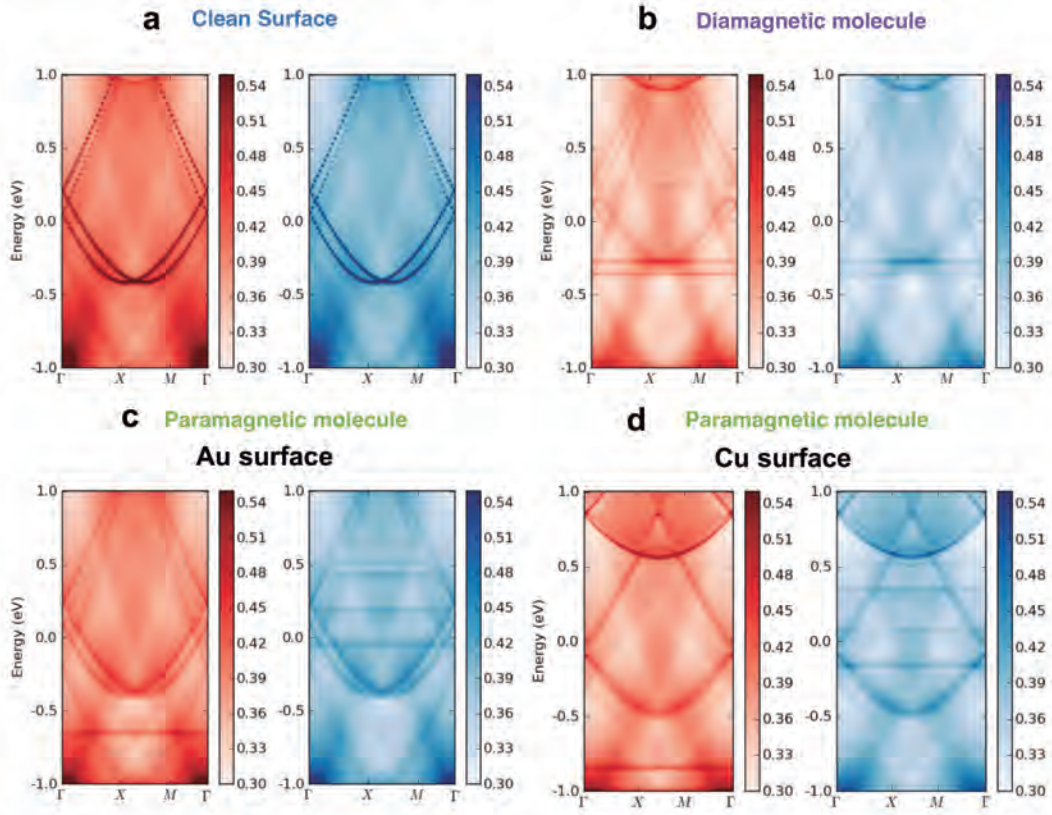

Figure S18. Maps of the logarithm of the DOS(ε,*k*) along the main directions of the (6x8)

Brillouin zone for the four studied systems corresponding to the three gold surface atoms coordinated to the molecule showing α-up (majority, red) and β-down (minority, blue) levels.

Such DFT electronic structure calculations for the interaction between a surface with strong spin-orbit coupling with a paramagnetic molecule have some intrinsic limitations: (i) the inherent single-determinant nature of the DFT methodology does not map directly in the multideterminant manifold of states for the system, which will be certainly present due to the existence of low lying excited states in the FeII complex and the metallic nature of the electrodes. (ii) The inclusion of spin-orbit effects employed in our DFT calculations is the best available approach for periodic systems, however, are less accurate than two-component DFT methods available for non-periodic DFT methods. In general any DFT method will have the limitation to use one single-determinant. Furthermore, CASSCF+RASSI calculations can handle these two limitations of DFT methods but cannot be performed by considering a surface, just a non-periodic small model.
Considering these limitations, we made some preliminary calculations that support a reasonable description of the system in a qualitative way. (i) the bare gold electrode calculations exhibit the characteristic band structure of the Rashba effect (ii) the spin state of the molecule is correctly described in the full system for all calculations (Au and Cu electrodes, spin-crossover and low spin molecules). (iii) we also tested a small model for the molecule electrode interaction (the molecule + a cluster of 4 gold atoms) by means of multireference methods (CASSCF + spin-orbit RASI, see section 5.2). It was observed that the magnetic anisotropy was not significantly affected by the coordination to the gold surface and the electronic configuration of the molecule remained robust, similar to the results of the periodic DFT calculations.

5.2. *Supporting CASSCF+RASSI calculations*
CASSCF+RASSI calculations to determine the zero-field splitting parameter D were performed for the isolated Fe^{II} complex and for a model of the complex coordinated in the 3-fold hollow site using a Au_4 cluster model using MOLCAS 7.8 code.[17] The magnetic anisotropy barrier is $D \cdot S^2$ (S = 2 for the studied Fe^{II} sytem). We used an all electron ANO-RCC basis set: Fe (6s5p4d2f), S (5s4p1d), N (4s3p1d), C (3s2p), H (2s) and Au(6s4p3d1f) with an active space considering the six d electrons of the Fe^{II} centers and the five d orbitals.

References

1 Chaudhuri, A.; Lerotholi, T. J.; Jackson, D. C.; Woodruff, D. P.; Dhanak, V. *Phys. Rev. Lett.* **2009**, *102*, 126101.
2 Jia, J. *et al. J. Phys. Chem. C* 2013, *117*, 9835-9842.
3 Pasquali, L. *et al. Langmuir* **2011**, *27*, 4713-4720.
4 Tanaka, A., Imamura, M. & Yasuda, H. *Phys. Rev. B* **2006**, *74*, 113402.
5 Battaglia, L. P. *et al. J. Chem. Soc. Dalton*, **1994**, 2651-2654.
6 Brefuel, N. *et al. Polyhedron* **2007**, *26*, 1745-1757.
7 Niel, V. *et al. Inorg. Chem.* **2003**, *42*, 4782-4788.
8 R. Skomski, *Simple Models of Magnetism*. (Oxford University Press, Oxford, 2008).
9 Rau, I. G. et al. *Science*, **2014**, *344*, 988-992.

10 Cobo, S.; Molnar, G. ; Real, J. A. ; Bousseksou, A. *Angew. Chem. Int. Edit.* **2006, 45,** 5786-5789.
11 Li, X. *et al. J. Am. Chem. Soc.* **2006**, *128*, 2135-2141.
12 Cerda, J.; Van Hove, M. A.; Sautet, P.; Salmeron, M. *Phys. Rev. B* **1997**, *56*, 15885-15899.
13 Soler, J. M. *et al. J. Phys.:Cond. Matter* **2002**, *14*, 2745-2779.
14 Cuadrado, R.; Cerda, J. I. *J. Phys.:Cond. Matter* **2012**, *24*, 086005.
15 Cuadrado, R. *et al. J. Chem. Phys.* **2010**, *133*, 154701.
16 Perdew, J. P.; Burke, K.; Ernzerhof, M. *Phys. Rev. Lett.* **1996, 77**, 3865-3868.
17 Aquilante, F. *et al.* Software News and Update MOLCAS 7: The Next Generation. *J. Comput. Chem.* **31**, 224-247 (2010).

2.2.3 Findings and Discussion

— *The main findings of this study were the following:*

- Ni-[Fe(tzpy)$_2$(NCSe)$_2$]-Au junctions showed more stability (longer junctions lifetime on *tapping* experiments) and a higher molecular conductance values than [Fe(tzpy)$_2$(NCS)$_2$] junctions, ca. factor 2.

- Junctions of both paramagnetic complexes of Fe(II) on Au substrate showed spin-dependent current to the α-↑Ni and β-↓Ni tip polarizations at RT and under *Au substrate-to-Ni tip* current sense, the observed conductance change was at least 100-fold under opposite Ni magnetic polarizations, like in the previous Co(II) complex. Oppositely, under the same experimental conditions the diamagnetic ([Fe(L)^A(NCS)$_2$]) complex did not show any dependence on the Ni tip polarization and its conductance presents a reduction of 5-fold respect the obtained for the [Fe(tzpy)$_2$(NCSe)$_2$] under β-↓Ni tip polarization.

- Under *Ni tip-to-Au substrate* current sense, both paramagnetic Fe(II) complexes did not show dependence on tip polarization, behavior already observed with Co(II) complex too.

- Single-molecule conductance measurements of [Fe(tzpy)$_2$(NCSe)$_2$] junctions under *substrate-to-Ni tip* current sense and employing Cu substrate electrodes did not show any kind of conductance dependence on the Ni tip magnetic polarization for all the experimental conditions.

- For the performed experiments under *Au substrate-to-Ni tip* current sense for Ni-[Fe(tzpy)$_2$(NCSe)$_2$]-Au junctions, if were applied successive decreasing T$_{working}$ below the T$_{CTC}$ (thus diamagnetic behavior) a progressive suppression of the spin-dependent current was observed. The obtained conductance values under the *high-spin* at RT configuration using β-↓Ni tips and the obtained for the *low-spin* electronic configuration at LT, both performed at the LT-STM, were statistically indistinguishable and showed an equivalent experimental error. Likewise was observed a ca. 2 fold of conductance difference between the measured *low-spin* [Fe(tzpy)$_2$(NCSe)$_2$] at LT and its *high-spin* state of measured at RT using the conventional STM under β-↓Ni tip polarization.

- Single-molecule conductance experiments performed under non-polarized electrodes (Au tips or non-magnetized Ni tips both with Au substrate) did not show any difference on the current response under both current senses. The obtained conductance values for all these cases was the same that the obtained for the [Fe(tzpy)$_2$(NCSe)$_2$] *high-spin* electronic configurations employing β-↓Ni tips.

- DFT transport calculations shows a large preference for the minority carriers in both high-spin d^6 Fe complexes (S=2) complexes, with five α and one β

electrons, HOMO and LUMO frontier orbital levels lie nearly to the electrode ε_F The α and β t_{2g} and e_g levels for the diamagnetic ($[Fe(L)^A(NCS)_2]$) complex are identically occupied.

— *The discussion of the results is summarized below:*

- The paramagnetic Fe(II) complexes were chosen by their spin-filter capabilities, widely explained in the preceding Section. In the presented experiments the $[Fe(tzpy)_2(NCSe)_2]$ transition to the S=0 *low-spin* electronic state due working at LT under the T_{CTC}, gradually shows the suppression of the MR effect according to the decrease of the working temperature until the complete transition. This monotonic transition directly related with the molecules population transited to the *low-spin* electronic state, is in agreement with previous studies about similar transitions of SCO molecules on a 2D Au-NP films.[315,347] The MR suppression effect is comparable to the showed by the *low-spin* $[FeL^A(NCS)_2]$ complex, also diamagnetic but at RT, because in both cases the α and β channels are equivalent occupied (spin balanced) then suppressing any spin-dependent transport as computational results confirm, unlike the spin unbalance for the *high-spin* electronic state at RT.

- Paramagnetism has a crucial role as evidenced in the previous point, but is revealed that also represents another crucial role for the Spinterface. As was expected, the Au surface is spin-polarized because its spin-texture is triggered by the SOC of the strong polarized axial ligand-Au bond, but unexpectedly these effects are dramatically amplified due the paramagnetic state (S≠0) of the molecule and the associated SOC interaction[188,189,192,193] like DFT calculations reflect. As a consequence, emerges the effective asymmetric hybridization of the complexes' molecular orbitals to the polarized Se-Au Spinterface which explains the favored transport of the spin *minority* α-carriers, pre-polarizing the current injected to the molecule-Au interface as was proposed on the previous Section's discussion due the observed MR suppression

- Despite the pre-polarization effect through the Spinterface is dramatically amplified by the paramagnetism of the molecule due its SOC, the net effect is not tuned by the paramagnetic molecule's magnetic moment direction. The experimental way to prove it, is through the observed invariance of the conductance values for all the cases employing $[Fe(tzpy)_2(NCSe)_2]$ when there is a detectable current signal, like under β-↓Ni tip polarization, diamagnetic *low-spin* electronic structure or employing non-polarized electrodes. Such phenomenon confirms that a permanent *minority* α-↑-(pre)polarized current is always injected to the molecular junctions for all the studied cases, which dominates the conducting state under any Ni tip's magnetic polarization or without it.

- The observed current switching effect presents a direct dependence on Ni tip's magnetic polarization due the molecule's magnetic moment-Ni tip alignment, as had been proved to the previous Section. But as a consequence of the

high SOC can be arised a magnetic anisotropy (MA),[166,348–353] a new plausible hypothetical scenario which had to be considered. As several precedents show,[196,219,350,354,355] MA represents a similar phenomenology to the presented when the molecule-surface ensemble is enough strong to keep its spin aligned in a fixed direction and consequently emits a polarized current. Using CASSCF+RASSI calculations the obtained magnitude of the MA barriers is around 20 K, a too low barrier value to explain the observed magnetoresistance effect at RT because the resulting magnetic moment is not enough strong[166,351,355,356] for avoiding be aligned by the Ni tip magnetic polarization, proving quantitatively the unlikeliness of such scenario. The rejection of the MA model validates that the Fe(II) complex molecule's magnetic moment remains aligned with the magnetic polarization of the Ni tip (like the previous calculated Co(II) complex case) resulting in the same spin-alignment for both subsystems, allowing the transmission of α-↑-(pre)polarized current from the Spinterface when Ni tip–molecule are β-↓ polarized or blocking it when Ni tip–molecule are α-↑ polarized.

- Despite a magnetized Ni electrode emits or accepts electrons more efficiently for the *minority* spin,[116] this behavior is not contributing to the observed magnetoresistance effect since the Ni tip induces the same spin-alignment to the complex molecules, as has been explained on the previous point. As a consequence, the Ni tip will be injected always by the same *majority* or *minority* carriers. Besides, since the performed calculations and previous works([288,299] show that Fe(II) complexes also presents preferences for *minority* spin-carriers, the matching for the carrier preferences presented for both Ni tip electrode and Fe complexes allows an efficient spin transfer from the molecule to the electrode, suppressing any kind of filtering or selection effect in the molecule-tip interface that could decrease the electronic transport efficiency at this final stage thus affecting the transport all the entire molecular wire.

- The already observed suppression of the of magnetoresistance effect when the electrons are injected from the Ni tip into the paramagnetic molecule, now can be justified by the mentioned Ni tip–molecule same spin-alignment which generates a permanent injection of *minority* carriers to the molecule independently to the Ni tip magnetic polarization, showing the no spin-filtering scenario.[288,299] However, assuming a non-perfect polarizing efficiency of the magnetized Ni tip source, is plausible the injection of a low population of *majority* spin-carriers which should generate a decrease of the molecular conductance due the MR effect. But paradoxically, assuming qualitatively a Spin-torque effect mechanism such transient *majority* carriers current coming from the tip could contribute to the MR suppression flipping the molecule's magnetic moment when both are anti-aligned (blockage current scenario) becoming aligned. Similar scenarios have been reported attributing the observed effects to the Spin-transfer torque mechanisms, widely studied for layered systems,[357–360] where the withdrawn (or reflected) electrons "accumulate" in the interfaces between layers proportionally to the current flowing through the structure,

until the accumulated electrons exceed the dumpling torque contribution and induce a magnetic reversal in the interface. The Spin-torque also can be an argument to explain the non-appreciable MR effect when the polarized electrons injected from the molecule to the Spinterface are unfavored for the latter.

- The metal substrate effects, already observed in the previous Section, prove again the Au substrate essential role for the spin-dependent transport. Now, with the obtained results can be asserted its interplay with the molecule to create the Spinterface; the asymmetric junctions of Fe(II) paramagnetic complexes using the Cu substrate due its lightness did not show a MR effect, contrary to the Au substrate. This fact represents a crucial control experiment because is in agreement with the performed calculations where the lack of large SOC contributions due the Cu atomic lightness has suppress the spin-polarizations of the surface even presenting the interaction with the paramagnetic complexes molecules. In this case the interface is not enough strong to polarize the injected current in contrast to the paramagnetic molecule scenarios of employing Au substrate, highlighting the relevant role of the metallic substrate and its electronic configuration.

- The role of the ligand in Spintronics terms is not affecting the single-mole device, because both metal complexes $[Fe(tzpy)_2(NCS)_2]$ and $[Fe(tzpy)_2(NCSe)_2]$ show the same MR efficiency in the employed current range given by the STM amplification. The observed effects are established over the lifetime of the junctions associated to the affinity of the anchoring group by the substrate, being the more stable and longer junction for the -SeCN compared to the obtained for the -SCN. This affinity can be related with the observed inherent resistance of the latter.

- In this Section, several complexes have been measured, some of them can not be attributed to spin-dependent effects, which are as follow. The observed shifting for the $[Fe(tzpy)_2(NCSe)_2]$ employing β-$\downarrow$Ni tips at RT versus the *low-spin* at LT, is due the employment of different equipment and dissimilitudes of the medium.[361–363] On the other hand the $[Fe(tzpy)_2(NCSe)_2]$ conductance 5-fold higher respect the one presented by ($[Fe(L)^A(NCS)_2]$) is due the different ligand field for the Fe(II) center in both complex molecules as well as the different anchoring groups, going from the more -SCN to the less resistive -SeCN.[50,97,364] The latter effect also justifies the differences of conductance (ca. 2 fold) between $[Fe(tzpy)_2(NCS)_2]$ and $[Fe(tzpy)_2(NCSe)_2]$.

2.3 Conclusions of the Chapter

As a consequence of the different proposed models and their development as well as the amount of key-concepts appeared throughout the two divisions of the Chapter, I found necessary gather and relate them along with the associated conclusions.

In this Chapter a single-molecule device with spin-filtering capabilities at RT has been developed and studied. The first proposed qualitative model to explain the MR observed effects was based on two key-parameters, a polarized current injected from a magnetized *(i)* STM Tip to a *(ii)* paramagnetic Co(II) complex with the capability to allow or block the current according its inherent spin properties. This model was invalidated for three reasons. Two of them were unpredicted effects consequence of employing Cu or Pt metal substrates and due the application of Ni tip-to-substrate current sense, both effects suppressed the MR effect despite in the initial model they should not present any interplay with the spin-dependent transport. Under such unsupported effects, the only reasonable strategy was reformulating the model replacing the electronic source's role of the Ni tip electrode by the metal substrate electrode, as well as assume that the interfacial pre-polarizing current mechanism occurred uniquely to the Au-molecule interface. The third reason for the invalidation of the proposed model, is the consequence of the not fixed molecular spin because it is orientated according the Ni tip magnetic polarization direction as calculations predicted. This simple feature has a large repercussion because explains why the experiment performed under the injected current from the Ni tip do not show any MR behavior since the molecule is permanently aligned according to the Ni tip, thus is injecting the same spin-carriers' population under any magnetic Ni polarization direction. Despite the mentioned drawbacks of the first model, some essential information was obtained comparing the response of Co(II), Mn(II) and Ni(II) metal complexes, since only the Co(II) case showed MR behavior. This fact defines two requirements for the molecule's electronic configuration to offer practical spin-filtering capabilities to the molecule apart form the paramagnetism, its orbitals (in the studied case empty) have to present enough strong interaction with the junction metal electrodes and the adequate energy difference to the ε_F for only one electron-polarization.

In the second Section, employing paramagnetic Fe(II) complexes which gather the above electronic conditions to present spin-filtering capabilities, were performed the single-molecule current measurements to prove the new assumed paradigms for the model, supported by several control experiments as well computational calculations. With the obtained results, the uncertainties were solved thanks to the confirmation of the proposed qualitative model based on the pre-polarization mechanism of the molecule-Au Spinterface. Since the polarized current only can be generated to the Au surface due its electronic properties and interplay with the paramagnetic molecules, therefore has to be emitted necessarily from it. These facts represent the most reasonable explanation for both suppressing effects, because explains why only Au can create enough powerful Spinterface and justifies the reason to be the source electrode. Moreover, The confirmation of the pre-polarization current on the

Spinterface also corroborates experimentally the proposed molecule's magnetic moment alignment according the Ni tip polarization direction, for the explained reasons above.

After the performed single-molecule current measurements and the reasoned validation of the second proposed model, the device phenomenology is qualitatively established. Below, are summarized other notable conclusions:

- The combination of the three asymmetric *key-parameters* proposed to build a single-molecule device with MR effects has been successfully developed using paramagnetic Fe(II) or Co(II) complex molecules trapped between a Au substrate electrode and a polarized ferromagnetic Ni tip electrode performing a stable junction. The junction conductance was switched by flipping the magnetic polarization of the Ni tip electrode, as a consequence of the following mechanism is proposed. Initially, the current injected from the Au substrate source electrode is induced to a defined polarization at the paramagnetic molecules/Au Spinterface, because here is generated a fixed spin-polarized Au surface due the hybridized spin-polarized states enhanced by the paramagnetic molecule's SOC, as a consequence, the *majority* β-polarized electron transmission is withdrawn and *minority* α-polarized electron transmission is favored dominating the conducting state of the junction. Such *minority* α-polarized current is injected to the molecule which presents spin-hybridized molecular levels close enough and strongly interacting with the electrodes ε_F, and finally is allowed the spin-filtering effect according the molecule's magnetic moment alignment with the Ni tip magnetic polarization ($\uparrow$ or $\downarrow$) directions. This mechanism causes the conductance switching between the two conductance states, giving a MR response of ca. 100-fold between both opposite Ni tip polarization directions.

- The observed current under non-polarized electrodes present the same conductance value than under β-$\downarrow$Ni tips, despite is contra-intuitive and it may be thought that the two different situation should present different conductance values because non-polarized current is a half-composed by α and β electrons, this assumed situation is not truth because according to the model exists a permanent *minority* α-(pre)polarized current always injected to the molecular junctions under any Ni tip's magnetic polarization or without it, therefore under non-polarized or β-$\downarrow$ Ni tips the phenomenology is equal because both of them do not present any penalty for the injected (α-$\uparrow$) electron.

- Is important to highlight that the observed MR effects are the direct consequence of a double spin-filtering behavior, because the transmitted current is selected in two different stages from different origin. The first selection is permanent and inherent to the S/Se-Au Spinterface which filters the current to a permanent α-polarization, and the second one is exerted by the molecule and tunable via the magnetic polarization of the Ni tip. Amongst the two spin-filtering stages, the interplay between the permanent α-polarized current and

the tunable molecule's spin preferences, represents the pillar of the spin-filter device, because the MR is switched at this intermediate stage since at this point the conducting state is totally dominated by the α-polarization which will be completely allowed or blocked by the molecule, according by the Ni tip magnetic polarization. The crucial role of the *Ni tip–molecule* spin-alignment reinforces the requirement of the open-shell electronic structure due its inherent paramagnetism.

- The identical spin-carriers preferences for the minority carriers presented for the Fe(II) and Co(II) complexes as well as for the Ni tip, avoid any current blockage in the molecule-Ni tip interface contributing to the high MR effect. Nevertheless, carrier preferences of other hypothetically used complexes can change due structural differences such as the ligands and/or metal centers affecting to the MR of the systems involved in. The carriers' preferences cannot be determined experimentally thus computational calculations should be performed.

- The proved experimentally and confirmed computationally *Ni tip–molecule* spin-alignment jointly with their matching preferences for the minority carriers, not only explain the suppression of the MR effect (spintronic diode) under *Ni tip-to-Au substrate* current sense, also can be the reason for the observed striking highly MR ratios, because they avoid any intermediate scenario between the totally blocked transport case (not detectable current) and the conducting state totally allowed (detectable current), due a unfavorable or favorable preferences for the spin-carriers respectively showed by Tip and molecule at the same time. This behavior, consequence of common spin preferences between Ni tip and molecule, can be changed just employing opposite preferences between molecule and electrodes, opening the gate to use the intermediate scenarios forbidden for the presented device but obtaining a spin-dependent variable resistor behavior instead a switch.

- DFT calculations overrates the Spinterface effects as a consequence of the not properly included SOC effects, so they cannot predict the huge current differences detected experimentally between both Ni tip polarizations.[365–367] Despite DFT predicts accurately the SOC effects on molecular and small systems it lacks on it incorporation on periodic systems like the electrodes.

- Despite the presented *set-up* can be used to build different single-molecule spin-filter devices, it presents some limitations. The most representative is the Au substrate requirement, because other material substrate could offer more stability like the proved Pt substrates or even offer additional spintronic capabilities to the system, like the graphene or graphite.[293,368–370] Other limitations are associated to the low assortment of paramagnetic molecules which gather both the required structural and stability properties for the junctions as well as the specific electronic configurations that allow and define the adequate spin-filtering capabilities found at this Chapter.

- The presented large magnetoresistance switching of two orders of magnitude and the "spintronic diode" effect is achieved at a near-zero bias voltage, which implies the molecular origin of the effect and the consequent use of very small currents and low power consumption, opening the gate to future real applications with a high efficient performance power.